AD-A086 000 NATIONAL MATERIALS ADVISORY BOARD (NAS-NAE) WASHINGTON DC F/G 11/6
AMORPHOUS AND METASTABLE MICROCRYSTALLINE RAPIDLY SOLIDIFIED AL--ETC(U)
MAY 80 N J GRANT, C F CLINE, L A DAVIS MDA903-78-C-0038
UNCLASSIFIED NMAB-358 NL

1 OF 2
AD A086 000

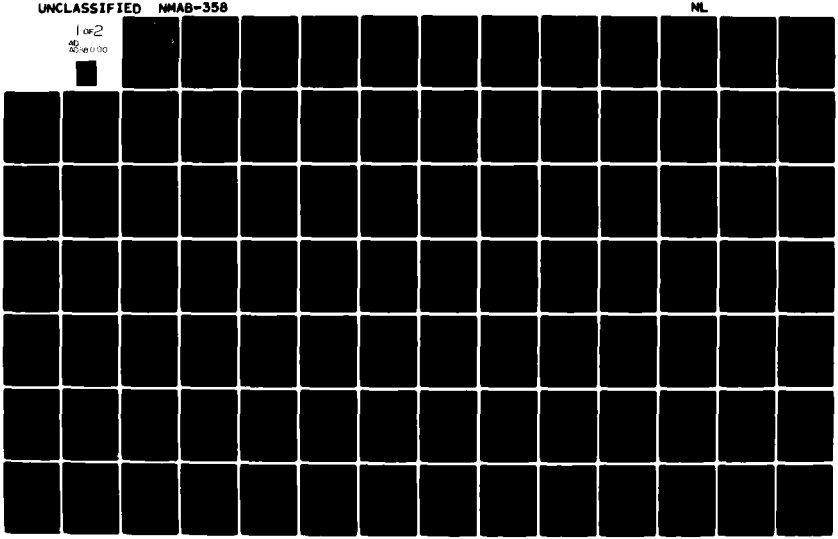

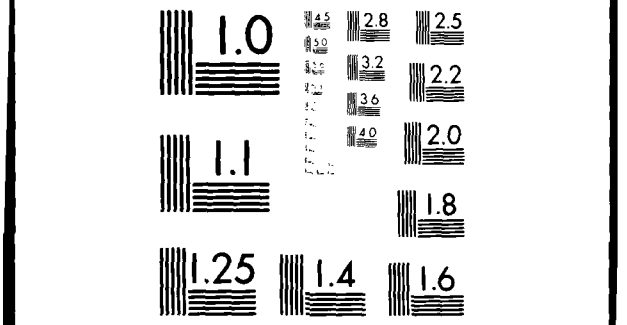

Amorphous and Metastable Microcrystalline Rapidly Solidified Alloys:

Status and Potential

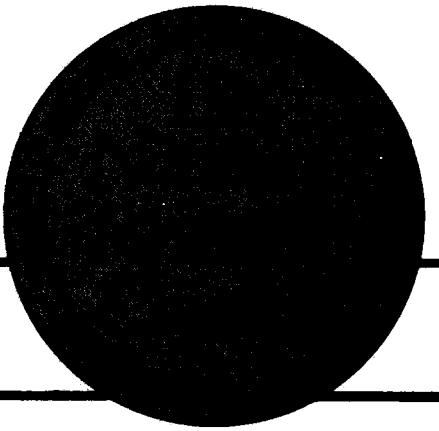

National Materials Advisory Board

Commission on Sociotechnical Systems

NMAB 358

NATIONAL RESEARCH COUNCIL
COMMISSION ON SOCIOTECHNICAL SYSTEMS
NATIONAL MATERIALS ADVISORY BOARD

Chairman:

Mr. William D. Manly
Senior Vice President
Cabot Corporation
125 High Street
Boston, MA 02110

Past Chairman:

Mr. Julius J. Harwood
Director, Materials Science Laboratory
Engineering and Research Staff
Ford Motor Company
P. O. Box 2053
Dearborn, MI 48121

Members

Dr. George S. Ansell
Dean, School of Engineering
Rensselaer Polytechnic Institute
Troy, NY 12181

Dr. H. Kent Bowen
Professor, Ceramic and Electrical Engineering
Massachusetts Institute of Technology
77 Massachusetts Avenue
Cambridge, MA 02139

Dr. Van L. Canady
Senior Planning Associate
Mobil Chemical Company
150 E. 42nd Street, Room 746
New York, NY 10017

Dr. George E. Dieter, Jr.
Dean, College of Engineering
University of Maryland
College Park, MD 20742

Dr. Joseph N. Epel
Director, Plastics Research and Development Center
Budd Corporation
356 Executive Drive
Troy, MI 48084

Dr. Larry L. Hench
Professor and Head
Ceramics Division
Department of Materials Science and Engineering
University of Florida
Gainesville, FL 32601

Dr. Robert E. Hughes
Professor of Chemistry
Executive Director, Materials Science Center
Department of Chemistry
Cornell University
Ithaca, NY 14850

Dr. John R. Hutchins III
Vice President and Director of Research and Development
Technical Staff Division
Corning Glass Works
Sullivan Park
Corning, NY 14830

Dr. Sheldon E. Isakoff
Director, Engineering Research and Development Division
E. I. DuPont de Nemours & Co., Inc.
Wilmington, DE 19898

Dr. Frank E. Jaumot, Jr.
Director of Advanced Engineering
Delco Electronics Division
General Motors Corporation
P. O. Box 1104
Kokomo, IN 46901

Dr. James W. Mar
Professor, Aeronautics and Astronautics
Building 33-307
Massachusetts Institute of Technology
Cambridge, MA 02139

Dr. Frederick T. Moore
Industrial Advisor
Industrial Development and Finance Department
World Bank
1818 H Street, N.W., Room D422
Washington, DC 20431

Dr. R. Byron Pipes
Director, Center for Composite Materials
Department of Mechanical and Aerospace Engineering
University of Delaware
Newark, DE 19711

Dr. Allen S. Russell
Vice President-Science and Technology
Aluminum Company of America
1501 Alcoa Building
Pittsburgh, PA 15219

Dr. John J. Schanz, Jr.
Senior Specialist
Congressional Research Service-ENR
Library of Congress
Washington, DC 20540

Dr. Arnold J. Silverman
Professor, Department of Geology
University of Montana
Missoula, MT 59801

Dr. Dorothy M. Simon
Vice President and Director of Research
AVCO Corporation
1275 King Street
Greenwich, CT 06830

Dr. William M. Spurgeon
Director, Manufacturing and Quality Control
Bendix Corporation
24799 Edgemont Road
Southfield, MI 48075

Dr. Roger A. Strehlow
Professor, Aeronautical and Astronautical Engineering
University of Illinois at Urbana
101 Transportation Building
Urbana, IL 61801

Dr. Michael Tenenbaum
1644 Cambridge
Flossmoor, IL 60422

Dr. William A. Vogely
Professor and Head, Department of Mineral Economics
Pennsylvania State University
University Park, PA 16802

Dr. Albert R. C. Westwood
Director, Martin Marietta Labs
Martin Marietta Corporation
1450 South Rolling Road
Baltimore, MD 21227

NMAB Staff

W. R. Prindle, Executive Director
R. V. Hemm, Executive Secretary

(1/18/80)

BIBLIOGRAPHIC DATA SHEET	1. Report No. (14) NMAB-358	2. AD-A086 000	3. Recipient's Accession No. AD-A085 600
4. Title and Subtitle (6) Amorphous and Metastable Microcrystalline Rapidly Solidified Alloys: Status and Potential,			5. Report Date (11) May 1980 6.
7. Author(s) Committee on Technological Potential for Amorphous and Metastable Materials for Military Applications			8. Performing Organization Rept. No. NMAB-358
9. Performing Organization Name and Address National Materials Advisory Board ~~National Academy of Sciences~~ 2101 Constitution Ave., N.W. Washington, D.C. 20418			10. Project/Task/Work Unit No. 11. Contract/Grant No. (15) MDA903-78-C-0038
12. Sponsoring Organization Name and Address Department of Defense and the National Aeronautics and Space Administration			13. Type of Report & Period Covered (9) Final Report, 14. (12) 190

15. Supplementary Notes (10) Nicholas J. Grant Carl F. Cline Lance A. Davis Bernard H. Kear Fred E. Lubarsky

16. Abstracts

The nature, properties, processing, and possible applications of two classes of materials are described: amorphous solids, particularly glassy metals, and metastable microcrystalline alloys. The thermodynamics and structural considerations of both amorphous and metastable metals and nonmetals are discussed in detail. The chemistry and properties of systems for which data are available also are described as are the processing limitations and methods. Application possibilities are discussed, and the report concludes with recommendations for research and development.

17. Key Words and Document Analysis. 17a. Descriptors

Amorphous materials	Anelasticity	Viscoelasticity
Metastable materials	Powder metallurgy	Heterogeneous nucleation
Noncrystalline materials	Glass formers	Atomization
Metal powders	Glassy state	Diffusion brazing
Alloy powders	Nonequilibrium materials	
Glassy metals and alloys	Rapid solidification	
Oxide glasses	Disordered materials	
Microcrystalline materials	Quenching	
Rapidly quenched materials	Splat cooling	
Superplasticity	Splat quenching	

17b. Identifiers/Open-Ended Terms

17c. COSATI Field/Group

DISTRIBUTION STATEMENT A
Approved for public release; Distribution Unlimited

18. Availability Statement	19. Security Class (This Report)	21. No. of Pages
This report is for sale by the National Technical Information Service, Springfield, Virginia 22151.	UNCLASSIFIED	163
	20. Security Class (This Page) UNCLASSIFIED	22. Price

405214

INSTRUCTIONS FOR COMPLETING FORM NTIS-35 (10-70) (Bibliographic Data Sheet based on COSATI Guidelines to Format Standards for Scientific and Technical Reports Prepared by or for the Federal Government, PB-180 600).

1. **Report Number.** Each individually bound report shall carry a unique alphanumeric designation selected by the performing organization or provided by the sponsoring organization. Use uppercase letters and Arabic numerals only. Examples FASEB-NS-87 and FAA-RD-68-09.

2. Leave blank.

3. **Recipient's Accession Number.** Reserved for use by each report recipient.

4. **Title and Subtitle.** Title should indicate clearly and briefly the subject coverage of the report, and be displayed prominently. Set subtitle, if used, in smaller type or otherwise subordinate it to main title. When a report is prepared in more than one volume, repeat the primary title, add volume number and include subtitle for the specific volume.

5. **Report Date.** Each report shall carry a date indicating at least month and year. Indicate the basis on which it was selected (e.g., date of issue, date of approval, date of preparation.

6. **Performing Organization Code.** Leave blank.

7. **Author(s).** Give name(s) in conventional order (e.g., John R. Doe, or J.Robert Doe). List author's affiliation if it differs from the performing organization.

8. **Performing Organization Report Number.** Insert if performing organization wishes to assign this number.

9. **Performing Organization Name and Address.** Give name, street, city, state, and zip code. List no more than two levels of an organizational hierarchy. Display the name of the organization exactly as it should appear in Government indexes such as **USGRDR-I.**

10. **Project/Task/Work Unit Number.** Use the project, task and work unit numbers under which the report was prepared.

11. **Contract/Grant Number.** Insert contract or grant number under which report was prepared.

12. **Sponsoring Agency Name and Address.** Include zip code.

13. **Type of Report and Period Covered.** Indicate interim, final, etc., and, if applicable, dates covered.

14. **Sponsoring Agency Code.** Leave blank.

15. **Supplementary Notes.** Enter information not included elsewhere but useful, such as: Prepared in cooperation with . . . Translation of . . . Presented at conference of . . . To be published in . . . Supersedes . . . Supplements . . .

16. **Abstract.** Include a brief (200 words or less) factual summary of the most significant information contained in the report. If the report contains a significant bibliography or literature survey, mention it here.

17. **Key Words and Document Analysis. (a). Descriptors.** Select from the Thesaurus of Engineering and Scientific Terms the proper authorized terms that identify the major concept of the research and are sufficiently specific and precise to be used as index entries for cataloging.
(b). Identifiers and Open-Ended Terms. Use identifiers for project names, code names, equipment designators, etc. Use open-ended terms written in descriptor form for those subjects for which no descriptor exists.
(c). COSATI Field/Group. Field and Group assignments are to be taken from the 1965 COSATI Subject Category List. Since the majority of documents are multidisciplinary in nature, the primary Field/Group assignment(s) will be the specific discipline, area of human endeavor, or type of physical object. The application(s) will be cross-referenced with secondary Field/Group assignments that will follow the primary posting(s).

18. **Distribution Statement.** Denote releasability to the public or limitation for reasons other than security for example "Release unlimited". Cite any availability to the public, with address and price.

19 & 20. **Security Classification.** Do not submit classified reports to the National Technical

21. **Number of Pages.** Insert the total number of pages, including this one and unnumbered pages, but excluding distribution list, if any.

22. **Price.** Insert the price set by the National Technical Information Service or the Government Printing Office, if known.

AMORPHOUS AND METASTABLE MICROCRYSTALLINE RAPIDLY SOLIDIFIED ALLOYS: STATUS AND POTENTIAL

Report of

Committee on Technological Potential for
Amorphous and Metastable Materials for Military Applications

NATIONAL MATERIALS ADVISORY BOARD
Commission on Sociotechnical Systems
National Research Council

Publication NMAB-358
National Academy of Sciences
Washington, D.C.

1980

NOTICE

The project that is the subject of this report was approved by the Governing Board of the National Research Council, whose members are drawn from the Councils of the National Academy of Sciences, the National Academy of Engineering, and the Institute of Medicine. The members of the Committee responsible for the report were chosen for their special competence and with regard for appropriate balance.

This report has been reviewed by a group other than the authors according to procedures approved by a Report Review Committee consisting of members of the National Academy of Sciences, National Academy of Engineering, and the Institute of Medicine.

This study by the National Materials Advisory Board was conducted under Contract No. MDA 903-78-C-0038 with the Department of Defense and the National Aeronautics and Space Administration.

This report is for sale by the National Technical Information Service, Springfield, Virginia 22151.

Printed in the United States of America.

FOREWORD

The National Materials Advisory Board (NMAB) assembled its Committee on Technological Potential for Amorphous and Metastable Materials for Military Applications to discuss the nature, processing, properties and possible applications of a new class of metallic materials that are obtained by rapid solidification. This is a new, rapidly evolving field out of which a number of extremely useful alloys and products have already emerged. The science and technology of rapidly solidified alloys, appropriate processing studies, and extensive property testing and evaluation are moving ahead rapidly. Both microcrystalline and amorphous (glassy) alloys are being developed side by side through this technology.

Amorphous and microcrystalline materials can also be produced by other techniques: vapor phase (atomic) quenching, sputtering, electroless deposition, etc. There are, however, basic features of rapid solidification which are conducive not only to an amazing degree of structure control, but also an unlimited range of alloy compositions, and full-scale commercial production of such alloys. Rather than take on the entire spectrum of processes for production of metastable alloys and materials, coverage in this report is restricted to rapid solidification. For historical reasons and as useful, valid background information, oxide glasses were reexamined during committee discussion since certain phenomena and basic behavior are common to metallic glasses produced by rapid quenching from the melt. The report, however, is confined to metals.

Although it was intended that the committee would assess possible applications of military interest, this proved to be impractical to accomplish except in very general terms. The nature of amorphous and metastable alloys and their properties are covered in detail, and this might permit subsequent matching of applications, as they evolve, and materials.

ABSTRACT

The nature, properties, processing, and possible applications of two classes of materials are described: amorphous solids, particularly glassy metals, and metastable microcrystalline alloys. The thermodynamics and structural considerations of both amorphous and metastable metals are discussed in detail. The chemistry and properties of systems for which data are available also are described as are the processing limitations and methods. Application possibilities are discussed, and the report concludes with recommendations for research and development.

These materials are at a relatively early stage of development; areas of great potential are indicated among:

- unusual, excellent corrosion resistance for some metallic glasses
- unusually high fracture strength for some metallic glasses
- excellent magnetic properties for metallic glasses
- high strength, toughness and excellent fatigue and crack growth resistance for fine-grained microcrystalline alloys
- superplastic behavior for appropriate microcrystalline alloy compositions and structures
- high specific modulus and high specific strength aluminum alloys
- a whole new world of alloys and alloy systems and structures which were never possible in the ingot world.

ACKNOWLEDGEMENTS

The contributions of A. Argon on anelasticity, R. Hasegawa on electrical applications, C.G. Levi and R. Mehrabian on heat flow and metastable crystalline aluminum, R.D. Maurer on use potential of oxide glass, Ian G. Palmer on survey of current aluminum technology, and R. Parrish on research needs are acknowledged with appreciation.

NATIONAL MATERIALS ADVISORY BOARD

COMMITTEE ON TECHNOLOGICAL POTENTIAL FOR
AMORPHOUS AND METASTABLE MATERIALS FOR MILITARY APPLICATIONS

Chairman

NICHOLAS J. GRANT, Professor, Department of Materials Science and Engineering, Massachusetts Institute of Technology, Cambridge, Massachusetts

Members

CARL F. CLINE, University of California, Lawrence Livermore Laboratory, Livermore, California

LANCE A. DAVIS, Manager, Strength Physics Department, Allied Chemical Corporation, Morristown, New Jersey

BERNARD H. KEAR, Senior Consultant, Science, United Technologies Research Center, East Hartford, Connecticut

FRED E. LUBORSKY, Metallurgy Laboratory, General Electric Company, Research and Development Center, Schenectady, New York

ROBERT MEHRABIAN, U.S. National Bureau of Standards, previously Professor, Department of Metallurgy and Mining Engineering, University of Illinois, Urbana, Illinois

DONALD E. POLK, Materials Research Corp. (formerly Institute for Chemical Analysis, Northeastern University), Watertown, Massachusetts.

STANLEY D. STOOKEY, Consultant, 12 Timber Lane, Painted Post, N.Y., formerly Director of Fundamental Chemical Research, Technical Staffs Div. of Corning Glass Works

THOMAS E. TIETZ, Manager, Metallurgy and Composites Laboratory, Lockheed Palo Alto Research Laboratory, Lockheed Missiles and Space Company, Inc., Palo Alto, California

Liaison Representatives

PHILLIP PARRISH, Metallurgy and Materials Science Division, U.S. Department of the Army, Army Research Office, Research Triangle Park, North Carolina

EDWARD S. BALMUTH, General Dynamics, Ft. Worth, Texas, formerly of the U.S. Department of the Navy, Naval Air Systems Command, Washington, D.C.

ATTWELL ADAIR, U.S. Air Force Materials Laboratory, Wright-Patterson Air Force Base, Ohio

JEROME PERSH, Staff Specialist for Materials and Structures (Engineering Technology), Office of Deputy Undersecretary of Defense for Research and Engineering, U.S. Department of Defense, Washington, D.C.

HUBERT PROBST, Materials and Structures Division, National Aeronautics and Space Administration, Lewis Research Center, Cleveland, Ohio

EDWARD C. VAN REUTH, Defense Advanced Research Projects Agency, Arlington, Virginia

NMAB Staff

JOSEPH R. LANE, Staff Metallurgist

CONTENTS

FIGURES AND TABLES

Chapter 1

SUMMARY

METASTABLE CRYSTALLINE AND AMORPHOUS MATERIALS

Nature of the Amorphous State

By definition, amorphous materials are those with no long-range order. However, differences in short-range order, such as pair ordering, can affect properties. Other departures from the purely amorphous state are two-phase structures that result because of partial crystallinity or impurities and strained lattices that result because of quenching stresses or mechanical work.

Thermodynamics and Kinetics

Amorphous solids are in metastable equilibrium because the normal transition on cooling to a crystalline state has been prevented by rapid cooling to the point at which the viscosity of the solid prevents diffusion to the more stable crystalline lattice. Heterogeneous nuclei, if present, tend to deter undercooling and, thus, aid crystallization. They also can catalyze the formation of nonequilibrium microstructures, affect grain size, and initiate subsequent crystallization of the glass.

Heat Flow Limitations

An upper limit on achievable heat-transfer coefficients can be calculated. In gas atomization, the factors influencing this limit are the specific heat, conductivity, velocity, density, and viscosity of the gas and the particle size of the metal. The average cooling rate in a liquid metal droplet is directly proportional to the heat-transfer coefficient and inversely proportional to the radius of the droplet. When solidification takes place against a metal substrate, the variables are the casting thickness and the conductivity and thermal diffusivity of the melt. As with gas cooling, the most effective way to increase the rate is to decrease the melt thickness (or the droplet size for gas cooling).

Processing Methods

Several methods can be used to achieve or approach the required quenching rates, the limits of which are described above. Early work involved splat cooling, but this process is not easily amenable to scale-up. More recent work has involved melt spinning and melt extraction and twin roller quenching. Other methods are high-velocity gas atomization (to

make powder), plasma spraying (which deposits the droplet on a surface), centrifugal atomization, and electric field atomization. Self-quenching can be used to convert a thin layer of liquid metal to glass on crystalline alloy surfaces.

Consolidation Methods

Since most glass production methods produce powder or splat, the key to commercialization is the conversion of such material into a solid of useful geometry and size. One of the procedures for doing this is in-situ consolidation. This can take the form of spray rolling of splat. Alternatively, cold compaction can be accomplished by closed die forging or by a high rate process involving explosive or magnetic means. For certain materials and applications, hot forming techniques such as slow strain rate hot-pressing and hot extrusion can be employed.

Metastable Crystalline Alloys

The microstructural modifications that can take place because of rapid solidification include:

a. Microstructural refinement,
b. Extension in solid solubility,
c. Morphological modifications,
d. Formation of nonequilibrium phases, and
e. Elimination of significant segregation.

These changes can have significant favorable influences on strength, toughness, elastic modulus, and fatigue crack initiation and propagation. Rapidly cooled alloys of the proper composition and structure exhibit superplastic behavior, thus permitting near-net shape closed-die-forged parts to be made and thin sheet to be rolled.

METALLIC GLASSES

Given only limited knowledge, it appears that only two major groups of metallic systems readily form glasses. The first group is referred to as metal-metalloid, $T^2_{1-x}X_x$, where T^2 is Mn, Fe, Co, Ni, Pd, Au, or Pt and X is B, C, N, Si, Ge, Al or P. The second group, referred to as intertransition, has the composition $T^1_{1-x}T^2_x$, where T^1 is a transition metal such as Fe, Co, Ni, Rh, Pd, and Cu and T^2 is as defined above. Other amorphous alloys also exist, leading to speculation as to whether there actually are any distinct systems. A narrow, deep eutectic at glass-forming compositions characterizes most systems. Nearly all glass-forming compositions belong to one of the following glass-forming element groupings: 15-25 percent, 25-35 percent, and 30-70 percent.

Glass-forming tendency has been correlated with phase diagram characteristics; differences in atomic size, valence or electronegativity, position in the periodic table, and composition considerations.

PROPERTIES OF AMORPHOUS MATERIALS

Magnetic Properties

Amorphous ferromagnets usually have a well defined magnetic ordering temperature, which is always significantly lower than that of crystalline alloys. Amorphous alloys display directional order anisotropy and are subject to stress-induced ordering. Their magnetic losses are at least ten times smaller than the losses of Fe-3-1/4% Si and two times smaller than the Permalloys.

Stability

The metallurgical stability of amorphous alloys of potential interest for magnetic applications has been found to be more than adequate. Lifetimes of the least stable of the alloys, $Fe_{80}B_{20}$, have been estimated to be 500 years at 175°C. Somewhat poorer mechanical stability is observed, but this is controllable during alloy preparation. There is no connection between ease of formation of the amorphous structure and the resultant stability.

Mechanical Properties

Many amorphous metals exhibit remarkable strengths. However, these alloys can be embrittled if heated for relatively short times at temperatures several hundred degrees below their glass transition temperatures.

The fracture toughness of amorphous metals is lower than that of tough steel but higher than that of other high-strength reinforcement materials such as oxide glasses. Under cyclic loading, the fatigue strengths of amorphous metals are comparable to or greater than those of steels. At very high stress levels, glassy alloys behave elastically which makes crack initiation difficult, and thus, prolongs low-cycle fatigue life.

Corrosion Properties

Some amorphous metals exhibit extraordinary high corrosion resistance. This is attributed, in part, to the absence of second phases and grain boundaries and to the formation of a protective film.

POTENTIAL APPLICATIONS AND LIMITATIONS

Magnetic Applications

Magnetic shielding and delay lines were among the first two applications reported, and cores, such as those used in current transformers and tensile stress transducers, also are described in the literature. Of greater economic importance is the potential for use in utility power transformers.

Structural Applications

Some structural elements of missiles, spacecraft, and aircraft are candidates for microcrystalline alloys, primarily because of the improved properties that may be developed in rapidly solidified materials in comparison with conventionally processed alloys. Alternatively, amorphous metal ribbons can provide multiaxial reinforcement in a composite, an improvement over the uniaxial strength offered by existing advanced fibers.

Brazing Alloy Applications

It is possible to produce thin, ductile strip and wire of near eutectic alloys. These materials may be useful for brazing applications.

CONCLUSIONS AND RECOMMENDATIONS

Potential for application of amorphous and microcrystalline alloys has been shown, but considerable development of alloys tailored to the process and to specific applications remains to be done. There is also a need for the development of consolidation techniques to provide greater bulk, particularly in the case of the glassy alloys.

Research and development on consolidation techniques, as well as techniques to increase the rate of solidification, are needed. More work is needed on alloy development: for microcrystalline alloys, for alloys uniquely suited to the production process, to obtain superplastic alloys, and to develop and understand alloys for corrosion-resistant service. While the field is ripe for development, fundamental work is also needed in developing certain phase diagrams, understanding the role of alloying elements, predicting glassy behavior from thermodynamic considerations, and understanding reasons for the limits of stability.

SECTION I

AMORPHOUS MATERIALS

Chapter 2

NATURE OF THE AMORPHOUS STATE

Amorphous materials are those that possess no long-range structural periodicity (i.e., those that are noncrystalline). Although some individuals prefer to reserve the term "glass" for its original meaning (i.e., an amorphous solid produced by cooling the corresponding liquid), the term "glassy" often is used interchangeably with the more general terms "amorphous" and "noncrystalline" and is applied to amorphous solids made by other techniques (e.g., sputtering).

An understanding of many aspects of the amorphous state (e.g., physical properties and processing techniques) depends upon an understanding of two of the fundamental characteristics of amorphous materials, their structure and their thermodynamic state. Each of these will be considered briefly before discussing the way in which nominally identical amorphous materials can differ.*

STRUCTURAL CHARACTERISTICS

The lack of long-range order (i.e., the absence of structural periodicity extending over distances of more than about 3 to 5 atomic or molecular diameters) is most readily evident in the diffraction behavior of amorphous materials. For example, the powder pattern of a crystalline material obtained with an x-ray diffractometer exhibits sharp, well defined maxima ("lines") that are related to the crystal structure by the well known Bragg relation. In contrast, the diffraction pattern (i.e., interference function) from an amorphous material exhibits only broad maxima, a pattern qualitatively similar to that observed for the corresponding liquid.

Diffraction data for amorphous materials provide only statistical information on the atomic structure; unlike the case for a crystal, a unique, fully specified atomic structural unit cannot be determined. Instead, structural information is contained in the radial distribution function (RDF) obtained by a Fourier transformation of the interference function. The RDF is the radial density of atoms averaged over all atom as the origin of the coordinate system. The problem with interpreting the RDF data is that there is no method for reversing the process and determining a one-to-one correlation between the RDF and the structure from which it arose (i.e., significantly different structures may have essentially the same interference functions). Also, slight differences in structures that do not measurably affect the interference function may

*These topics are treated in greater detail in Chapter 1, "Overview of Principles and Applications," by Polk and Giessen in Metallic Glasses (ASM, 1978).

affect specific properties of interest. Within these limitations, a powerful method for investigating the structure of amorphous materials is to produce structural models and compare the calculated diffraction behavior, and other calculated properties, of these models to those that are observed for the actual material. Finally, the fact that the "lines" seen in the diffraction pattern for crystalline material progressively broaden as crystallite size decreases has led to suggestions that the amorphous structure is made up of more highly ordered clusters of atoms of the order of 4-5 Å in diameter. Although this cannot be ruled out at the present time, the weight of the evidence now supports the view that glasses have a "continuous random" atomic structure.

The central problem in structural studies of amorphous materials involves the accurate definition of their short-range order. A full knowledge of the short-range order would specify the distribution about individual atoms of the near neighbors. These near-neighbor data must specify the number of neighbors, their distance, their chemical identity (since most glasses of interest contain more than one element), and the angular correlation between the neighbors. The first three can be derived from RDF measurements, but the last is more complex and, in most cases, its determination may require structural modeling.

Additional information on short-range order can be determined: a) by gathering interference patterns, and thus, RDFs from different radiations where the individual chemical components have different relative scattering power; b) by using a technique such as extended x-ray absorption fine structure (EXAFS) measurements to probe the environment around a single atomic species; or c) by using indirect methods such as Mössbauer spectroscopy to infer information about the local arrangements from other measurements. Additionally, comparative techniques, through which fraction changes upon in-situ annealing are measured, or energy dispersive x-ray diffraction (EDXD), through which anomalous dispersion can be used to obtain partial structure factors, can provide further detailed information. These structural characterization techniques will be discussed in greater detail below.

THERMODYNAMIC CHARACTERISTICS

A glass is a nonequilibrium state of matter; it is metastable with regard to alternative crystalline phases and generally is unstable relative to other lower energy glassy structures. Annealing can, therefore, lead to structural changes by crystallization, and hence, to property changes by "relaxation."

The thermodynamic nature of the glassy state can be understood by considering the process of cooling a liquid to a glass. Assuming that crystallization does not occur, a metastable liquid-like structure (which remains in internal equilibrium) is retained as the liquid is cooled below the equilibrium melting temperature. As further cooling

occurs, the relaxation time of this structure (i.e., the time required for the structure to change its atomic configurations to those characteristic of a slightly different temperature) increases and eventually a point is reached at which the relaxation time is greater than the time interval allowed by the cooling rate. Internal equilibrium is no longer achieved with further cooling, but rather the structure characteristic of the higher temperature is frozen in. Thus, the glass has a characteristic fictive temperature, the temperature at which the equilibrium structure best approximates that of the glass. In most cases, the specific heat of the undercooled liquid is greater than that of the glass, and a relatively sudden change in the specific heat is seen when the system leaves equilibrium, the glass transition. The fictive temperature of the glass (i.e., the temperature at which the glass transition occurs) depends, of course, on the cooling rate. The atomic mobilities in the glass are very low (i.e., well below the glass transition temperature) and no further structural changes occur.

The process competing with glass formation upon continued cooling of the liquid is, of course, crystallization. This first-order transformation is governed by both thermodynamic and kinetic factors; the crystallization rate can thus be expressed by temperature-time-transformation (TTT) diagrams. This subject will be discussed later, but one must note at this point that the cooling rate, and hence, the attainable fictive temperatures are limited by the competing crystallization process. For example, one might wish to form a glass with a very low cooling rate in order to minimize the fictive temperature and the relaxation effects that occur later, but the alternative of crystallization always imposes a minimum cooling rate for glass formation.

Further, the nonequilibrium nature of the amorphous state means that, in many cases, it can be achieved only by very specialized processes that produce high cooling rates in metallic systems. In addition, the time-temperature profile during preparation can differ so that amorphous materials of the same composition often have different properties.

DIFFERENCES BETWEEN AMORPHOUS MATERIALS OF THE SAME COMPOSITION

A major problem in the study of an amorphous material of a given composition is that its structure, and thus, some of its properties can vary in subtle ways from sample to sample and for the same sample as a function of time. This is enhanced by the nonequilibrium nature of the material, and studies are hampered by the fact that much structural information for these materials is statistical in nature. These differences can come about during preparation (e.g., by different, generally unknown time-temperature relations during the cooling of the liquid or the taking up of gaseous impurities) or can be due to subsequent treatments (e.g., mechanical deformation, thermal annealing, or irradiation). The differences that can exist between nominally

identical glasses are reviewed below. In most cases, a careful analysis of the sample(s) using an appropriate technique (e.g., transmission electron microscopy) may permit identification of differences; however, in other cases, the amorphous nature of the sample should be characterized by x-ray diffraction, Mössbauer measurements, RDF's, magnetic properties, etc.

Partial Crystallinity

When attempting to prepare an amorphous material, whether by cooling of the liquid or by a deposition process, it is possible that a two-phase material, a mixture of an amorphous phase with a crystalline phase or a mixture of two glassy phases, will be obtained instead. If only a small percentage of the material is crystalline, it may not be detected by x-ray diffraction examination as generally practiced; this is especially true if the crystal phase has a complex structure, if the crystallite sizes are small, etc. Similarly, the very beginning of crystallization upon thermal annealing of the glass also will not be readily detectable by such examination.

Gaseous Impurities

The processing techniques used to produce an amorphous alloy can result in the contamination of the final product with a wide range of gaseous elements that are homogeneously dispersed throughout the structure. This is of special importance in the case of metallic glasses (e.g., oxygen can be picked up during the initial alloy preparation or during the rapid liquid quenching process, hydrogen may be incorporated into samples made by electrodeposition, and argon may be incorporated into samples made by atomization or sputtering). Such contaminants may have a major effect on the stability of the amorphous phase, both in terms of formation of the glass and in terms of its subsequent crystallization upon annealing.

Impurity Particles

A glass may have embedded in it particles of a composition very different from that of the matrix. In systems where the oxygen solubility in the liquid is low, these may be oxide particles initially present in the liquid; alternatively, an element present at very low levels may have combined with a second element to produce a solid dispersion in the liquid at the temperature from which the liquid is cooled. In other cases, gaseous impurities dissolved in the glass may precipitate upon annealing for time-temperature conditions not sufficient to begin the crystallization of the matrix.

Internal Stresses

The processes used to form the amorphous phase may result in a material having macroscopic internal stresses. This can occur, for example, because of the temperature gradients present during the sputtering process or in a sample being subjected to rapid liquid quenching. Such stresses can lead to variations in magnetic behavior (via magnetostrictive interactions) or mechanical behavior. "Annealing" can be used to remove such effects.

Mechanically Deformed Material

At temperatures well below the glass transition temperature, many glasses will deform plastically in a nonhomogeneous manner upon the imposition of an appropriately applied force at a slow rate of strain. Although there is no evidence of the existence of line defects (analagous to dislocations in crystals) after deformation ends, it is clear that, at least in the case of metallic glasses, the regions which have undergone deformation differ from the original matrix material. Plastic deformation can introduce internal stresses into the sample. It is agreed that there is no cold work response in terms of work hardening, but the high elastic limit and localized deformation characteristic of these materials can lead to internal stresses. This occurs, for example, when a shear band moves only part way through the substance.

Compositional Segregation

Glasses are potentially more compositionally homogeneous than crystals; for crystalline alloys, two-phase fields are more common, and grain boundary segregation is usual. As noted above, impurity precipitants also can occur in a glass. Further, phase separation where both phases are amorphous can occur and is especially important for silicate glasses. Segregation of one of the components in the glass to the surface of impurity particles within the glass also may occur and affect the properties.

Glasses Formed by Different Methods

It is known that metallic glasses formed by different techniques (e.g., rapid liquid quenching and sputtering) can have different properties although the interference functions appear similar; the ductility of metallic glasses is an example of such a property. It is not yet known whether the difference is due to subtle differences in the structure (e.g., the amount and distribution of free volume) or to extrinsic differences (e.g., different impurity content or internal stresses).

Pair Ordering

In a glass of more than one component, it is possible that the relative number of A-B near-neighbor pairs can vary as a function of preparation process or annealing treatments. Further, the short-range order may not be spatially isotropic; a preferred direction can be related to heat flow during preparation, deposition direction, or applied magnetic fields. Very small differences in pair distribution can have a major effect on magnetic properties; this is a further complication since it imposes another requirement on the already difficult task of fully defining the short-range order.

Relaxation Effects

The discussion, begun above, of the variability of structure related to changes of the fictive temperature must now be continued. This is, in many respects, the most fundamental difference between glasses of the same composition and would appear to be the one most difficult to characterize. Further, annealing well below the glass transition temperature may cause relaxation to a lower energy glass structure that is different from that obtained by cooling at a lower rate. In either case, it is clear that the lower energy state will be slightly more dense. Although glasses of different fictive temperature must have a different structure, the local rearrangements leading to these changes cannot be uniquely determined even when differences in RDF's can be demonstrated by careful comparative measurements. One problem in a study of the results of changes in the fictive temperature involves separating these effects from those caused by other mechanisms (e.g., the beginning of crystallization).

OTHER STRUCTURAL CHARACTERISTICS

In addition to direct calculation of the RDF from diffraction data, other experimental techniques can provide information on the amorphous structure.

Extended x-ray absorption fine structure (EXAFS) measurements provide radial density data for the atomic distributions around a given atomic species (i.e., RDF data where only one kind of atom serves as the origin) (Pampillo, 1975). This is especially useful in determining the surroundings for elements that are a minor component of the alloy and/or have low relative scattering power. In addition, it may be useful in investigating small variations (e.g., between the environments and dynamical interactions of Ni and of Fe atoms in an alloy containing both) or the changes in an amorphous material caused by annealing insufficient to produce observable crystallization. However, there are still uncertainties involved in the interpretation of EXAFS results; these primarily are associated with uncertainty concerning the

phase shifts and the evaluation of the amorphous data based on crystalline reference materials.

Energy dispersive x-ray diffraction (EDXD) measurements have been used to investigate the small changes in $I(k)$, and thus, the RDF caused by annealing (Pampillo and Polk, 1974). Small changes can be accurately characterized since effects from fluctuations of the intensity of the x-ray source are eliminated. White incident radiation is used, and the diffracted intensity is recorded at a fixed angle as a function of energy with all of the energy channels counted in parallel. Further, the annealing can be done in place, and since no movement is involved, optical misalignment is eliminated.

Information on partial RDFs also can be obtained using only one radiation by carrying out an isomorphic substitution of one element for another in amorphous alloys. An example of this approach is the comparison of *Hf-Cu and Zr-Cu metallic* glasses (Masumoto and Maddin, 1975).

Standard small-angle scattering measurements also have proven to be valuable for structural characterization. Rather than giving information on the atomic structure (e.g., short-range order), such data can be interpreted to characterize the larger scale inhomogeneities that sometimes occur in amorphous materials. As discussed below, this technique can be useful in differentiating between amorphous metals that exhibit very similar large-angle diffraction behavior.

The density of an amorphous material obviously is directly dependent on its structure. Thus, measured densities provide a ready additional test for structural models.

Standard transmission electron microscopy (TEM) has provided little direct information on the atomic structure of amorphous metals. High-resolution dark field micrographs generally exhibit graininess with characteristic dimensions of 5 to 15 Å; however, it is not clear whether such contrast is due to coherently scattering domains (Chen and Wang, 1970) or is an instrumental artifact. TEM studies are expected to be of value in the study of the inhomogeneities having larger characteristic domains (e.g., voids and phase separation) that are discussed below.

The newly available scanning transmission electron microscope (STEM) may be more useful than TEM in structural studies of amorphous metals because of its high resolution. In addition, the ability to do chemical analysis using x-ray emission on volumes about 0.05 μm in diameter will be useful in studying compositional segregation, precipitation, and impurities.

Atom probe microanalysis also may be of use in the study of compositional segregation in amorphous metals; this technique is believed

to offer spatial resolution superior to that of the STEM. The atom probe consists of a time-of-flight mass spectrometer system combined with a field ion microscope, allowing one to both "see" and identify the individual atoms on a metal's surface. Controlled sectioning of the specimen, using "field evaporation," permits the quantitative determination of chemical composition at the nanometer level.

STRUCTURAL MODELS

Since all details of the structure of an amorphous material cannot be determined experimentally, investigations have attempted to infer these details by comparing experimental data to the corresponding data calculated from models. Clearly, good structural models are necessary in order to calculate the physical properties of the amorphous metals, and thus, gain a predictive capability.

A wide range of models has been considered for amorphous metals. These can be grouped into three categories: microcrystalline, continuous random, and noncrystallographic cluster models.

Microcrystalline models assume the existence of highly ordered regions (i.e., microcrystals of $\sim$10 Å diameter) having atomic configurations identical to those of an ordinary three-dimensional crystal. Generally, the microcrystals are proposed to be assembled without orientational correlations; although about one-half of the atoms are on the surface of the microcrystal for such small grain sizes, the details of atomic configurations at the microcrystalline boundaries are not given.

Continuous random models are based on Zachariasen's concepts, which have been widely accepted for silicate glasses. Noncrystallographic, dense, randomly packed configurations of hard spheres (DRPHS) (Bernal, 1959) have been produced both physically and with computer algorithms. An important difference from the microcrystalline structures is that the DRPHS structure is statistically homogeneous and does not contain the internal boundary regions intrinsic to microcrystalline models.

Noncrystallographic cluster models are similar to microcrystalline models except that they are based on clusters that cannot be the basis of an extended three-dimensional crystal. These noncrystallographic clusters often contain a fivefold rotational axis.

Whichever model is considered, a relaxation of the model structure is necessary if the model is to accurately reflect the behavior of a true alloy. The hard sphere interatomic potential generally used to generate DRPHS structures clearly is unrealistic for metals; similarly, the idealized atomic arrangements of the crystal-like or noncrystallographic clusters would be distorted once these clusters of atoms were assembled to a dense solid. Relaxation is achieved by assigning an interatomic potential to the atoms and following an interactive process involving small

changes in the atomic positions so as to minimize the energy of the structure.

Presently, no model can be considered to be an exact representation of the amorphous structure; however, it appears that the continuous random models or, the noncrystalline cluster models, can account for experimental observations better than can the microcrystalline models. The DRPHS models have been the most extensively developed (e.g., they have been extended to large numbers of atoms and subjected to relaxation), and thus, will be referred to below in discussions of the possible differences between amorphous materials of the same composition.

Additional experimental work directed towards the measurement of RDFs and the evaluation of structural models would be highly desirable. Only high-quality RDFs are likely to advance present understanding of amorphous structures, but obtaining high-quality RDF's is made difficult because I(k) is not available for all values of k and because there are several other experimental and computational problems (Chen and Wang, 1970). Similarly, only critical studies of structural models that are large enough to be considered free of surface effects, that have fully defined atomic coordinates, and that are not unstable to atomic rearrangements when subjected to reasonable interatomic potentials, are likely to be useful.

STRUCTURAL VARIATIONS

One of the problems often encountered in the study of amorphous metals is that the properties, especially magnetic and mechanical behavior, can vary significantly for samples of identical composition and nominally identical RDFs. This is due to the fact that the RDF is relatively insensitive to small structural changes and is not typically determined accurately enough to indicate these small changes when two RDFs are compared. The structural differences that can be expected to occur can be divided into two categories: those that are relatively homogeneous throughout the material and those that are, by definition, inhomogeneous.

HOMOGENEOUS VARIABILITY

In addition to being metastable, amorphous alloys generally are in a quasi-equilibrium state (i.e., the structure is unstable relative to other amorphous structures of lower energy). This can readily be understood as the possible variation in the fictive temperature of a glass, where the fictive temperature is the temperature at which the topology of the amorphous structure in metastable equilibrium best approximates that which exists in the low-temperature glass.

Briefly, as the liquid is cooled at a given rate, it eventually reaches a temperature at which the rearrangements necessary to maintain the equilibrium structure can no longer occur in the time available; the structure at that point, the glass transition, is then "frozen in," and this becomes the fictive temperature of the glass. This structure of a given fictive temperature thus has a given topology and, at any specified lower temperature, a given internal energy, specific volume, compositional ordering, etc. However, changes in the structure can occur at much lower temperatures when sufficiently long times are available (i.e., structural annealing can occur wherein the structure "relaxes" to one of lower internal energy). These changes may or may not be exactly equivalent to the structural differences that would occur by decreasing the cooling rate to obtain a glass of lower fictive temperature. In any case, the relaxed glass is expected to have a different topology, and thus, slightly different short-range order; this will be reflected in changes in the packing density and/or in the compositional ordering in the glass.

Such variability in the short-range order can be understood readily by considering features of DRPHS structures. Even for one sphere size, such structures can exist with a range of packing densities, presumably related to the variability of the interstitial hole distribution which can exist from structure to structure. Using different construction procedures can result in slightly different RDFs as well. Consideration of two or more components introduces the obvious variable of compositional ordering; the number of like versus unlike near-neighbors can vary between the extremes for complete randomness or maximum ordering.

These subtle differences are difficult to document, but they can affect properties dependent on the short-range order and therefore become important. High-precision measurements of the short-range order in metallic glasses is an area of research requiring more work. Although many annealing effects are seen in metallic glasses, it often is not clear whether they are due to the relaxation discussed above or to the development of inhomogeneities such as those discussed below.

INHOMOGENEOUS VARABILITY

The idealized amorphous material generally is thought of as isotropic and compositionally uniform, but a wide variety of structural and compositional inhomogeneities have been shown to occur in real amorphous materials. Compositional segregation is known to occur in amorphous solids. When the segregation involves two amorphous phases of different composition that co-exist with each other, it is labelled phase separation. Alternatively, segregation can occur as the very first stage of crystallization although the overall material still appears amorphous to standard diffraction examinations. Segregation also can

occur at surfaces, either at free surfaces or at the surface of included particles (e.g., oxides). Small-angle scattering and transmission electron microscopy are especially useful for studies of such segregation.

Well defined structural defects such as cracks or voids also occur in amorphous materials. Voids are most likely to be formed in materials made from vapor (i.e., by thermal evaporation or sputtering); large numbers of cracks also are most commonly found in materials made by deposition techniques, especially electrodeposition. Again, small-angle spectroscopy and TEM studies, as well as optical microscopy to identify cracks, are the most direct ways of monitoring these effects.

Because of the preparation techniques that must be used in the production of amorphous metals, these materials may contain significant levels of gaseous contaminants. Oxygen, hydrogen, and/or nitrogen can be picked up readily from the gaseous atmosphere or crucible when samples are made by rapid liquid quenching. Hydrogen often is incorporated in amorphous films made by electrodeposition. Materials made by thermal evaporation often contain large amounts of oxygen. Sputtered films can contain significant amounts of the sputtering gas. These gases, especially oxygen, can segregate to form well defined impurity particles embedded in an amorphous matrix.

Fully amorphous, compositionally uniform materials also may be nonisotropic, generally due to details of the preparation technique. This is especially likely for materials made by deposition techniques; the structure in the growth direction can be different than that in a perpendicular direction. This means that the atomic density function need not be spherically symmetric; the variation can be due to topological and/or compositional variation. There also can be a compositional gradient in the growth direction since the composition of the alloy is generally a sensitive function of the deposition parameters that may not be controlled sufficiently well to prevent such fluctuations.

Amorphous materials also can vary because of mechanical effects. Internal stresses can be introduced during material preparation for both liquid quenched and deposited materials. In addition, amorphous metals deform plastically well below the glass transition temperature along planar shear bands (i.e., nonhomogeneously); although there is no evidence for the presence of discrete dislocations following deformation, it has been shown that the material in the shear bands behaves differently from the undeformed matrix (Pampillo, 1972).

Finally, the amorphous material may be partly crystalline. If the crystals have a proper combination of small size and complex structure and are present in small amounts, they will not be readily observable in macroscopic diffraction examinations.

Nonreproducibility and instability of properties are two of the factors limiting the applications of amorphous metals at this time.

Both types of property variation must be related to variations in the short-range atomic structure or the macrostructure. Clearly, then, an increased effort to characterize accurately the structural variations that exist and to correlate these with property variations should receive increased attention.

REFERENCES

Chen, H.S., and T.T. Wang. 1970. J. Appl. Phys., Vol. 41, p. 5338.

Masumoto, T., and R. Maddin. 1975. Mater. Sci. Eng., Vol. 19, p. 1-24.

Pampillo, C.A. 1972. Scripta Met., Vol. 6, p. 915.

Pampillo, C.A. 1975. J. Mat. Sci., Vol. 10, p. 1194.

Pampillo, C.A., and D.E. Polk. 1974. Acta Met., Vol. 22, p. 741.

Chapter 3

THERMODYNAMICS AND KINETICS

THERMAL STABILITY OF AMORPHOUS ALLOYS

Three types of change occur when amorphous alloys are heated: high-temperature thermal exposures result in crystallization and relatively low-temperature exposures cause structural relaxations without causing crystallization. These structural relaxations are seen as broad exothermic peaks in differential scanning calorimetry (DSC) and often are accompanied by changes in mechanical and magnetic properties. Low-temperature exposures in the presence of a magnetic field result in magnetic reorientation of the easy axis in the amorphous ferromagnetic alloys. The low-temperature effects or the higher temperature crystallization process may be the limiting factors in controlling the life of the amorphous alloy in a particular application.

Crystallization

The formation and resultant stability of amorphous alloys are important topics both theoretically and technologically. The theoretical analysis of the factors controlling the ease of formation and the stability of the resultant amorphous alloys have been discussed in many reviews [e.g., in the extensive general review by Jones (1973), from the thermodynamic viewpoint by Turnbull (1974), and, most recently, by Takayama (1976)]. The ability of an alloy to be quenched into the glassy state generally is measured by the magnitude of the quantity:

$$\Delta T_g = T_m - T_g, \tag{1}$$

where T_m and T_g are the melting and glass temperatures, respectively. In a similar manner, the stability of the glass after formation generally is measured by the magnitude of the quantity:

$$\Delta T_x = T_x - T_g, \tag{2}$$

where T_x is the temperature for the onset of crystallization. As the temperature decreases from T_m, the rate of crystallization increases rapidly but then falls rapidly as the temperature decreases below T_g. Thus, if one quenches a molten alloy rapidly enough to a temperature below T_g, a quasi-equilibrium amorphous phase is obtained. Note that there is no direct relation between the ease of formation and the resultant stability of an amorphous alloy. It has been noted that the composition most favorable for glass formation is near a deep eutectic; the deeper the eutectic, the

better is the glass-forming ability. At such a point, the liquid is particularly stable against crystallization.

There have been three approaches to explaining the stability of the glass (i.e., its resistance to crystallization). The first is based on Bernal's model of randomly packed hard spheres as developed by Cargill (1970), Bennet, et al. (1971), Polk (1972), and Turnbull (1974). In this model, the metal atoms are assumed to form a random network of close packed hard spheres and the smaller metalloid atoms fill the holes inherent in such a structure. The most stable configuration occurs when all the holes are filled, corresponding to about 20 percent. This is near the eutectic composition of many of the alloys and is in the range of the stable glass compositions. Although this simple geometrical model has been successful in accounting for the observed glass-forming ability of many metallic alloys, it would be surprising if only the atomic radii were important.

The second approach to understanding glass stability is discussed by Chen (1974). He considered the effects of atomic sizes and interatomic interactions (i.e., chemical bonding) and suggested that chemical bonds are the dominating factor in glass formation and stability.

The third approach was suggested by Nagel and Tauc (1976) and is based on the role of the electron gas. They showed that under certain circumstances a nearly free electron gas will produce a barrier against crystallization.

Luborsky (1977) has clearly shown that the end-of-life as far as magnetic applications are concerned corresponds to the onset of crystallization. At the onset of crystallization, the coercive force and losses increase and the remanence and permeability decrease, all at a very rapid rate for a small increase in temperature. The available information on the time-temperature behavior for the onset of crystallization in amorphous alloys containing transition metals is summarized in Figure 1. The results were obtained by transmission electron microscopy and diffraction studies for alloys of FePC, CoSiB, and NiSiB. Calorimetric studies were used for NiP, NiPBAl, and FeCoPBAl alloys. Both calorimetric and magnetic tests were used to obtain the crystallization results on FeB, FeNiB, and FeNiPB. It is of interest to note that some of the time-temperature curves are discontinuous (e.g., the curves for CoSiB, NiSiB, and FePC). These discontinuities are the result of the formation of different phases. At temperatures below the break, a single metastable crystalline phase forms while at temperatures above the break, small metastable crystals form in the amorphous phase. It is therefore apparent that extrapolation of high-temperature results to lower temperatures may be very misleading.

The results in Figure 1 are close to straight lines represented by an Arrhenius relation for the time for the onset of crystallization:

$$t_x = T_{o,x} \exp(\Delta E_x/kT). \qquad (3)$$

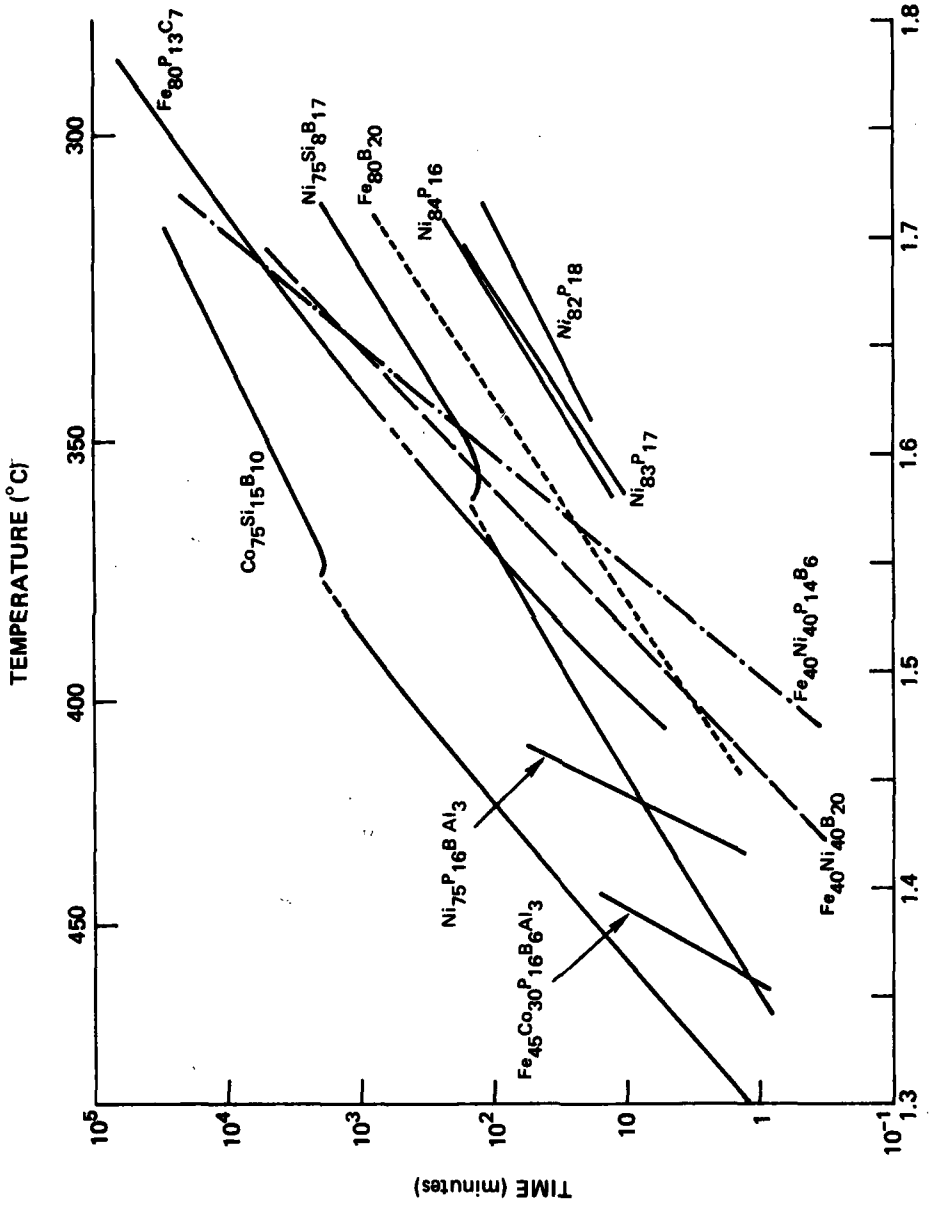

FIGURE 1 Time for the start of crystallization as a function of temperature. FePC from Masumoto and Maddin (1975) and Masumoto, et al. (1976); CoSiB, NiSiB from Masumoto, et al. (1976); NiP from Clements and Cantor (1976); NiPBAl, FeCoPBAl from Coleman (1976); FeB, FeNiB, FeNiPB from Luborsky (1977).

These incubation times are a common feature of phase transformations. They may be considered to be the time required for a population of nuclei characteristic of the annealing temperature to be achieved. The existence of an incubation time implies that no nuclei of suitable size exist in the as-quenched glass. Davies, et al. (1974) applied this approach to the interpretation of the formation and stability of some glasses, and Davies (1976) recently reviewed this subject. It can be readily shown that Equation 3 can be derived from transformation theory where ΔE_x is the activation energy for viscous flow. Other terms have been omitted because they have an insignificant temperature dependence in this region of temperature.

Luborsky (1977) showed that the activation energies for the onset of crystallization, ΔE_x, obtained from the slopes of the lines in Figure 1 correlate well with the values of ΔT_x for the stability of amorphous alloys as given by Equation 2 and as obtained from scanning calorimetry. The values of ΔE_x also appear to correlate well with the number of atomic species in the alloy; the more complex the alloy, the greater is ΔE_x. Some results are shown in Table 1. Similar correlations between thermal stability as measured by ΔT_x and ΔE_x were discussed experimentally and theoretically by Chen (1976) who used the time of transformation to the peak in the exotherm rather than to the start of the exotherm to obtain ΔE_x. The effect of this difference in measurement on ΔE_x appears to be negligible for all alloys studied.

The effect of alloying elements on the crystallization temperature has been studied by Naka, et al. (1974) in the $Fe_{80-x}M_xP_{13}C_7$ alloy series by Luborsky (1977) in the $Fe_{80-x}Ni_xP_{14}B_6$ and $Fe_{80-x}Ni_xB_{20}$ alloys. Calorimetric measurements were made at a heating rate of 5 deg/min and 40 deg/min, respectively, to determine T_x, the temperature for the beginning of the crystallization exotherm. Although the use of a constant rate of heating will give interesting correlations, the results cannot be extrapolated to other temperatures of interest and do not necessarily correlate with isothermal results as seen by comparing the 2-hour anneal results for the FeNiPB alloys with the scanning results in Figure 2; the trends are in opposite directions. Naka, et al. (1974) concluded that the atomic size of the alloying elements had little or no effect on T_x, that the electronegativity also had little or no effect, but that the relative valency did seem to correlate with the trends in T_x. Their results concerning T_x as a function of average outer electron concentration show this correlation, taking for the number of outer electrons for Ti, V, Cr, Mn, Fe, Co, and Ni, 4 through 10 respectively. Thus, they concluded that the crystallization temperature is predominantly governed by the nature and strength of the bonding of the atoms in these alloys.

Structural Relaxation

Irreversible structural changes are observed at times and temperatures well below those necessary to initiate crystallization, and both magnetic and mechanical properties can be drastically altered.

TABLE 1 Activation Energy for Crystallization of Various Amorphous Alloys

Alloy	ΔE eV[x]	T_g, °C	T_x-T_g, °C	Reference
$Ni_{75}P_{16}B_6Al_3$	6.5	417	10[c]	Coleman, 1976
	6.7[a]			
$Fe_{45}Co_{30}P_{16}B_6Al_3$	5.5	456	16	Coleman, 1976
$Fe_{75}P_{16}B_6Al_3$	4.8[a]	477	-50[c]	Chen, 1976
$Fe_{79}P_{13}C_7Ti_{0.5}Cr_{0.5}$	4.5			Scott and Ramachardrarao, 1977
$Fe_{29}Ni_{44}P_{14}B_6Si_2$	4.4			Scott, 1978
	4.0			Scott, 1978
$Fe_{40}Ni_{40}P_{14}B_6$	3.9	405	9	Luborsky, 1977
$Co_{75}P_{16}B_6Al_3$	3.2[a]	487	-87[c]	Chen, 1976
$Fe_{80}P_{13}C_7$	3.1	–	–	Masumoto et al., 1976
	2.4[b]			Masumoto and Maddin, 1975
$Fe_{40}Ni_{40}B_{20}$	3.0	442	9	Luborsky, 1977
$Co_{75}Si_{15}B_{10}$	2.8	–	–	Masumoto et al., 1976
	1.6[b]			
$Fe_{80}B_{20}$	2.1	441	7	Luborsky, 1977
$Ni_{75}Si_8B_{17}$	2.0	–	–	Masumoto et al., 1976
	2.0[b]			
$Ni_{83}P_{17}$	2.0	–	–	Clements and Cantor, 1976
$Ni_{84}P_{16}$	1.9	–	–	Clements and Cantor, 1976
$Ni_{82}P_{18}$	1.6	–	–	Clements and Cantor, 1976

NOTE: From Luborsky, 1977.
[a]Evaluated from time to reach peak in crystallization exotherm.
[b]The low temperature activation energy. T_x from DSC at 40 deg/min.
[c]T_x from DSC at 20 deg/min by extrapolation.

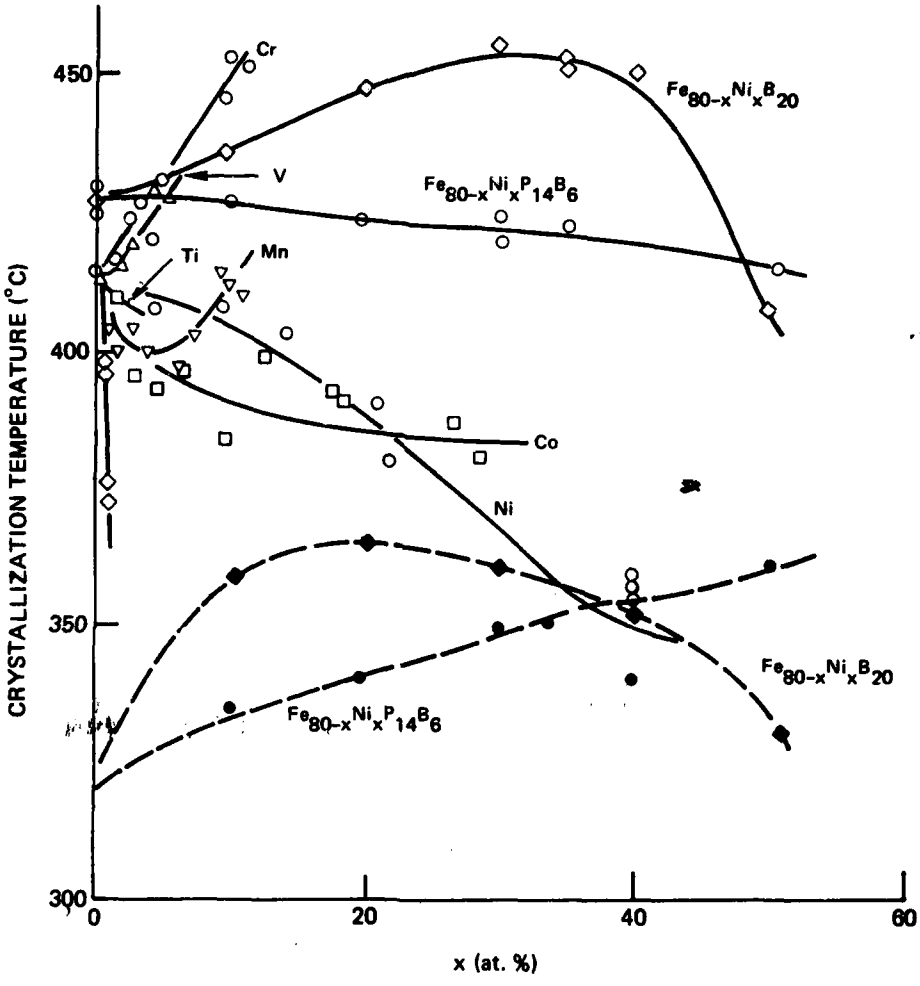

FIGURE 2 Temperatures for the start of crystallization. For $Fe_{80-x}M_xP_{13}C_7$ alloys from Naka, et al. (1974) using a 5°C/min heating rate, open symbols. For $Fe_{80-x}Ni_xP_{14}B_6$ ● and $Fe_{80-x}Ni_xB_{20}$ ◆ from Luborsky (1977) at a 40°C/min heating rate and dashed lines for two hour anneals.

Heating as-cast samples results in two broad peaks in differential scanning calorimetry indicating two different modes of rearrangement as discussed by Chen and Coleman (1976). These structural changes produce a small change in Curie temperature without a significant change in saturation moment. This change in T_c after structural relaxation is mostly the result of the change in the interatomic distances but also may be affected by the change in average coordination number. An additional and major change that is associated with the relaxation of internal strain was first noted by Luborsky, et al. (1975). By minimizing the internal strains, the strain-magnetostriction interaction and the resultant anisotropy are minimized, leading to a reduction in coercive force and losses and an increase in permeability and loop squareness. This stress-relaxation occurs at temperatures below T_x in most alloys of interest.

Structural Results

Diffraction results are the principal source of information on the atomic arrangements in amorphous alloys. It is now clear that the DRPHS model qualitatively accounts for the major features in the radial distribution functions. However, recent results concerning the partial interference functions associated with individual atomic pairs are not in complete agreement with the calculations of the DRPHS model as discussed recently by Cargill (1976).

The annealing of amorphous structures reported by Waseda and Masumoto (to be published) indicates that detectable changes occur in the atomic structure in amorphous $Fe_{80}P_{13}C_7$ before any indication of crystallization is detected by transmission electron microscopy or by appearance of crystalline features in x-ray interference functions. The first two maxima in I(k) become slightly higher after anneals at 300°C for varying times. The magnitude of oscillations at larger k values also appears to increase. Luborsky, et al. (1976), on the other hand, reported no detectable change in the diffuse x-ray scattering pattern from amorphous $Fe_{40}Ni_{40}P_{14}B_6$ after both cold rolling and annealing to temperatures just below detectable crystallization.

Small-angle x-ray scattering provides results related to compositional homogeneity. Luborsky, et al. (1976) reports that cold rolling the $Fe_{40}Ni_{40}P_{14}B_6$ alloy reduces the intensity of the small-angle scattering, interpreted as improving the homogeneity, while annealing increased the small-angle scattering, which suggested the possibility of phase separation. A more detailed analysis of these results by Walter, et al. (1977) indicated that the scattering regions in the as-cast material are ∿32Å in diameter and ∿250Å apart and constitute about 1 percent of the volume of the sample. Their size is not changed by annealing but their number increases. These changes appear to have no direct effect on magnetic properties. Cold rolling produced a completely flat I(k) versus k curve indicating no inhomogeneities were present, but subsequent annealing again developed scattering regions. The rolling also produced very large increases in coercivity

and decreases in remanence. Subsequent annealing returned these parameters to values representative of annealed specimens that had not been rolled. Small-angle x-ray scattering also has been used to characterize the inhomogeneities in Co-P. Chin and Cargill (1976) have interpreted their results as showing that this electroless deposit contained anisotropic inhomogeneities—$\sim$100-300 Å (10-30mμ) in the film plane and $\gtrsim$2000 Å (200mμ) normal to the film plane. It is believed that these regions influence the magnetic properties. After annealing, these inhomogeneities decreased in size in contrast to the results on the melt-quenched $Fe_{40}Ni_{40}P_{14}B_6$.

Most amorphous ferromagnetic materials have non-zero magnetostriction, λ. Internal strains, σ, that may be uniform or nonuniform, arise from the original solidification or from subsequent fabrication. These strains couple with λ to produce an anisotropy, k_λ. Uniform strains often are induced in evaporated, sputtered or electrodeposited films due to the differential thermal expansion between the film and the substrate. The magnitude of λ and the direction and magnitude of σ then will determine the direction and magnitude of k_λ. An important example of nonuniform strains is observed in drum-quenched alloys of the $(TM)_{80}(P,B,Al...)_{20}$ type. The nonuniform strains develop during the preparation of the ribbon and result in a periodic fluctuation in the perpendicular component of anisotropy along the length of the tape. Thermal annealing removes the internal strains causing the anisotropy to disappear. The domain structure and its disappearance after annealing reflect this perpendicular k_λ and its removal. This has been discussed by Becker (1976) and Fujimori, et al. (1976). There is also excellent experimental evidence for pair and stress induced magnetic anisotropies in evaporated rare-earth transition metal alloys.

Directional Order Relaxation

In contrast to the irreversibility of the crystallization and structural relaxation effects, directional ordering is a reversible process. Directional ordering, produced by annealing in either a magnetic field or a mechanically stressed condition, results in a magnetic anisotropy that can markedly influence the magnetic properties of the amorphous alloy. The relaxation or reorientation of this anisotropy occur at quite low temperatures in some amorphous alloys (e.g., under the influence of its own self-demagnetizing field, externally applied field, or stressed condition). The rate at which this occurs may limit the usefulness of some of the alloys in applications where the initial ordering direction is different from the resultant magnetic or stress fields encountered during use. This directional order may arise from Fe-Fe and Ni-Ni pair ordering and from metalloid-netal ordering, both similar to that found in conventional crystalline alloys or to a single atom anisotropy. This ordering again emphasizes the fact that these amorphous alloys are far from being homogeneous structureless arrays of atoms.

REFERENCES

Becker, J.J. 1976. AIP Conf. Proc., No. 29, p. 204.

Bennett, C.H., et al. 1971. Acta Met., Vol. 10, p. 1295.

Cargill, G.S., III. 1970. J. Appl. Phy., Vol. 41, p. 2248.

Cargill, G.S., III. 1976. In Proc. Second Int. Conf. on Rapidly Quenched Metals, p. 293. Edited by N.J. Grant and B.C. Giessen. MIT Press, Cambridge, Ma.

Chen, H.S. 1974. Acta Met., Vol. 22, p. 1505.

Chen, H.S. 1976. Appl. Phys. Lett., Vol. 29, p. 12.

Chen, H.S., and E. Coleman. 1976. Appl. Phys. Lett., Vol. 28, p. 245.

Chin, G.C., and G.S. Cargill, III. 1976. Mat. Sci. Eng., Vol. 28, p. 155.

Clements, W.G., and B. Cantor. 1976. In Proc. Second Int. Conf. on Rapidly Quenched Metals, p. 267. Edited by N.J. Grant and B.C. Giessen. MIT Press, Cambridge, Ma.

Coleman, E. 1976. Mat. Sci. Eng., Vol. 23, p. 161.

Davies, H.A. 1976. Phys. Chem. Glasses, Vol. 17, p. 159.

Davies, H.A., et al. 1974. Scripta Met., Vol. 8, p. 1179.

Fujimori, H., et al., 1976. Sci. Repts. Res. Inst. (Tohoku Univ.), Vol. A-26, p. 36.

Jones, H. 1973. Rep. Prog. Phys., Vol. 36, p. 1425.

Luborsky, F.E. 1977. Mat. Sci. Eng., Vol. 28, p. 139 and in Amorphous Magnetism, Vol. 2, pp. 345-68. Edited by R.A. Levy and R. Hasegowa. Plenum Press, N.Y.

Luborsky, F.E., et al. 1975. IEEE Trans. Magnetics, Vol. 11, p. 1644.

Luborsky, F.E., et al. 1976. IEEE Trans. Magnetics, Vol. 12, p. 936.

Masumoto, T., and R. Maddin. 1975. Mater. Sci. Eng., Vol. 19, pp. 1-24.

Masumoto, T., et al. 1976. Sci. Repts. Res. Inst. (Tohoku Univ.), Vol. A-26, p. 26.

Nagel, S.R., and J. Tauc. 1976. In Proc. Second Int. Conf. on Rapidly Quenched Metals, p. 337. Edited by N.J. Grant and B.C. Giessen. MIT Press, Cambridge, Ma.

Naka, A., et al. 1974. J. Japan. Inst. Met., Vol. 38, p. 835.

Polk, D.E. 1972. Acta Met., Vol. 20, p. 485.

Scott, M.G. 1978. J. Mat. Sci., Vol. 13, p. 291.

Scott, M.G., and P. Ramachandrarao. 1977. Mat. Sci. & Eng., Vol. 29, p. 137.

Takayama, S. 1976. J. Mat. Sci., Vol. 11, p. 164.

Turnbull, D. 1974. J. de Physique, Vol. 35, p. C4-1.

Walter, J.L., et al. 1977. Mater. Sci. Eng., Vol. 29, p. 161.

Chapter 4

HEAT FLOW LIMITATIONS IN RAPID SOLIDIFICATION PROCESSING

The term "rapid solidification processing" (RSP) is equally applicable to the formation of both crystalline and noncrystalline solid phases by quenching of a material from an initial liquid state. During RSP, the cooling rate in the liquid prior to solidification affects nucleation (undercooling) and growth phenomena in important ways; it influences undercooling in crystalline solidification and is an overriding factor in the formation of noncrystalline structures. On the other hand, the fineness of a crystalline microstructure (e.g., segregate spacing, size of second phase particles) usually can be correlated to average cooling rate during solidification or time available for coarsening. Thus, a clear distinction must be made between cooling rates in the liquid (or during noncrystalline solidification) and during crystalline solidification; the latter is significantly lower at equivalent rates of external heat extraction due to the heat of fusion.

Some general relationships between cooling rates during crystalline and noncrystalline solidification and process variables in different RSP techniques are discussed below. Calculations are presented to show the heat-flow characteristics and limitations in the general areas of RSP: atomization and solidification against substrates with and without significant resistance to heat flow at the liquid-substrate interface.

HEAT FLOW DURING ATOMIZATION

During solidification of small spherical alloy droplets, heat flow is controlled by both convection at the surface and by radiation. However, there are no accurately established values for the combined radiative and convective heat-transfer coefficient, and direct measurement of the cooling rate or heat flux during solidification of an atomized droplet would be extremely difficult, if not impossible. In gas atomization, the convective heat-transfer coefficient is overriding and usually is estimated from the following equation:

$$\frac{hD}{k_f} = 2.0 + 0.60Re^{1/2}Pr^{1/3} \quad , \tag{4}$$

where: Re = Reynold's number = $vD\rho_f/\mu_f$, Pr = Prandtl number = $C_{pf}\mu_f/k_f$, C_{pf} = specific heat of the gas, D = particulate diameter, k_f = conductivity of the gas, h = heat transfer coefficient, v = gas velocity relative to particle, ρ_f = density of the gas, and μ_f = viscosity of the gas.

An upper limit on achievable heat-transfer coefficients can be deduced from Equation 4. For example, the calculated heat-transfer coefficients during argon gas atomization, with a high relative velocity of 1 Mach between the gas and the metal droplets, are 5.86×10^3 and $\sim 1.1 \times 10^4$ W/m^2K for droplet diameters 75 μm and 25 μm, respectively (Mehrabian, et al., 1978). The use of higher conductivity gases and finer particles results in calculated heat-transfer coefficients of less than 10^5 W/m^2K.

Indirect estimates of heat-transfer coefficients in various atomization processes also have been made by comparison of measured segregate (dendrite arm) spacings in crystalline alloy powders with predetermined relationships between these spacings and average cooling rate during solidification. Table 2 shows the various heat-transfer coefficients during atomization of maraging 300 steel determined by this method. Note that the heat-transfer coefficient for gas atomization is the same order of magnitude as that estimated above from Equation 4.

TABLE 2 Calculation of Heat-Transfer Coefficients from DAS

Atomization Process	Particle Size, μm	DAS μm	$\epsilon_{Avg.}$ °K/sec	h (Calculated) S.I.	hr_o/k_L
Argon Atomized Fine Powder	75	~ 2	$\sim 2.1 \times 10^4$	9.6×10^3	0.0084
REP	170	~ 3	$\sim 5.5 \times 10^3$	5.4×10^3	0.011
Steam Atomized Coarse Powder	1000	~ 6.5	$\sim 4.2 \times 10^2$	2.5×10^3	0.029
Vacuum Atomized	650	~ 6.5	$\sim 4.2 \times 10^2$	1.63×10^3	0.0123

NOTE: Data from Mehrabian et al., 1978.
Maraging 300 Steel: $d = 39.8\ \epsilon_{Avg.}^{-0.30}$
d = secondary dendrite arm spacing, DAS.
$\epsilon_{Avg.}$ = average cooling rate during solidification.
Biot number = hr_o/k_L.

In general, a limitation on the achievable heat-transfer coefficient at a liquid metal droplet-environment interface can be translated into a limitation on the important dimensionless variable, Biot number, governing the rate of heat extraction from the droplet. For example, a heat-transfer coefficient $h < 10^5$ W/m^2K translates to a limitation on the range of Biot numbers of $10^{-2} < Bi < 1.0$ for atomized droplets of liquid aluminum in the size range of 1 μm to 1000 μm:

$$Bi = \frac{hr_o}{k_L} \quad , \tag{5}$$

where h is the heat-transfer coefficient at the metal droplet-environment interface, r_o is the radius of the droplet, and k_L is the conductivity of the liquid metal.

Figure 3 shows calculated dimensionless temperature distribution in a liquid droplet for various Biot numbers and initial temperatures at the instant the droplet surface reaches its melting point. These data show that for Biot numbers less than $\sim$0.01 there is no significant temperature gradient in the droplet and the simple Newtonian cooling expressions can be used for crystalline and noncrystalline solidification.

An important variable that affects undercooling prior to crystalline solidification or formation of amorphous structures is the cooling rate in the liquid droplet. A generalized expression relating the instantaneous average cooling rate, ε_{avg}, in a liquid metal droplet to the Biot number and dimensionless surface temperature has been derived (Mehrabian, et al., 1978):

$$\varepsilon_{avg} = \left(\frac{d\theta}{dFo} \right)_{avg} = 3 \times Bi \times \theta_{SURFACE} \qquad (6)$$

where: $\varepsilon_{avg} = -3\int_0^1 (r/r_o)^2 \left(\frac{d\theta}{dFo} \right) d(r/r_o)$, $\frac{r}{r_o}$ = fractional radius,

$\theta = \frac{T - T_g}{T_M - T_g}$, $Fo = \frac{\alpha_L t^2}{r_o}$, T = temperature in the droplet, T_g = temperature of the environment, T_M = melting point of the droplet, α_L = thermal diffusivity of the liquid metal, r_o = radius of droplet, and t = time. If thermal properties of a noncrystalline solid are assumed to be equal to the liquid, Equation 6 would apply throughout solidification and subsequent cooling of amorphous droplets.

Equation 6 indicates that the average cooling rate, $(\partial T/\partial t)_{avg}$ in a liquid metal droplet is directly proportional to the heat-transfer coefficient at the droplet-environment interface and inversely proportional to the radius of the droplet. Thus, considering an upper limit for achievable heat-transfer coefficients, the only other method for increasing cooling rate is to decrease particle size. For example, using $h = 10^5$ W/m^{2}K and Equation 6, the average cooling rates of 8.3×10^5 K/s and 8.3×10^6 K/s are calculated for iron droplets of 100 μm and 10 μm, respectively, when their surface reaches the melting point.

Figure 4 shows the effect of process variables on the normalized crystalline solidification time of three different metal droplets. This time is normalized by dividing it by the Newtonian prediction of net solidification time which is:

$$t_f(\text{Newtonian}) = \frac{r_o k_s}{3\alpha_s h \text{Ste}} , \qquad (7)$$

$$\theta_i = \frac{T_i - T_g}{T_M - T_g}$$

$$Bi = \frac{hr_o}{k_L}$$

NOMENCLATURE

θ_i	BIOT NUMBER			
	1.0	0.5	0.1	0.01
1.1	1	2	6	9
1.2	2	4	7	10
1.3	3	5	8	11

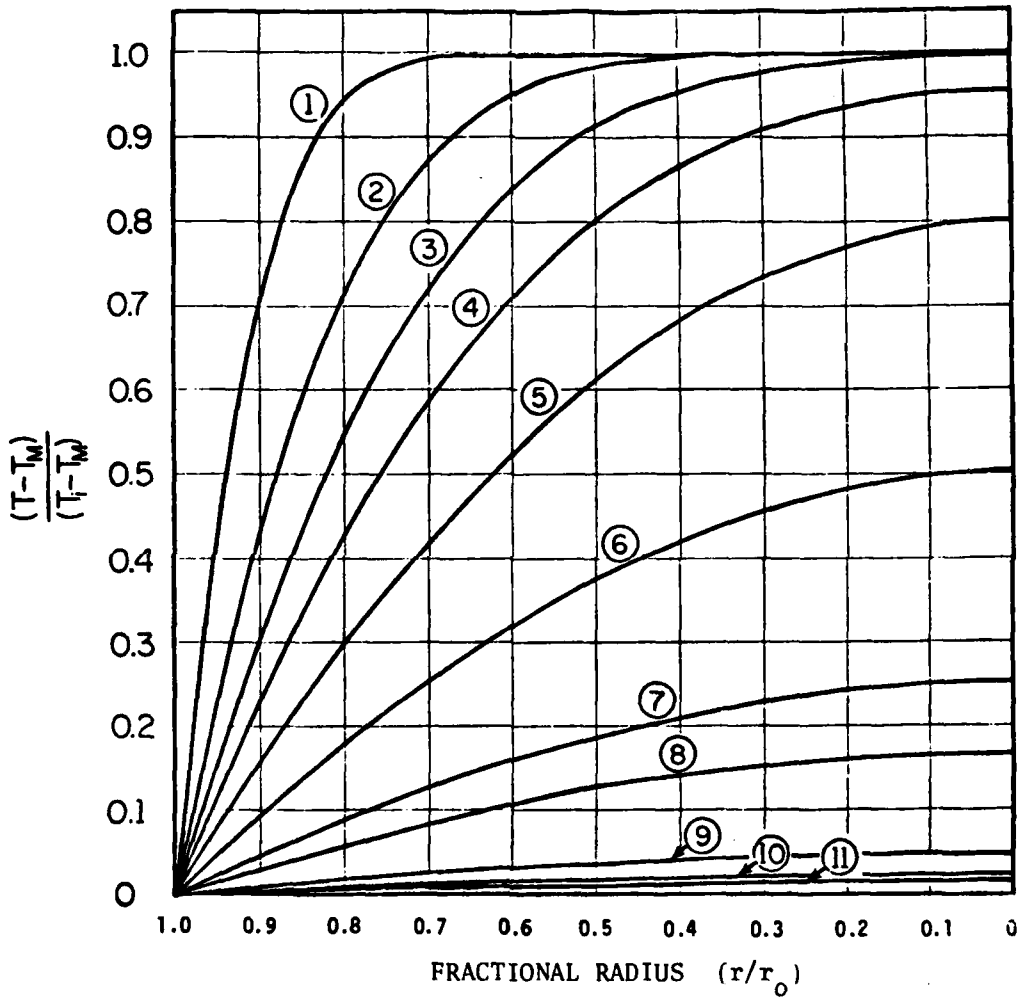

FIGURE 3 Normalized temperature distribution in a liquid droplet when its surface reaches the melting point, as a function of fractional radius, for different Biot Numbers and initial dimensionless temperatures θ_i (Mehrabian, et al., 1978).

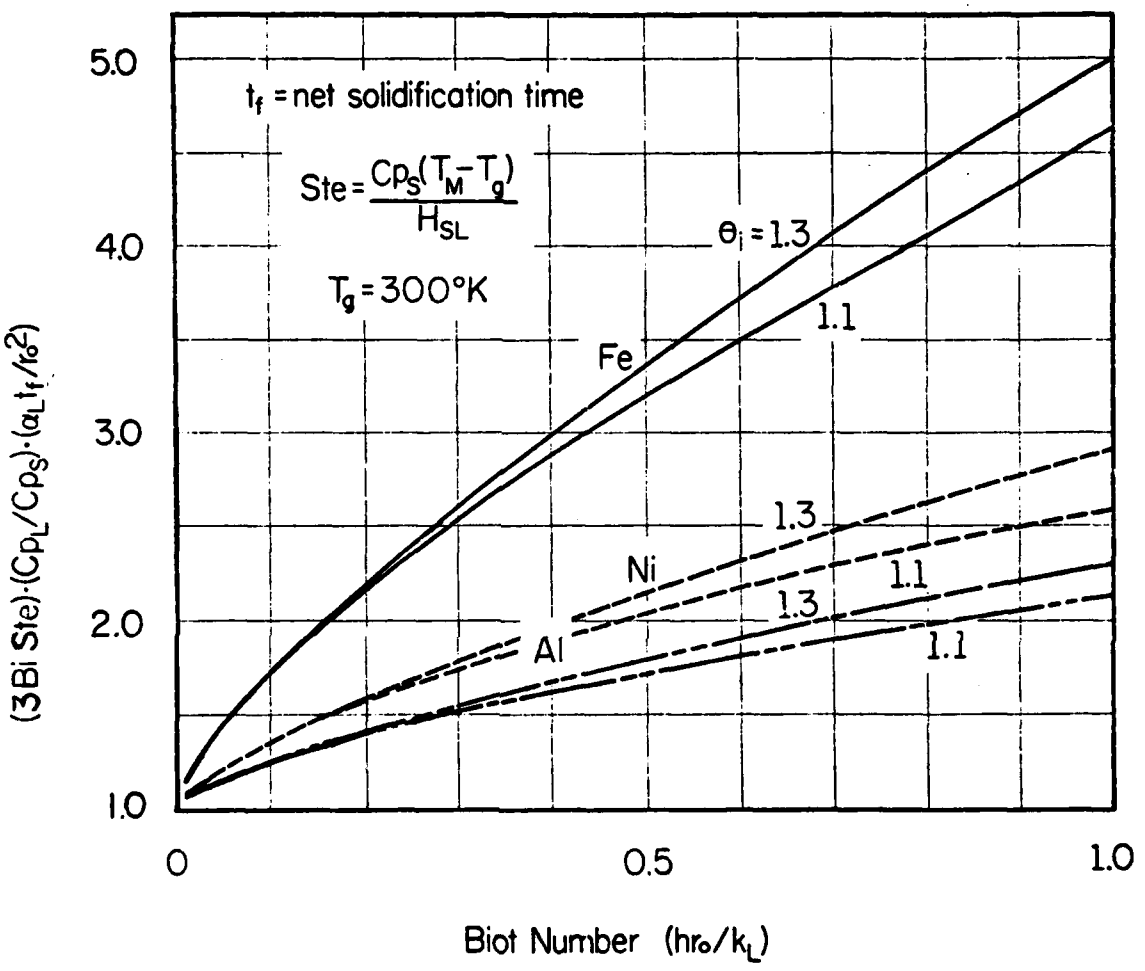

FIGURE 4 Normalized solidification time, $3 \cdot Bi \cdot Ste \cdot (\alpha_L\ t_f/r_o^2)$ for liquid droplets of Al, Fe and Ni as a function of Biot Number, for different initial dimensionless temperature θ_i • t_f designates the net solidification time (Mehrabian, et al., 1978).

where Ste is the Stefan number as defined in Figure 4.

Crystalline solidification time is the most important variable affecting segregate spacings, inclusion size, etc. It gives a better indication of time available for coarsening phenomena to occur than average cooling rate during solidification. The general trend established in Figure 4 for this normalized solidification time indicates that once heat transfer at the droplet-environment interface is maximized, this time can be reduced only by decreasing particle size. As example, net solidification times of 9.8×10^{-4} seconds and 5.3×10^{-5} seconds are calculated for iron droplets of 100 μm and 10 μm in size, respectively.

HEAT FLOW DURING SOLIDIFICATION AGAINST A METAL SUBSTRATE

A large number of innovative batch and continuous techniques for production of rapidly solidified material against a metal substrate have been developed recently. Determination of exact cooling rates during solidification of crystalline and noncrystalline structures in these processes have required estimates of heat-transfer coefficients between the melt and the substrate. Two measurements of heat-transfer coefficient in splat cooling have been reported (Predecki, et al., 1965; Harbur, et al., 1969). Table 3 shows these values along with measured heat-transfer coefficients for the case of a pressurized (89.7 MN/m^2) aluminum casting against a steel mold (Ramati, et al., 1978) and liquid aluminum die cast against a steel mold at 55 m/s metal flow velocity (unpublished paper by S. Hong, D.G. Backman, R. Mehrabian). Again, it appears that an upper limit exists for practically achievable heat-transfer coefficients between liquid metals and substrates. It is probably in the range of $h = 10^5$ to 10^6 W/m^2K.

TABLE 3 Measured Heat-Transfer Coefficients for Aluminum

Technique	Thickness of Casting	h, S.I.
Splat on Ni Substrate (Predecki et al., 1965)	1 μm	1.1×10^5 to 2.8×10^5
Drop Smash on Fe Substrate (Harbur et al., 1969)	150 μm	1.7×10^4 - 1.2×10^5 - 1.8×10^5
Pressure Cast in Steel Mold (Ramati et al., 1978)	10^4 μm	3.1×10^3 89.7 MPa 3.3×10^4
Die Cast in Steel Mold (unpublished paper by S. Hong, D. G. Backman, R. Mehrabian.)	1.6×10^3 μm	7.94×10^4 Metal flow velocity 55 m/s Pressure 175 MPa

NOTE: Data from Mehrabian et al., 1978.

Computer heat-flow calculations carried out for solidification of a noncrystalline aluminum melt are shown in Figures 5 and 6. The data are presented in terms of the dimensionless variables:

$$Bi = \frac{hL}{k_L} \qquad \text{and} \quad Fo = \frac{\alpha_L t}{L^2} \quad , \tag{8}$$

where L is casting thickness, k_L is melt conductivity, t is time, and α_L is thermal diffusivity of the melt. There is no evidence that aluminum has been made amorphous by rapid solidification; however, the numbers generated in these calculations are useful in that they again present the upper limit of achievable cooling rates; heat of fusion did not have to be removed during solidification.

As expected, for Biot numbers less than $\sim$0.05, temperature gradients in the melt are negligible (Figure 5a and the linear portion of the curve in Figure 6). The maximum melt thickness for this region of the plot is $\sim$40 μm for a heat transfer coefficient h = 4.18 x 10^5 W/m^2K (which is higher than those reported in Table 3). At Biot numbers larger than $\sim$10, resistance to heat flow is primarily within the aluminum melt (cooling is essentially ideal) and average cooling rate is independent of the Biot number. For Biot numbers in the Newtonian and ideal cooling ranges, the average cooling rate in the liquid increases by one and two orders of magnitude, respectively, as the melt thickness is decreased by one order of magnitude. Thus, as in the case of metal droplets, the most effective way to increase cooling rate is to decrease melt thickness.

Similar calculations have been reported for crystalline solidification of iron splats against a copper substrate (Ruhl, 1967). It was found that for Biot numbers less than $\sim$0.015 and more than $\sim$30, cooling was Newtonian and ideal, respectively.

Analytical expressions are available for plane front interface velocity for the case of Newtonian and ideal cooling, Equations 9 and 10, respectively:

$$R = \frac{h}{\rho_s H_{SL}} (T_M - T_O) \quad , \tag{9}$$

and

$$R = \frac{2\gamma^2\alpha}{S} \quad , \tag{10}$$

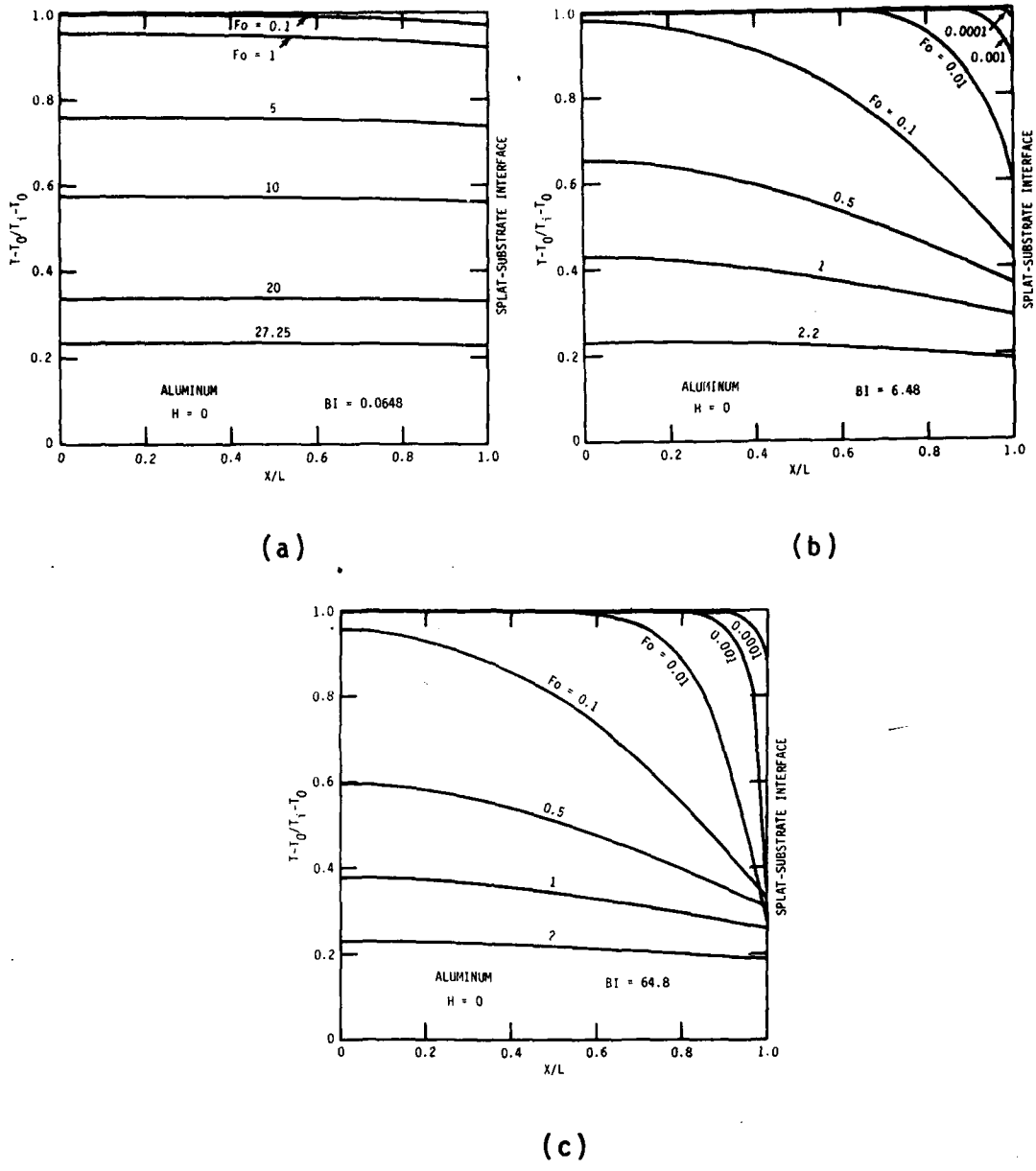

FIGURE 5 Calculated temperature distributions during cooling and noncrystalline solidification of splats of aluminum against a copper substrate. T, and T_i and T_o denote instantaneous and initial aluminum melt and initial copper substrate temperatures, respectively. X/L is fractional distance from the free surface of the aluminum (Mehrabian, et al., 1978)

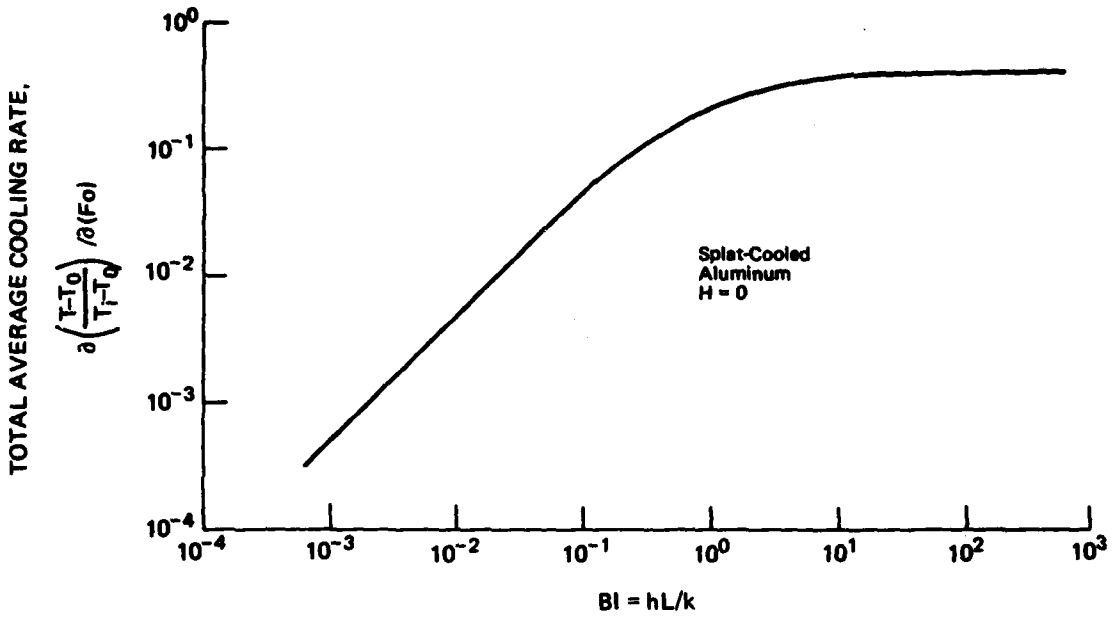

FIGURE 6 Cooling rate averaged over melt thickness and temperature to reach half the melting point for noncrystalline solidification of an aluminum melt against a copper substrate at initial temperature of T_0 (Mehrabian, et al., 1978)

where R = interface velocity, α = thermal diffusivity of the solid forming, S = distance solidified, γ = argument of the error function solution of the temperature distribution and is determined from a characteristic equation which contains metal and substrate thermal constants, T_0 = temperature of environment, T_M = temperature at melting point, h = heat of fusion, ρ_s = solid density, and L = melt depth.

The change in temperature with time in the liquid is $G_L \cdot R$ where G_L is the temperature gradient and R is the liquid-solid interface velocity. Approximate analytical solutions are available for Biot numbers between these two extremes; however, numerical solutions such as those described above can be readily employed.

Several attempts have been made to predict critical cooling rates in the liquid during RSP for the formation of noncrystalline structures (Shingu and Ozaki, 1975; Uhlmann, 1976; Spaeper and Turnbull, 1975). Heat-flow calculations usually are combined with theories of nucleation, growth, and transformation kinetics. This area, as well as rapid solidification of undercooled crystalline structures, remains fertile for future investigations.

REFERENCES

Harbur, D.R., et al. 1969. Trans Met. Soc. AIME, Vol. 245, p. 1055.

Mehrabian, R., et al. 1978. In Proc. Sagamore Army Materials Res. Conf. on Recent Advances in Metals Processing. Syracuse Univ. Press, N.Y.

Predecki, P., et al. 1965. Trans. Met. Soc. AIME, Vol. 233, p. 1581.

Ramati, S.D.E., et al. 1978. Met. Trans. B, Vol. 9B, p. 279.

Ruhl, R.C. 1967. Mat. Sci. Eng., Vol. 1, p. 313.

Shingu, P.H. and R. Ozaki. 1975. Met. Trans. A, Vol. 6A, p. 33.

Spaepen, F., and D. Turnbull. 1975. In Proc. Second Int. Conf. on Rapidly Quenched Metals, p. 205. MIT Press, Cambridge, Ma.

Uhlmann, D.R. 1976. J. Non-Cryst. Solids, Vol. 7, p. 337.

Chapter 5

CHEMISTRY OF METALLIC ALLOY GLASS SYSTEMS

The classification of metallic alloy glass systems has not yet progressed very far, but some of the major types of known representatives can be described. Polk and Giessen (1978) recently summarized the literature and Table 4 presents their scheme for classifying the alloy families. A list of glass-forming compositions (Table 5) also has been compiled by Takayama (1974), and a periodic table representation of glass forming elements (Figure 7) was published by Masumoto and Maddin (1975).

The two major groups of known systems that readily form glasses are listed as Nos. 1 and 2 of Table 4; less well delineated groups and groups of lesser importance are summarized as No. 3. Also listed because of its technical importance is a type of thermally stable amorphous metal that requires an atomic deposition process for its preparation.

The first group is referred to as the metal-metalloid systems T^2-$X_{1-x}X_x$, where T^2 is Mn, Fe, Co, Ni, Pd, Au, and Pt and X is B, C, N, Si, Ge, Al, and P, generally with compositions x = 0.15 to 0.25. Both T and X can be combinations of elements from each group, and this often increases the glass-forming tendency. A good example of this effect is shown by $Fe_{80}P_{13}C_{07}$, an alloy with a substantially greater forming tendency (Duwez and Lin, 1964). Limited amounts of aluminum (and possibly other B-metal elements) as well as early transition metals can be added to a system of this type.

Fe-based systems (e.g., Fe-B) and Pd-Si systems (Figure 8) have been widely studied (Davis, et al., 1976; Duwez, et al., 1965; Chen and Turnbull, 1969; Hansen, 1958; Elliott, 1965, Shunk, 1969; Moffatt, 1976). Each falls into the region of a narrow, deep eutectic at approximately the same composition, and models explaining their occurrence both on structural and electronic grounds have been developed (Bennett, et al., 1971; Nagel and Tuac, 1975).

The second group is referred to as the inter-transition metal systems, $T^1_{1-x}T^2_x$, where T^1 is an early transition metal such as Fe, Co, Ni, Rh or Pd, and Cu and T^2 is as defined above; x = 0.3 to 0.65. The T^1 - T^2 systems appear to fall into three subgroups: (1) systems such as Zr-Cu (Figure 8c) with a wide glass-forming composition range accessible by liquid quenching (Ray, et al., 1968); (2) systems in which glasses form preferentially at T^1-rich compositions (e.g., the Ti-Ni system where glasses can be formed between 30 and 40 at.% Ni) (Polk, et al., 1978); and (3) systems in which glasses are retained more readily at T^2-rich composition such as Nb-Ni (Figure 8d) and Ta-Ni (Giessen, et al., 1976; Ruhl, et al., 1967). It is possible that there are no fundamental differences between these three subgroups and that the compositional differences in glass-forming tendency are only a

TABLE 4 Families of Amorphous Metals Based on Chemical Classification of Constituents

Alloy System	Representative Systems	Typical Composition, at pct.	Preparation Method
1. T^2-(or Noble) Metal + Metalloid (X)	Pd-Si,Co-P Fe-P-C,Ni-P-B	 15-25 X	 LQ,ED
2. T^1-Metal	Zr-Cu	30-65 Cu	LQ,SP
+ T^2-Metal (or Cu)	Y-Cu,Ti-Ni	30-40 T^2,Cu	LQ
	Nb-Ni,Ta-Ni	40-65 Ni	LQ,SP
3. Miscellaneous systems			
a) A-Metal + B-Metal	Mg-Zn	25-35 Zn	LQ
b) T^1-Metal + A-Metal	(Ti-Zr)-Be	20-60 Be	LQ
c) Actinide + T^1-Metal	U-V,U-Cr	20-40 T^1	LQ
4. "Thermally stable" amorphous metal not formed by liquid quenching			
T^2-Metal + Rare earth Metal	Co-Gd Co-Gd-Mo	~20 Gd	SP

A-Metal = Li, Mg groups
T^1-Metal = early transition metal (Sc,Ti,V Groups)
T^2-Metal = late transition metal (mn,Fe,Co,Ni groups)
B-Metal = Cu,Zn,Al groups
Metalloid = B,C,Si,Ge,P

ED = Electrodeposition
LQ = Liquid quenching
SP = Sputtering

NOTE: From Polk and Giessen, 1978.

TABLE 5 Amorphous Phases of Some Materials

System	Composition Range x (at. %)	Method	Reference
$Pd_xNi_yP_z$	y = 8-73 z = 10-23	SQ	Maitrepierre, 1969; Hasegawa, 1972c; Takayama, 1974
$(Pd_{60-x}Pt_xNi_{40})_{75}P_{25}$	0-60	SQ	Boucher, 1971
$Pt_{100-x}Ge_x$	17-30	SQ	Crewdson, 1966
$Pt_{100-x}Sb_x$	33-37	SQ	Crewdson, 1966
$Pt_{100-x}Si_x$	23,25,68	SQ	Crewdson, 1966
$(Pt_{100-x}Ni)_{80}P_{20}$	10-80	SQ	Chen, 1974
$(Pt_{100-x}Ni_x)_{75}P_{25}$	20-70	SQ	Shinha, 1970
$(Pt_{70}Ni_{30-x}Cr_x)_{75}P_{25}$	1.5-6	SQ	Shinha, 1971b
$(Pt_{70}Ni_{30-x}V_x)_{75}P_{75}$	0-3	SQ	Hasegawa, 1972b
$Rh_{78}Si_{22}$	–	SQ	Crewdson, 1966
Rh-Ge	?	SQ	Cresdson, 1966
$Sn_{99}Cu_{10}$	–	SQ,EV	Buckel, 1954; Ruhl, 1954
$Te_{100-x}Ga_x$	10-30	SQ	Willens, 1962; Luo and Duwez, 1963; Luo, 1964
$Te_{100-x}Ge_x$	10-25	SQ	Willens, 1962; Luo and Duwez, 1963; Luo, 1964
$Te_{100-x}In_x$	10-30	SQ	Willens, 1962; Luo and Duwez, 1963; Luo, 1964
$Te_{70}Cu_{25}Au_5$	–	SQ	Hasegawa and Tsuei, 1970b
$Tl_{100-x}Te_x$	15-60	EV,SQ	Cutler and Mallon, 1966; Ferrier et al., 1972
$Tl_{100-x}Au_x$	25-60	SQ	Luo, 1967
$Zr_{72}Co_{28}$	–	SQ	Ray et al., 1968
$Zr_{100-x}Ni_x$	20-40	SQ	Ray et al., 1968
$Zr_{100-x}Cu_x$	40-75	SQ	Ray et al., 1968
$Zr_{100-x}Pd_x$	20-35	SQ	Ray, 1969
Y-Fe	?	SQ	

NOTES: EV = vapour deposition, ED = electrolyte deposition, CD = chemical deposition (electroless), P = plasma-jet deposition, SQ = splat quenching.

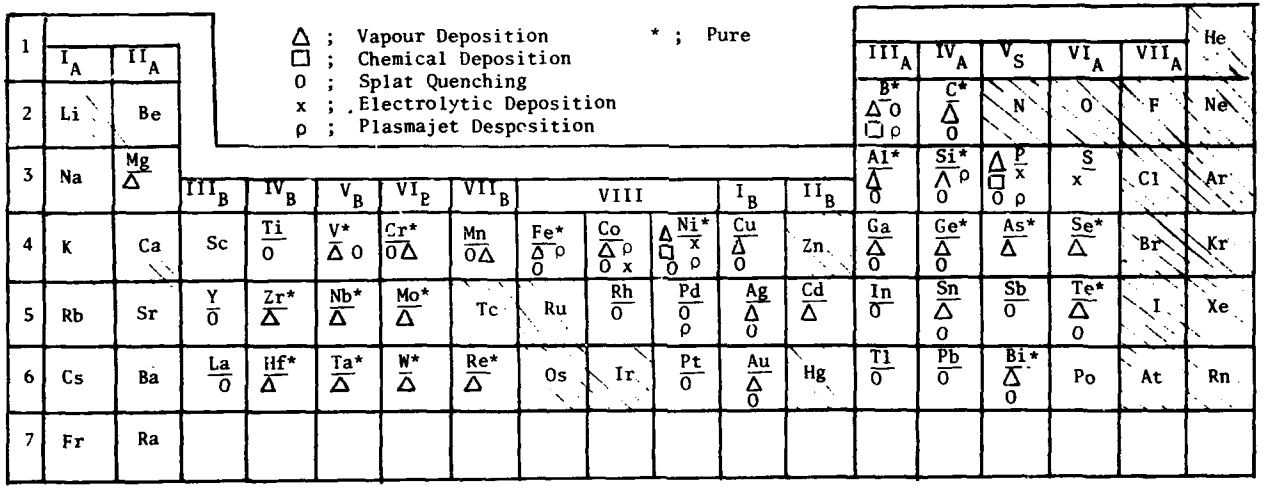

FIGURE 7 The periodic table representation of amorphous elements (Masumoto and Maddin, 1975).

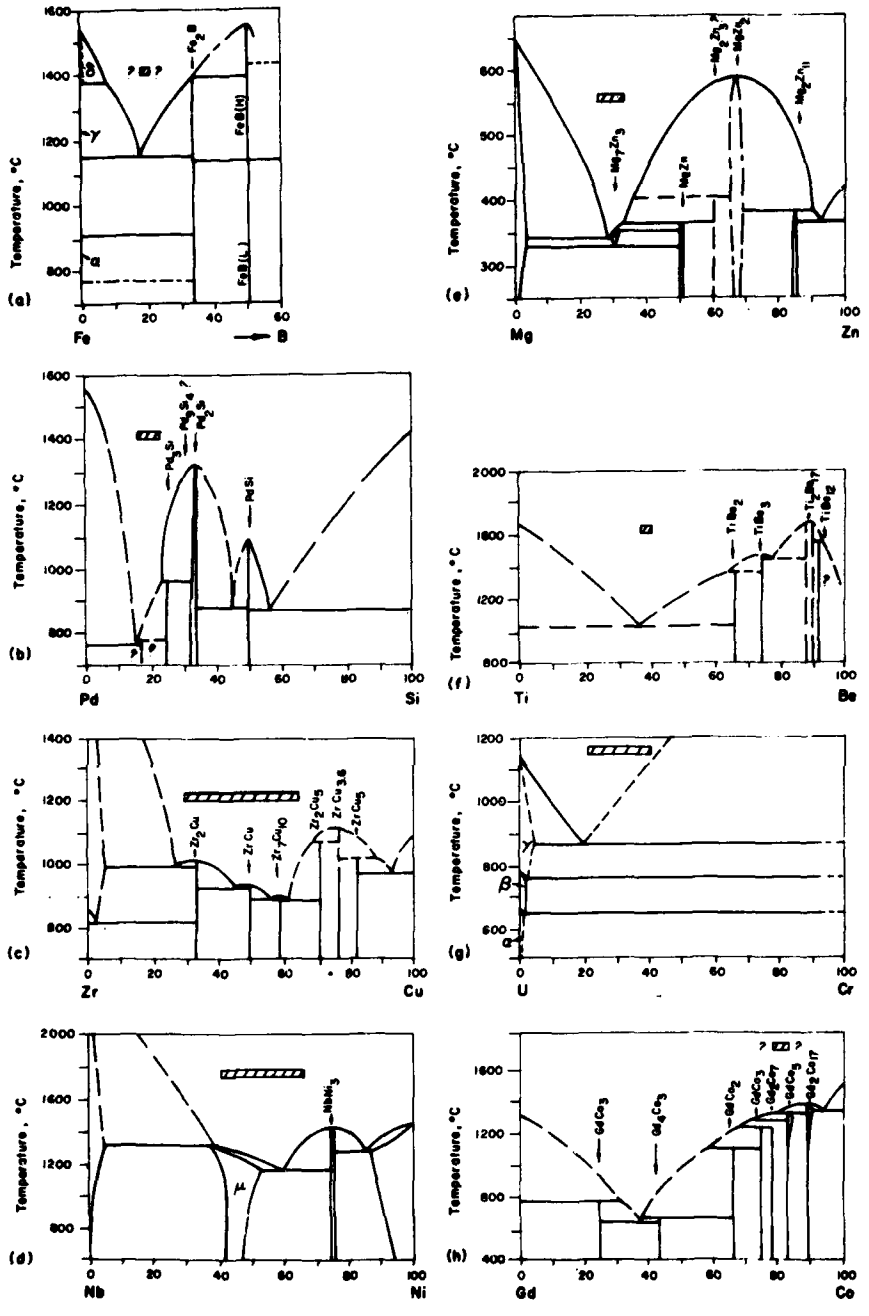

FIGURE 8 Constitution diagrams: (a) to (g) representative of binary alloy systems that readily form glasses (composition ranges of glasses obtained by rapid liquid quenching are indicated); (h) of Gd-Co system showing composition range of amorphous alloys formed by sputtering (from Polk and Giessen, 1978).

result of phase diagram features (e.g., high melting temperatures for alloy compositions with low glass-forming tendency). There are, however, characteristic crystal chemical differences between the system types: In the Ti-Ni system there is a fairly stable CsCl-type phase; occurence of a phase with this simple structure type generally inhibits glass formation at its composition. By contrast, the Nb-Ni system (Figure 8d) is characterized by a Frank-Kasper phase μ of complex structure near the equiatomic composition with low melting point, whereas at higher Nb (or Ta) contents the steep rise of the liquidus will rapidly reduce T_g/T_m. By contrast, Cu-Zr combines low melting points over a broad composition range with the presence of complex intermetallic phases.

A number of other T^1- T^2 alloy systems as well as systems formed by combining a rare earth or actinide metal with a T^2 metal have not yet been explored and can be expected to yield glasses. In a survey of Zr systems (Ray, 1969), additional glasses were found; superconducting amorphous Zr-Rh alloys were reported recently (Togano and Tachikawa, 1976); and some Y-rich Y-T^2 glasses have been prepared (unpublished work by B.C. Giessen, R. Roman, R. Ray, and M. Segnini).

The glass-forming systems listed here as miscellaneous systems were reported only recently. In the Mg-Zn system (Figure 8e), glasses were obtained in alloys with 25-35 at.% Zn (i.e., bracketing the deep eutectic) (Calka, et al., 1977). This was the first amorphous metal to be prepared from a melt that consisted only of "simple" metals (i.e., did not contain either transition metals or metalloids) and the constituents are isovalent.

A technically interesting series of amorphous alloys combining Ti, Zr, or Ti-Zr with Be (Figure 8f) is commercially available (Tanner and Ray, 1977); besides their remarkable mechanical properties, these alloys are constitutionally of interest because the region of glass formation widens from only 4 at.%. Be in the binary system Ti-Be to ∿40 at.%. Be (at constant Ti/Zr ratio) in the ternary system.

Melt spun amorphous U alloys also have been described recently (Ray and Musso, 1976); the T^1 melts V and Cr were added at levels of 20-40 at.% to produce glasses (Figure 8g). The ability to form glasses despite the small melting point depression at the eutectic (especially for U-V)* indicates that a propensity of U and possibly other actinides have a glass-forming tendency that may be related to the participation of f-electrons in their bonding.

Co-Gd, a technically interesting alloy formed by sputtering, is an example of an alloy that is thermally stable well above room temperature but that has not been formed by liquid quenching (Figure 8h). The high melting points (relative to the cohesive energy) indicate

*R. Elliot, Los Alamos Scientific Laboratory, reported in early 1979 that he could not form U-V glasses. It is also interesting that the best glass composition in the U-Cr system is at 70 at.% U and not at the eutectic composition of 80 at.% Cr.

that these alloys probably cannot be prepared as glasses from the melt. Binary compositions of interest for magnetic bubble domain memory devices center around 80 at.% Co; Mo may be added at levels between 10-20 at.% to modify the magnetic properties (Chandhari, et al., 1975).

One can change the present chemical classification of alloy glasses into one founded on glass forming composition ranges; based on the extent of that range, nearly all relatively simple systems belong to one of the following groupings: 15-25 percent, 25-35 percent, and 30-70 percent. The significance of these ranges is not yet clear; however, they must be interpreted in terms of the criteria outlined below.

Glass formation at a given cooling rate requires that T_{gr} exceed some critical value. The effect of kinetic parameters is well represented by a model proposed by Uhlmann (1972) and based on the theories of homogeneous nucleation and crystal growth. It permits the construction of temperature-time-transformation curves for each glass-forming composition using the melt viscosity, η, and a site fraction, f, as partly adjustable parameters. This construction permits calculation of the T_c required to avoid formation of a measurable amount of crystalline alloy in the melt during cooling (Chandhari, et al., 1975; Uhlmann, 1972). T_c depends on T_{gr} via η.

T_g varies somewhat, but not drastically, with the experimental conditions. It appears to vary smoothly with composition in binary systems; however, since T_g was found to decrease with increasing Zr content in Cu-rich Zr-Cu glasses despite a concomitant increase of the cohesive energy of these alloys, its change with composition cannot always be monotonic (Kerns, et al., in press). Fundamentally, T_g has been related to a potential barrier, $\Delta\mu^*$, for cooperative atomic transition and, hence, to the slope of the repulsive potential (Takayama, 1976). Davis, et al. (1974) has related T_g to the cohesive energy. This useful relation can serve as a first approximation, but it shows too much scatter to stand without modification. Although a comprehensive theory of T_g in terms of more fundamental parameters (e.g., elastic or anelastic constants) still has not been presented, T_g probably is not primarily responsible for the wide variations of the glass-forming tendency with composition (Chen, 1974).

When focusing on low T_m values, glass-formation theories become identical with theories concerning the formation of stable liquid alloys; however, this field has not yet really advanced beyond enlightened empiricism (Beer, 1972). Based on the available empirical evidence, a number of alloy characteristics that appear to be more or less associated with glass-forming have been proposed. These characteristics, which are listed in Table 6, are highly correlated, not independent.

The primary phenomenological requirement of a low "relative" T_m for a glass-forming alloy has led to the introduction of several

TABLE 6 Alloy Chemical Criteria for Easy Glass Formation

Property	Characteristic Parameter	Examples	Reference
Phase diagram characteristics (low liquidus temperatures T_m)			
Narrow low T_m region (single deep eutectic)	$\Delta T_{mr} \sim 0.41^a$	Pd-Si, Mg-Zn	Cohen and Turnbull, 1959; Duwez et al., 1965; Calka et al., 1977
Low T_m over extended composition range	$\Delta T_{mr} \sim 0.33^a$	Nb-Ni,Zr-Cu	Ray et al., 1968; Giessen et al., 1976
Atomic properties of constituents			
Size difference	r_1/r_2 = 0.79 to 1.41	Fe-B,Pd-Si, Zr-Cu	Takayama, 1976; Ray et al., 1968; Giessen et al., 1976
Valence difference	Δ_n = 4-5 el/atom	Pd-Si, Nb-Ni	–
Electronegativity difference	irregular	–	Takayama, 1976
Position in periodic table		Ni-P,Zr-Cu	–
Compositional properties			
Stoichiometry and compositional ordering	A_4B, A_2B	Pd-Si,Mg-Zn	Polk, 1972; St. Amand and Giessen, in press; Hume-Rothery and Anderson, 1960; Nagel and Tauc, in press
Valence electron concentration (Nagel-Tauc theory)	VEC~1 el/atom	Pd-Si	Nagel and Tauc, 1976
	VEC~5-7 el/atom	Nb-Ni	Nagel et al., 1977
Complex equilibrium phases	Frank-Kasper phases, Fe_3C type phases	Nb-Ni,Mg-Zn	Takayama, 1976; Suzuki et al., 1976; Shoemaker and Shoemaker, 1969
Confusion principle		Fe-P-C Fe-Ni-P-B	Duwez and Lin, 1964

$^a T_{mr} = (\bar{T}_m - T_m)/\bar{T}_m$ is the normalized depression of the melting point from the weighted average.

expressions:

1. A reduced melting temperature, $\tau_m = kT_m/\Delta H_v$; here ΔH_v, the heat of vaporization, can be understood as a measure of the resistance of the system against the atomic motions required for equilibration (Polk, 1972). The glass-forming tendency increases with decreasing τ_m.

2. The reduced melting point depression, $\Delta T_{mr} = (\overline{T}_m - T_m)/\overline{T}_m$ is the weighted average of the melting points of the components. The glass-forming tendency should increase with increasing ΔT_{mr}.

3. The reduced melting point depression, $T_{mr}^{id} = (T_m^{id} - T_m)T_m^{id}$, which measures the depression of T_m from T_m^{id}, the hypothetical liquids temperature given by ideal solution theory (Marcus and Turnbull, 1976); again glass-forming tendency and ΔT_{mr}^{id} should scale together.

In some systems, very low melting points occur only in a very narrow composition range, e.g., for Pd-Si (Figure 8b) or Au-Si. It was initially thought that equilibrium solidification at these low melting compositions of easy glass formation required the nucleation and growth of phases differing in composition from that of the homogeneous eutectic liquid, providing a constraint against equilibration and enhancing the glass-forming tendency; however, it has since been realized that even in systems with very low melting eutectics, there are stable or metastable intermetallic compounds at or within a few percent of the eutectic composition, e.g., in Pd-Si (Nylund, 1966), Au-Si (Giessen, 1969), and Mg-Zn (Hansen, 1958; Elliott, 1965; Shunk, 1969; Moffatt, 1976). Regarding the glass forming T^1-T^2 compounds such as Zr_7Cu_{10}, there can be no thermodynamic stabilization of the melt with respect to a single phase solid (Turnbull, 1971), and the high glass-forming tendency at these compositions is essentially a kinetic effect.

On the other hand, in T-T metal systems such as Zr-Cu, the glass-forming tendency is high over a broad composition range, and it is not possible to assess the glass-forming tendency of such a system using the departure from an ideal solution (Marcus and Turnbull, 1976) since the calculated liquidus curves fall below the actual melting points of glass forming intermetallics in the Zr-Cu system (Spaepen and Turnbull, 1976).

Several atomic properties of the constituent elements of glass-forming systems have been connected with the glass-forming tendency. Size difference appears to be of major importance; most alloys readily forming a glass have nominal component size ratios as measured by $r_1/r_2 = (\overline{V}_1/\overline{V}_2)^{1/3}$, taking molar volumes in the metallic state (Pearson, 1972) appreciably different from unity (Takayama, 1976; Giessen and Wagner, 1972).

For the liquid-quenched glasses in Table 4, r_1/r_2 (where r_1 is the radius of the majority atom species) ranges from 1.41 (for Y-Cu) to 0.79 (for Cu-rich Zr-Cu) with the values for most glasses lying between 1.15 and 1.25. For some metal-metalloid glasses, however, nominal size ratios near unity occur, e.g., for Pd-Si (Giessen and Wagner, 1972). A better measure of the size ratio can be determined by observing its occurrence in a crystalline phase of similar composition (Polk, 1972) or, when available, its value in the amorphous alloy; this may differ from the ratio calculated from the elemental values due to charge transfer or differing coordination numbers for the components in the glass or intermetallic phase. A recent analysis of the partial distribution functions of $Pd_{80}Si_{20}$ using x-ray and neutron diffraction (Suzuki, et al., 1976) yielded Pd-Si distances of 2.35Å and Pd-Pd distances of 2.90Å, indicating a substantial size difference of the components in the glass; crystalline Pd_3Si shows a similar size relation (Aronsson and Nylund, 1960).

Thus, it appears that an appreciable size difference ($r_1/r_2 < 0.88$ or > 1.12) of the components in the glassy alloy is a necessary requirement for ready glass formation; no counter-example is known among the several dozen readily formed glasses examined to date. Recent data on A-metal + A-metal glasses (St. Amand and Giessen, 1978) suggest that the size factor may be the only factor active in some metallic glasses, somewhat in analogy to its role in some crystalline Laves phases. It had been suggested (Polk, 1972) that, at least in the case of metal-metalloid glasses such as Pd-Si, such size differences make possible a random packed structure with a packing density much higher than that possible for dense random packing of spheres of one size (Finney, 1975); this high packing density, together with the proposed compositional ordering (Polk, 1972), can result in an amorphous structure that is relatively stable to the fluctuations necessary for crystallization to occur.

Valence differences also may be an important factor in promoting glass formation. In T^2-x and in T^1-T^2 diagrams, fairly large differences (Δn = 3-5 and 5-6, respectively) between the valences of the components are observed. These large differences simply may be coincidental with the size by a reduction in the magnetic moment of the metal atom (Sinha, 1971a); for T^1-T^2 metals, d-electron transfer from T^2 antibonding orbitals to T^1 bonding orbitals is assumed to take place. In any case, the valence differences are not a necessary criterion for glass formation, as shown by the example of Mg-Zn where both components are divalent.

The role of electronegativity differences (Takayama, 1976) is more uncertain. The differences between the Gordy electronegativities χ of the glass components (Pearson, 1972) are generally small, $-0.3<\chi<0.2$, and vary irregularly (i.e., $\chi_{Pd}>\chi_{Si}$, but $\chi_{Ni}<\chi_{P}$). With regard to crystalline alloys, the electrochemical factor derived from the values

for the elements often may not be meaningful for small differences of χ.

The qualitative criterion related to position in the periodic table may be stated as follows: Elements promoting glass formation with a given element tend to be located in different sections in the periodic table (i.e., in sections such that the differences of relevant properties between the components are sufficiently large but not too large). It is not known whether this criterion could be adequately quantified (e.g., analogously to a Darken-Gurry plot) (Pearson, 1972); however, it is sometimes found to be qualitatively useful in searching for a new amorphous metal.

The composition dependence of the glass-forming tendency suggests that composition-dependent factors are effective in most systems. Considered first is compositional ordering, which most frequently has been considered for T^2-X glasses. Noting the deep eutectics present in some of these systems, Hume-Rothery and Anderson (1960) attempted to connect melt stability with ideal, quasi-stoichiometric compositions such as A_6B and A_3B on the basis of an assumed icosahedral coordination of liquid atoms around a reference atom. Chemical ordering has been an important consideration in some structural models (Polk, 1972). Chen and Park (1973) have ascribed such ordering to covalently directed T^2-$_X$ bonds, whereas Turnbull (1974) has associated the relative stability of binary alloy glasses with the softness of the repulsive potential between pairs of atoms of different species, which would favor the liquid and, hence, the glass by lowering the energy of crystallization. Recently, the short-range order of the liquid, as expressed by the absence of minority atom contacts in T^2-$_X$ glasses, has been treated theoreticlaly using a semi-quantitative pseudopotential argument (Nagel and Tauc, in press). It is pointed out that such ordering, which results in a minimization of the number of first-nearest-neighbor contacts between like atoms, is also a common characteristic of crystalline intermetallic phases.

Favorable values of the valence electron concentration (VEC) have been correlated with the glass-forming tendency by Nagel and Tauc (1975) somewhat in analogy to the corresponding argument for crystalline Hume-Rothery phases. In their approach, the glass-forming tendency has a maximum at the composition where $2k_F$, the "spanning vector" of the Fermi surface, equals q_p, the maximum of the structure factor, determined by the atomic structure of the glass. When this is the case, the density of states D(E) will have a minimum at the Fermi energy and the amorphous state at this composition has a reduced energy. Presence of a kinetic barrier against fluctuations leading to crystallization also has been inferred (Nagel and Tauc, 1975). Reduced $D(E_F)$ values, as required by this theory, have been observed by ultraviolet photoelectron spectroscopy (UPS) for Pd-Si glasses (Nagel, et al., 1976) and also were found recently for amorphous Nb-Ni alloys (Nagel, et al., 1977).

Systematic UPS measurements on glasses at compositions of high and low glass-forming tendency would be required to confirm this theory; however, the occurrence of metallic glasses in preferred VEC ranges (e.g., for T^1-T^2 glasses) suggests an electronic contribution to the glass-forming tendency. Weaknesses of this theory are that it relies on the rigid band model and that it does not express the large qualitative differences in glass-forming tendency between elements of the same valence.

Another indication of a valence electron effect on the glass-forming tendency comes from a survey of the crystalline equilibrium phases found at the composition of many metallic glasses. These phases tend to be of complex structure types involving a range of coordination numbers and interatomic distances such as Frank-Kasper phases of the σ, μ, or M types (Shoemaker and Shoemaker, 1969); the Fe_3C (cementite) type; or others (Giessen and Wagner, 1972; Shoemaker and Shoemaker, 1969). Thus, at or near the glass-forming $Mg_{70}Zn_{30}$ eutectic composition, there is a complex orthorhombic phase with about 150 atoms per unit cell. The occurrence of Frank-Kasper phases is known to depend strongly on the average VEC, and VEC values of 6-7 are favorable both for Frank-Kasper phase and metallic glass formation.

Although it is an argument clearly containing a kinetic component, the "confusion principle" is listed here and is often taken recourse to by designers of metallic glass compositions. According to this concept, the glass-forming tendency is enhanced at compositions corresponding to low-temperature invariant melting point where the equilibrium alloy consists of as many crystalline solids as is possible and compatible with alloy design, such as a ternary eutectic or, at least, a two-phase composition in a ternary system involving a binary solid solution. An example is the ternary Fe-P-C glass which consists in pseudo-equilibrium of Fe, Fe_3C, and Fe_3P (considering the metastability of Fe_3C) (Duwez and Lin, 1964).

REFERENCES

Aronsson, B., and A. Nyland. 1960. Acta Chem. Scand., Vol. 14, p. 1011.

Beer, S.Z., Ed. 1972. Physics and Chemistry of Liquid Metals. M. Decker, New York, N.Y.

Bennett, C.H., et al. 1971. Acta Met., Vol. 19, p. 1295.

Boucher, B.Y. 1971. Calif. Inst. Tech. Report CALT 822-35.

Buckel, W. 1954. Z. Phys., Vol. 138, p. 136.

Calka, A., et al. 1977. Scripta Met., Vol. 11, p. 65.

Chandhari, P., et al. 1975. Conf. Proc. 24, AIP, p. 562.

Chen, H.S. 1974. Acta Met., Vol. 22, p. 1505.

Chen, H.S., and B.K. Park. 1973. Acta Met., Vol. 21, p. 395.

Chen, H.S. & D. Turnbull. 1969. Acta Met., Vol. 17, p. 1021.

Cohen, M.H., and D. Turnbull. 1959. J. Chem. Phys., Vol. 31, p. 1164.

Crewdson, R.C. 1966. Calif. Inst. Tech. Rept. CALT-221-20 and 21.

Cutler, M., and C.E. Mallon. 1966. Phys. Rev., Vol. 114, p. 642.

Davis, L.A., et al. 1974. Scripta Met., Vol. 8, p. 1179.

Davis, L.A., et al. 1976. Scripta Met., Vol. 10, p. 541.

Duwez, P., and S.C. Lin. 1964. J. Appl. Phys., Vol. 38, p. 4096.

Duwez, P., et al. 1965. J. Appl. Phys., Vol. 36, p. 2267.

Elliott, R.P. 1965. Constitution of Binary Alloys-First Supplement, McGraw-Hill, N.Y.

Ferrier, R.P., et al. 1972. J. Non-Cryst. Sol., Vol. 8-10, p. 798.

Finney, J.L. 1975. J. de Physique, Vol. 36, p. C2-1.

Giessen, B.C. 1969. In Developments in the Structural Chemistry of Alloy Phases, p. 227. Plenum Press, N.Y.

Giessen, B.C., and C.N.S. Wagner. 1972. In Liquid Metals, Chemistry and Physics, p. 633. Edited by S.Z. Beer. Marcel Decker, New York, N.Y.

Giessen, B.C., et al. 1976. In Proc. Second Int. Conf. on Rapidly Quenched Metals, p. 145. Edited by N.J. Grant and B.C. Giessen. MIT Press, Cambridge, Ma.

Hansen, M. 1958. Constitution of Binary Alloys. McGraw-Hill, N.Y.

Hasegawa, R. 1972b. Phys. Let., Vol. 38A, p. 5.

Hasegawa, R. 1972c. Phys. Rev. Let., Vol. 28, p. 1376.

Hasegawa, R., and C.C. Tsuei. 1970. Calif. Inst. of Tech. Rept. CALT-221-90.

Hume-Rothery, W., and E. Anderson. 1960. Phil. Mag., Vol. 5, p. 383.

Kerns, A., et al. In press. Mat. Sci. and Eng.

Luo, H.L. 1964. Calif. Inst. Tech. Report No. 22.

Luo, H.L. 1967. Abst. Bull. IMD-AIME, Vol. 2, No. 1, p. 44.

Luo, H.L., and P. Duwez. 1963. Appl. Phys. Let., Vol. 2, p. 21.

Maitrepierre, P.L. 1969. J. Appl. Phys., Vol. 40, p. 4826.

Marcus, M., and D. Turnbull. 1976. In Proc. Second. Int. Conf. on Rapidly Quenched Metals, p. 211. Edited by N.J. Grant and B.C. Giessen. MIT Press, Cambridge, Ma.

Masumoto, T., and R. Maddin. 1975. Mat. Sci. Eng., Vol. 19, p. 1.

Moffatt, W.G. 1976. Binary Phase Diagrams Handbook. General Electric, Schenectady, N.Y.

Nagel, S.R., and J. Tauc. 1975. Phys. Rev. Let., Vol. 35, p. 380.

Nagel, S.R., and J. Tauc. 1976. In Proc. Second Int. Conf. on Rapidly Quenched Metals, p. 337. Edited by N.J. Grant and B.C. Giessen. MIT Press, Cambridge, Ma.

Nagel, S.R., and J. Tauc. In press. Solid State Comm.

Nagel, S.R., et al. 1976. Phys. Rev., Vol. B13, p. 3284.

Nagel, S.R., et al. 1977. Solid State Comm., Vol. 22, p. 471.

Nylund, A. 1966. Acta Chem. Scand., Vol. 20, p. 2381.

Pearson, W.B. 1972. The Crystal Chemistry and Physics of Metals and Alloys, Wiley-Interscience. N.Y.

Polk, D.E. 1972. Acta Met., Vol. 20, p. 485.

Polk, D.E., and B.C. Giessen. 1978. "Overview of Principles and Applications." Met. Glasses, ASM, Metals Park, Oh.

Polk, D.E., et al. 1978. Acta Met., Vol. 26, p. 1097.

Ray, R., and E. Musso. 1976. U.S. Patent No. 3981722.

Ray, R., et al. 1968. Scripta Met., Vol. 2, p. 357.

Ray, R. 1969. ScD Thesis, MIT, Cambridge, Ma.

Ruhl, R. 1954. Z. Phys., Vol. 138, p. 121.

Ruhl, R., et al. 1967. Acta Met., Vol. 15, p. 1693.

St. Amand, R., and B.C. Giessen. 1978. Scripta Met., Vol. 12, p. 1021.

Shoemaker, C.G., and D.P. Shoemaker. 1969. In Developments in the Structural Chemistry of Alloy Phases, p. 107. Edited by B.C. Giessen. Plenum Press, N.Y.

Shunk, F.A. 1969. Constitution of Binary Alloys, Second Supplement. McGraw-Hill, N.Y.

Sinha, A.K. 1970. Phys. Rev., Vol. B1, p. 4541.

Sinha, A.K. 1971a. J. Appl. Phys., Vol. 42, p. 338.

Sinha, A.K. 1971b. Calif. Inst. Tech. Report CALT-822-31.

Spaepen, F., and D. Turnbull. 1976. In Proc. of Sec. Int. Conf. on Rapidly Quenched Metals, p. 205. Edited by N.J. Grant and B.C. Giessen. MIT Press, Cambridge, Ma.

Suzuki, K., et al. 1976. In Proc. Second Int. Conf. on Rapidly Quenched Metals, p. 215. Edited by N.J. Grant and B.C. Giessen. MIT Press, Cambridge, Ma.

Takayama, S. 1974. PhD Thesis. Univ. of Pennsylvania.

Takayama, S. 1976. J. Mat. Sci., Vol. 11, p. 164.

Tanner, L.E., and R. Ray. 1977. Scripta Met., Vol. 11, p. 783.

Togano, K., and K. Tachikawa. 1976. In Proc. Second Int. Conf. on Rapidly Quenched Metals. Edited by N.J. Grant and B.C. Giessen. MIT Press, Cambridge, Ma.

Turnbull, D. 1971. In Solidification, p. 1. ASM, Metals Park, Oh.

Turnbull, D. 1974. J. de Physique, Vol. 35, p. C4-1.

Uhlmann, D.R. 1972. J. Non-Cryst. Solids, Vol. 7, p. 337.

Willens, R.H. 1962. J. Appl. Phys., Vol. 33, p. 3269.

Chapter 6

PROCESSING METHODS

During the past two decades, increasing emphasis has been placed on the development of new techniques for the rapid solidification processing of metallic materials. Some of these are pictured in Figure 9. Initially, efforts were focused on splat quenching techniques and production capabilities were limited. More recently, interest has shifted towards the development of processes for manufacturing tonnage quantities of splatted material, continuous thin filamentary material, and fine powders. In addition, new methods that make use of recent advances in laser and electron beam technologies have been introduced for the surface treatment of materials by self-substrate quenching techniques. These developments in RSP are reviewed below, and an attempt is made to define problem areas as well as promising areas for future development.

MELT SPINNING

Melt spinning of thin filaments involves jetting the melt through a small orifice into an appropriate substrate or chill block (Pond and Maddin, 1969; Hubert, et al., 1973; Pond, et al., 1974). In free-flight, the liquid metal is delivered to an appropriate rapidly rotating copper disc, wheel, or drum, that may be cooled for large-scale production. Current practice favors a downwards directed jet (0.3-1.5mm in diameter), inclined at 15 degrees to the disc radius with the nozzle tip at about 3mm from the disc surface and set back about 25mm from its crest. The disc rotates at up to 20,000 rpm. Provided that the melt properly wets the surface of the disc, this simple jetting technique readily produces rapidly solidified filaments up to about 3mm in width, with thicknesses that range from 25 to 200 μ. Ribbons up to 15cm in width can be produced by melt spinning, (widths up to 30cm are claimed to be feasible), but this requires careful positioning and design of the actual nozzles. An optimum configuration appears to be a nozzle with a slotted orifice and angled tip that is positioned to be almost in contact with the surface of the rotating disc. This stabilizes the melt pool formed under steady state conditions in contact with the disc.

The time of contact of the solidifying material on the chill block is of decisive importance in the fabrication of amorphous metallic filaments. If the filament detaches from the disc too soon, crystallization and phase decomposition will occur during secondary cooling from the melt in the solid state. In extended chill melt spinning, this is avoided by deliberately increasing the filament contact time by employing a spring-loaded auxiliary disc in contact with the main melt spinning disc (Bedell, 1975). In centrifugal spin quenching, the extended chill effect occurs quite naturally since the melt is jetted onto the

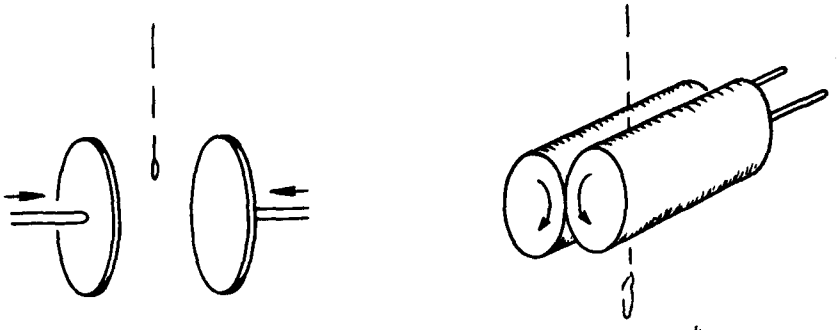

10^6

(a)

5×10^4

(b)

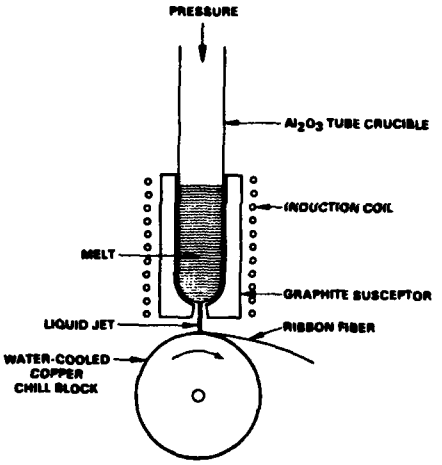

$10^5 - 10^6$

(c)

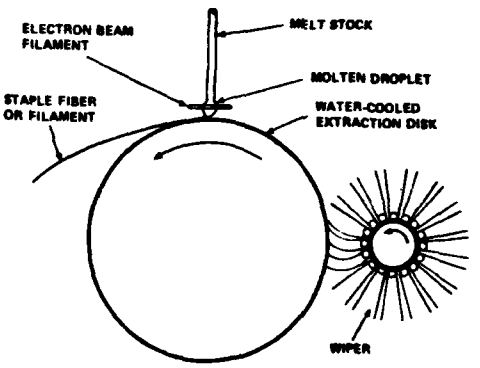

5×10^4

(d)

FIGURE 9 Schematic representation of quenching techniques; typical cooling rates are indicated: (a) piston and anvil, (b) roll quenching, (c) melt spinning, and (d) pendant drop melt extraction (Collings, Maringer and Mobley, 1978)

inner surface of a rapidly rotating drum (Chen and Miller, 1976). The problem here is not to extend the contact time, but rather to induce detachment of the filament from the surface of the drum after completion of solidification and solid state cooling. This can be done most effectively by using an inclined chill surface on the inside edge of the rotating drum or by using a doctor blade to detach the ribbon since centrifugal forces acting on the sloping surface encourage detachment of the filament. As would be expected, the filament contact time decreases as the slope of the inclined chill surface increases. The greater the slope, the greater the tendency to form a ribbon of unequal thickness across its width.

Although considerable progress has been made in the technology of melt spinning, much remains to be done. Foremost among the technical problems remaining to be resolved are those associated with the scale-up of manufacturing operations, such as nozzle and wheel erosion, and the efficient collection of the spun product. Other difficulties (e.g., control of edge definition, surface smoothness, especially of the contact side, and width of filaments or ribbons) appear to be close to solution. Improved nozzle design, control of puddle geometry and the use of inert gas at reduced pressure in the processing chamber have contributed to improvements in the overall quality of the melt-spun product. Interest also is developing in high-speed processing as a means to produce splatted powder. Further in the future, the processing of laminated composites can be expected and will involve metal-metal, metal-semiconductor, and possibly, metal-ceramic combinations. Quench rates for melt spinning, depending on ribbon thickness and alloy composition are about 10^{5}°C/sec.

MELT EXTRACTION

Melt extraction is slightly different from melt spinning in that the melt source is stationary, and the edge of a rotating disc or wheel picks up the melt to form rapidly quenched filamentary or particulate material (Pond, et al., 1974; Maringer and Mobley, 1974). Quench rates are similar to those attained in melt spinning, about 10^{5}°C/sec. The melt may be contained in a crucible or a special arrangement may be employed that does not require a crucible (e.g., pendant-drop melt extraction). A variety of water-cooled copper disc designs have been employed, including notched or serrated discs for the purpose of making short fibers or particulates, not continuous filaments. A typical disc for thin filament production is about 20cm in diameter and has a wedge-shaped edge. To achieve steady state processing conditions, the melt is fed to the edge of the disc in a continuous manner by raising the molten bath in the crucible process and by lowering the feedstock in the pendant drop process. Electron beam melting of the tip of a solid bar under high vacuum conditions is a unique feature of the pendant-drop process and makes it especially attractive

for the processing of reactive, high-melting-point materials. The pendant-drop process appears to be more suitable than the crucible process for the high rate production of thin (∿25μ) filaments. In the processing of thicker (up to ∿500 μ) filaments by the crucible process, the sides of the disc are protected from the melt either by a maskant or by a slot in the template cover on the melt surface. Thus, the filament is constrained by essentially one-dimensional heat flow to grow radially on the disc.

The large-scale production capabilities of melt extraction processing already have been demonstrated. Problems remaining to be resolved are similar to those identified for melt spinning processing (e.g., extending the useful life of extraction wheels).

TWIN ROLLER QUENCHING

The mechanics of twin-roller quenching are similar to those of melt spinning, except that a pair of counter-rotating chills replaces a single rotating chill for the purposes of melt quenching (Chen and Miller, 1970; Babic, et al., 1970). Typically, the melt stream is directed vertically downwards between a pair of water-cooled rolls made of a broad variety of alloys. Thin filaments are formed by rapid melt quenching in the pinch of the rolls. In order to produce filaments of uniform thickness, the roll surfaces and shafts must be machined to close tolerances and precision bearings must be used. Ribbons varying from about 50 to 200 μm in thickness are formed when the rolls initially are in rolling contact under some pressure. Thicker ribbons can be made by controlling the roll gap. Owing to the limited contact time of the solidified material with the rolls, twin-roll quenching is not as efficient as melt spinning in producing amorphous metallic solids. However, it is quite suitable for making extended solid solution or metastable phases and has the advantage that the material can be obtained in thicker sections (Davies, et al., 1977). Some problems remain to be resolved (e.g., fold-forming tendency and surface cracking), but they do not appear to be insuperable. Roll life is a problem similar to that for melt spinning and extraction.

Future work probably will be directed towards extending the capabilities of twin-roller quenching to the fabrication of wide sheet material. It also seems likely that the technique will be exploited to produce a variety of thin-walled shapes by the simple expedient of using matching pairs of contoured rolls as opposed to flat rolls.

SELF-QUENCHING

Self-quenching involves surface localized melting of bulk material followed by rapid solidification and subsequent solid state cooling (Jones, 1969; Breinan, et al., 1976). Processing

is accomplished by rapidly traversing a sharply focused energy beam (plasma, electron, or laser beam) over the material surface, usually with incident power densities of $\sim 10^6$ W/cm^2 and interaction times of $\sim 10^{-5}$ secs. Experience has shown that laser surface melting, using continuous wave systems, can be controlled to depths of ~ 25 μ, which corresponds with a maximum average cooling rate of $\sim 10^8$ ^{o}C/sec. Even higher cooling rates are possible using pulsed laser systems because of the higher power densities available. Reproducible and controllable surface melting using pulsed lasers has been achieved in surface layers as thin as ~ 1000 Å. Typical operating conditions in this regime of laser processing are power densities of $\sim 5 \times 10^7$ W/cm^2 and interaction times of $\sim 10^{-8}$ secs. Pulsed laser treatments are being employed to anneal out irradiation damage in ion-implanted semiconductors. On the other hand, laser surface melting using continuous wave systems is being exploited to enhance the fatigue, corrosion, erosion, and wear properties of material surfaces. A wide variety of surface microstructures (e.g., amorphous metallic solids, extended solid solution phases, metastable phases, ultrafine eutectics, refined dendritic structures) has been produced by this technique.

Currently, interest is focused on process modifications to permit controlled surface alloying in conjunction with self-quenching (e.g., by melting in surface deposits of prealloyed powder). The influence of preheating the substrate also is being examined since this may be a way to overcome the hot cracking problem encountered in the self-quenching of hard materials.

GAS ATOMIZATION

Conventional gas atomization involves the interaction of a melt stream with a symmetrical arrangement of converging high velocity gas jets (Klar and Shafer, 1972). Atomization occurs in the interaction zone by dissipating the kinetic energy of the gas phase. Most commonly, the working fluid in conventional gas atomization is air, steam, nitrogen, or argon. In the special case of soluble gas atomization, the working fluid is hydrogen (Wentzell, 1976). The gas is dissolved under pressure in the melt, and atomization is achieved by explosive decompression of the saturated melt as it passes through a small orifice into a massive vacuum chamber.

Current developments in gas atomization are directed towards increasing the average cooling rate of the atomized product. In ultrasonic atomization, this is achieved by increasing the yield of very fine particles, which naturally experience higher average cooling rates (Grant, 1977). Using a Hartman shock wave tube, exit gas velocities up to Mach 2 are possible. At these high velocities, the melt is atomized into very fine particles in a single step, typically <30 μ in diameter, and often with yields of 80 to 90 percent. Higher cooling rates also

are achieved by techniques of spray deposition, where the atomized particles are deposited onto a chilled substrate. The rapidly solidified material is collected simply by scraping off the splats as fast as they are formed.

Future work probably will be concerned mainly with process refinements to increase yields of powder particles having a well defined particle size range. At the same time, more attention will be given to the problem of generating very clean powders (i.e., free of insoluble inclusions and other extraneous matter). This will require improvements in primary melting practice and the introduction of new techniques for separating inclusions from the atomized product.

CENTRIFUGAL ATOMIZATION

Many schemes have been devised for producing fine particles by rotary or centrifugal atomization. In the rotating electrode process, fine particle generation is achieved by melting off the tip of a rapidly rotating electrode (feedstock) using a tungsten arc or some other directed energy source (e.g., plasma, electron beam, or laser beam) (Aldinger, et al., 1975). The technique is useful for processing high-melting-point and/or reactive materials. Low-melting-point materials can be atomized by spraying the melt from a rotating crucible or by passing the melt through the walls of a rotating cylindrical sieve (Grant, 1977).

Only a few practical systems have been optimized specifically to generate rapidly solidified powders. Typical of these is the Rapid Solidification Rate process, which employs a high-speed disc atomizer for particle generation and high mass flow He gas quenching to obtain high cooling rates (Cox, et al., 1976). Cooling rates of $\sim 10^5$ ^{o}C/sec in particles of ~ 50 μ in diameter have been achieved in a variety of commercial alloys. Good wetting between melt and disc appears to be a prerequisite for efficient production of fine spherical powders. This is best achieved by forming and maintaining a thin solid skull on a water-cooled copper disc. Currently, efforts are being made to extend the cooling rate capabilities of the RSR process by substituting splat quenching for gas quenching. This is being done by surrounding the rotary atomizer with a system of water-cooled copper chills. Average cooling rates of $\sim 10^7$ ^{o}C/sec appear feasible by spray deposition on water-cooled rotating/reciprocating substrates.

ELECTRIC FIELD ATOMIZATION

Electric field atomization is a technique for generating fine particles from the melt by the application of an intense electric field to a molten metal surface in a very restricted space (e.g., a liquid

meniscus located at the tip of a capillary tube) (Clampitt, et al., 1975; Perel, et al., 1977). When the applied field reaches a critical value ($\sim 10^5$ V/cm), it disrupts the meniscus and small droplets of the melt are expelled. The particles typically are ~ 0.1 μ in diameter and attain velocities of about ~ 20 km/sec. The process may be used as a fine particle generator or as a means to produce thin metastable layers by splat quenching on cold substrates.

PLASMA SPRAYING

Very hot, highly ionized plasma jets commonly are employed to melt and to spray prealloyed powder onto cold substrates. Metastable structures normally are produced because of the high cooling rates characteristic of splat quenching (Cahn, 1977; Giessen, et al., 1977; Krishnanand and Cahn, 1976). Thick deposits of extended solid solution phases, with varying degrees of phase decomposition due to self-annealing as the deposit builds up in thickness, have been produced in a variety of materials. Some success has even been obtained in forming a thick deposit of an amorphous metallic solid. To minimize the effect of self-annealing, it appears necessary to employ a rotating water-cooled copper substrate coupled with cross-blasting to divert the plasma jet at a point just in front of the substrate without diverting the molten particles. The adherence of the plasma-sprayed deposit to the substrate is generally good, provided that the substrate surface is suitably roughened (e.g., by grit blasting).

Two major problems have been encountered in plasma spraying technology that tend to limit the range of applications. First, the strength of the bond between substrate and deposit is not always acceptable in situations involving dissimilar materials (e.g., metallic-ceramic or metallic-intermetallic combinations). The problem is particularly acute when the coated part is subjected to thermal cycling, which gives rise to high stresses at the coating-substrate interface. Second, the mechanical properties of the as-deposited material are far from ideal, due to the presence of internal stresses and microporosity. Attempts are being made to overcome these difficulties by thermomechanical treatments applied after spray deposition.

REFERENCES

Aldinger, F., et al. 1975. Westinghouse Electric Corporation Technical Report AFML TR-76-65.

Babic, E., et al. 1970. J. Phys. E. Sci. Inst., Vol. 3, p. 1014.

Bedell, J. 1975. U.S. Patent No. 3,862,658 (Jan. 29).

Breinan, E.M., et al. 1976. Superalloys—Metallurgy and Manufacture, p. 435. AIME, New York.

Cahn, R.W. 1977. In Proc. Int. Conf. on Rapid Solidification Processing, p. 129.

Chen, H.S., and C.E. Miller. 1970. Rev. Sci. Inst., Vol. 41, p. 1237.

Chen, H.S., and C.E. Miller. 1976. Mat. Res. Bull., Vol. 11, p. 49.

Clampitt, R., et al. 1975. J. Vac. Sci. and Tech., Vol. 12, p. 208.

Collings, E.W., R.E. Maringer, and C.E. Mobley. 1978. Amorphous Glassy Metal and Microcrystalline Alloys for Aerospace Applications, Tech. Rept. AFML-TR-78-70. Battelle Columbus Lab, Columbus, Oh.

Cox, A.R., et al. 1976. Superalloys—Metallurgy and Manufacture, p. 45. AIME, New York.

Davies, H.A., et al. 1977. In Proc. Int. Conf. on Rapid Solidification Processing, p. 78.

Giessen, B.C., et al. 1977. Met. Trans., Vol. 8A, p. 364.

Grant, N.J. 1977. In Proc. Int. Conf. on Rapid Solidification Processing, p. 230.

Hubert, J.C., et al. 1973. Z. Metallkde Bd., Vol. 64, p. 835.

Jones, H. 1969. J. Mat. Sci. Eng., Vol. 5, No. 1, p. 1.

Klar, E., and W.M. Shafer. 1972. In Powder Metallurgy for High Performance Applications, p. 57. Syracuse U. Press, N.Y.

Krisknanond, K.D. and R.W. Cahn. 1976. In Rapidly Quenched Materials, p. 67. MIT Press, Cambridge Ma.

Maringer, R.E. and C.E. Mobley. 1974. J. Vac. Sci. Tech., Vol. 11, p. 1067.

Perel, J., et al. 1977. In Proc. Int. Conf. on Rapid Solidification Processing, p. 258.

Pond, R.B. and R. Maddin. 1969. Trans. Met. Soc. AIME, Vol. 245, p. 2475.

Pond, R.B., et al. 1974. In New Trends in Materials Processing, p. 128, ASM, Metals Park, Oh.

Wentzell, J.M. 1976. Paper presented at 42nd Meeting of the Structures and Materials Panel, AGARD, Ottawa, Ontario, Canada.

Chapter 7

CONSOLIDATION METHODS

Three distinct approaches are being investigated for the production of bulk rapidly solidified structures: in-situ consolidation, cold compaction, and hot forming. In-situ consolidation is being applied to the processing of all types of rapidly solidified materials. Cold compaction has the more limited objective of consolidation of amorphous metallic solids when the processing temperature is not permitted to exceed the crystallization temperature. Hot forming currently is applied extensively in the processing of all classes of microcrystalline alloys when exposure to elevated temperatures is necessary to obtain the flow and bonding of the quenched particles.

IN-SITU CONSOLIDATION

An established procedure in gas atomization is to increase the average cooling rate of the atomized product by allowing the atomized spray to undergo splat quenching on a chilled substrate (e.g., a water-cooled mandrel or drum). If sufficient care is exercised in controlling deposition rate, heat-transfer characteristics and other process variables, a thick deposit of rapidly solidified material can be built up by simply bonding together one splatted layer to another in a continuous manner. In spray rolling, the spray deposition rate is adjusted so that individual droplets of melt undergo efficient splat quenching prior to full densification in the pinch of the rolls (Singer, 1970; Latimer, et al., 1973). In the Osprey process, the atomized spray is collected in a mold at a location in the atomizing chamber where most of the particles are in the partially solidified, or mushy condition, producing hot pre-forms which are greater than 95 percent dense, usually 97-98 percent dense (private communication from A.R.E. Singer). When the mold is full, the hot pre-form is converted into the desired shape by closed-die forging. In spray casting, massive ingots are formed by slowly filling the mold with a spray of fine particles generated by the soluble gas atomization technique or some other atomization method (private communication from N.J. Grant).

Another development of some interest is the adaptation of the principles of self-quenching to the fabrication of bulk rapidly solidified material (Breinan and Kear, 1977). This is being done by the incremental buildup of deposited material on a rotating mandrel, making use of a sharply focused laser or electron beam to fuse one deposited layer to another in a continuous manner. The feedstock may be delivered to the mandrel in the form of a thin wire, a molten jet, or as a steady stream of powder particles.

Future work probably will be concerned with improving existing systems and with uncovering new opportunities for in-situ consolidation.

For example, an obvious next step in centrifugal atomization, specifically by the RSR process, would be to attempt spray deposition of a thin-walled cylindrical shape using a water-cooled rotating/reciprocating substrate surrounding the central rotary atomizer. A particular advantage of this technique is that the entire operation can be conducted in high vacuum, including subsequent hot forming to achieve full densification. Thus, any possibility of deleterious environmental interactions (e.g., surface gas reactions, and/or entrapment of insoluble gases) is eliminated.

COLD COMPACTION

Methods for the consolidation of amorphous metallic solids currently are limited to high-energy-rate forming techniques because of the characteristic high strengths of these materials and the need to conduct the operation at relatively low temperatures. High-energy-rate forming involves the rapid and efficient conversion of stored energy (chemical or electrical) at high energy densities into mechanical work at high strain rates. Energy densities of $\sim$0.1-1.0 kJ/cm^3 are sufficient for many shaping operations, whereas higher energy densities of $\sim$10-100 kJ/cm^3 are required for the joining of materials or the consolidation of powders. In explosive forming, the workpiece is located at some distance ($\sim$10-100 cm) from the explosive charge to even out the pressure distribution and to maintain the integrity of the workpiece surface (Thornton and Garrett, 1977). In explosive bonding, this separation is unnecessary and usually is avoided. For efficient energy transfer, the space between the charge and workpiece is filled with a medium of low compressibility, attenuation, and dispersion (e.g., water). Arrays of shaped charges are employed to profile the pressure distribution as required in the forming of complex shapes. About 25 percent of the initial stored energy is converted into mechanical work in well designed systems. This occurs typically in a time constant of $\sim 10^{-4}$ sec, which corresponds with the decay of the primary shock wave. Average strain rates are 100 sec^{-1}. In electrohydraulic forming, the energy released by capacitance discharge is rapidly deposited into a small volume element or channel in order to achieve the requisite high energy densities (Waniek, 1976). Using energy deposition rates of $\sim 10^{-5}$ sec, energy densities of $\sim$2 kJ/cm^3 are readily attainable, with energy conversion efficiencies of $\sim$20 percent. These parameters are comparable with those encountered in explosive forming; however, there are more restrictions on processing geometry in electrohydraulic forming owing to the reduced stand-off distance ($\sim$1 cm) for efficient hydraulic coupling. In electromagnetic forming, controlled mechanical deformation is achieved by the application of an appropriately high magnetic pressure to the workpiece. Working with magnetic field intensities in the range 50 kOe-1MOe, the effects in conducting materials range from cold deformation to melting. Deformation velocities are high and may amount to 10^5 cm/sec (Mach 3) with a field of 0.5 MOe.

In properly engineered systems, up to 90 percent of the stored electrostatic energy is transferred to the forming coil, and up to 25 percent appears as mechanical work. Electromagnetic forming offers extreme flexibility in the adjustment and control of operating parameters. Pressures, dynamic times, and force profiles can be selected to satisfy a range of practical requirements.

Although the processing of conventional materials by high-energy-rate forming techniques has been widely used in industry for some time, the application of these novel techniques to the processing of rapidly solidified materials has only just begun. The most notable achievement to date has been the utilization of explosive forming techniques to achieve full densification of amorphous metallic powder compacts and to bond amorphous metallic filaments to conventional crystalline material substrates (Cline, et al., 1977). It remains now to explore the potential of the whole range of available high-energy-rate forming techniques. Future work in this regard probably also will include exploring the potential of hybrid techniques. For instance, the combination of explosives and magnetic fields has led to the development of flux-compression techniques capable of yielding field intensities up to 20 MOe, which corresponds to 10^7 atm pressure. Compaction of large powder aggregates should be feasible by this method. Another likely development is the integration of the technologies of high-energy-rate forming and mechanical alloying (Benjamin, 1970). The latter is an established method for producing composite powder particles with controlled microstructures by the simple expedient of repeated cold welding and fracture of mixtures of powder particles in a high energy ball mill. Conceivably, this technique can be used to disperse amorphous particles in a soft, ductile matrix. This being the case, high-energy-rate forming techniques can be employed to obtain some strikingly novel microstructures in bulk components.

HOT FORMING

Hot forming techniques have been used to consolidate rapidly solidified powders or thin filaments in situations where the principal benefits of rapid solidification are seen to be improvements in homogeneity in distribution and volume content of hardening phases and unusual alloy and phase combinations in the finished product. Currently, the most widely used techniques are hot extrusion and hot isostatic pressing but some work has been done with hot mechanical pressing. Hot extrusion is favored because of the inherent possibilities for control of microstructure by varying extrusion parameters. Hot isostatic pressing is favored because of its near-net-shape processing capabilities and potential for reducing manufacturing costs.

The most sophisticated developments in hot forming technology have occurred in the processing of superalloy hardware (Bourdeau and Moore, 1977). Three distinct processing steps are employed to achieve the desired

microstructures starting from rapidly solidified superalloy powder. First, the powder is consolidated to theoretical density by hot extrusion, making sure that the extrusion parameters are adjusted to give an ultra-fine grained structure. Second, the extruded billet is hot worked into shape by controlled strain rate, isothermal forging--superplastic forging. Third, a textured columnar-grained structure is developed by directional recrystallization in a gradient annealing furnace. The significant property improvements attained by this processing sequence may be attributed to reduced segregation in the initial rapidly solidified powder. So far, this work has been restricted to conventional γ' precipitation hardened superalloys. Future work almost certainly will be directed towards combining γ' precipitation hardening with inert particle (e.g., carbides, borides) dispersion strengthening. This will necessitate higher melt quenching rates in order to achieve the requisite degree of supersaturation in the initial powder.

Other developments of equal significance have been made in the processing of Ti-, Al-, and Fe-base alloys. The titanium case is interesting in that the critical processing steps are performed in high vacuum (Maringer and Mobley, 1977). Thus, the initial rapid solidification of high aspect ratio filaments is carried out under vacuum by the pendant-drop technique, and subsequent consolidation is achieved by hot isostatic pressing using a hermetically sealed, evacuated container. In the aluminum case, new alloys are being developed specifically to exploit the extended solid solubilities that are readily attainable by rapid solidification. The parameters for hot forming are selected not only to achieve a fully dense product but also to yield the optimum phase decomposition strengthened microstructure. Much of the work on iron-base alloys has been concerned with generating novel microstructures by rapid solidification of conventional alloys (e.g., the tool steels). Some unique distributions of carbides phases have been produced by rapid solidification followed by hot isostatic pressing.

REFERENCES

Benjamin, J.S. 1970. Met. Trans., Vol. 1, p. 2943.

Bourdeau, R.G., and J.B. Moore. 1977. In Proc. Int. Conf. on Rapid Solidification Processing, p. 334.

Breinan, E.M., and B.H. Kear. 1977. In Proc. Int. Conf. on Rapid Solidification Processing, p. 87.

Cline, C.F., et al., 1977. In Proc. Int. Conf. on Rapid Solidification Processing, p. 308.

Latimer, K.G., et al., 1973. Paper presented at the Institute of Metals Conference on Modern Metallurgy, Oxford, England.

Maringer, R. and C. Mobley. 1977. In Proc. Int. Conf. on Rapid Solidification Processing, p. 208.

Singer, A.R.E. 1970. Met. and Mat., Vol. 4, p. 246.

Thornton, H.R. and D.R. Garrett. 1977. SAMPE Quart., Vol. 8, No. 4, p. 38.

Waniek, R.W. 1976. In New Trends in Materials Processing. ASM, Metals Park, Oh.

Chapter 8

PROPERTIES OF METALLIC GLASSES

MAGNETIC PROPERTIES

The magnetic properties of amorphous metallic alloys have been covered in several reviews. Wright (1976) critically evaluated the results on almost pure transition metal amorphous elements. The behavior of alloys was reviewed by Cargill (1975), Mizoguchi (1976), Tsuei (1976), Hasegawa, et al. (1976), Alben, et al. (1971), and Luborsky (1978). Amorphous alloys, viewed as soft magnetic materials for potential application, were reviewed by Egami, et al. (1975), Gyorgy, et al. (1976), and Luborsky (1977).

This discussion will be restricted to the transition metal-metalloid, TM-M alloys, which appear to be the most technologically significant. Both the fundamental and applications-oriented properties of these alloys will be summarized.

The local environment around each atom in an amorphous solid differs from site to site in contrast to that in a regular crystalline lattice. The effect of the resulting distribution of hyperfine interactions is not apparent in the magnetic moments, critical behavior, or anisotropies but is necessary to account for the details of the Mössbauer spectra and nuclear magnetic resonance. However, the major difference between the properties of amorphous and crystalline alloys comes from the change in the electronic environment around each atom caused by the metalloids, not from the structural disorder. Short-range order generally is maintained in amorphous alloys and is evidenced by similar trends in the properties that depend, to various degrees, on short-range order (e.g., saturation moment, Curie temperature, and magnetostriction).

Magnetic Moments

The moments of most amorphous alloys are lower than those of the pure crystalline transition metals they contain. However, the direct effect of the structural disorder is small. The moments are lower because of the change in the local chemical environment provided by the metalloids. The effects of the metalloids are apparent in Figure 10, which presents a comparison of the amorphous and crystalline alloys of both Fe and Co. The simplified rules based on the rigid-band model suggest that the moments of Fe and Co should fall linearly with addition of metalloid at a slope depending on the electrons available (e.g., 3 μ_B [Bohr magnetons] for each P, 2 μ_B for each Si or C, and 1 μ_B for each B atom). The results for Co all fall approximately linearly as expected, but the slopes of the curves for -P and -Si are essentially the same. The results for the Fe alloys are very different. Large additions of

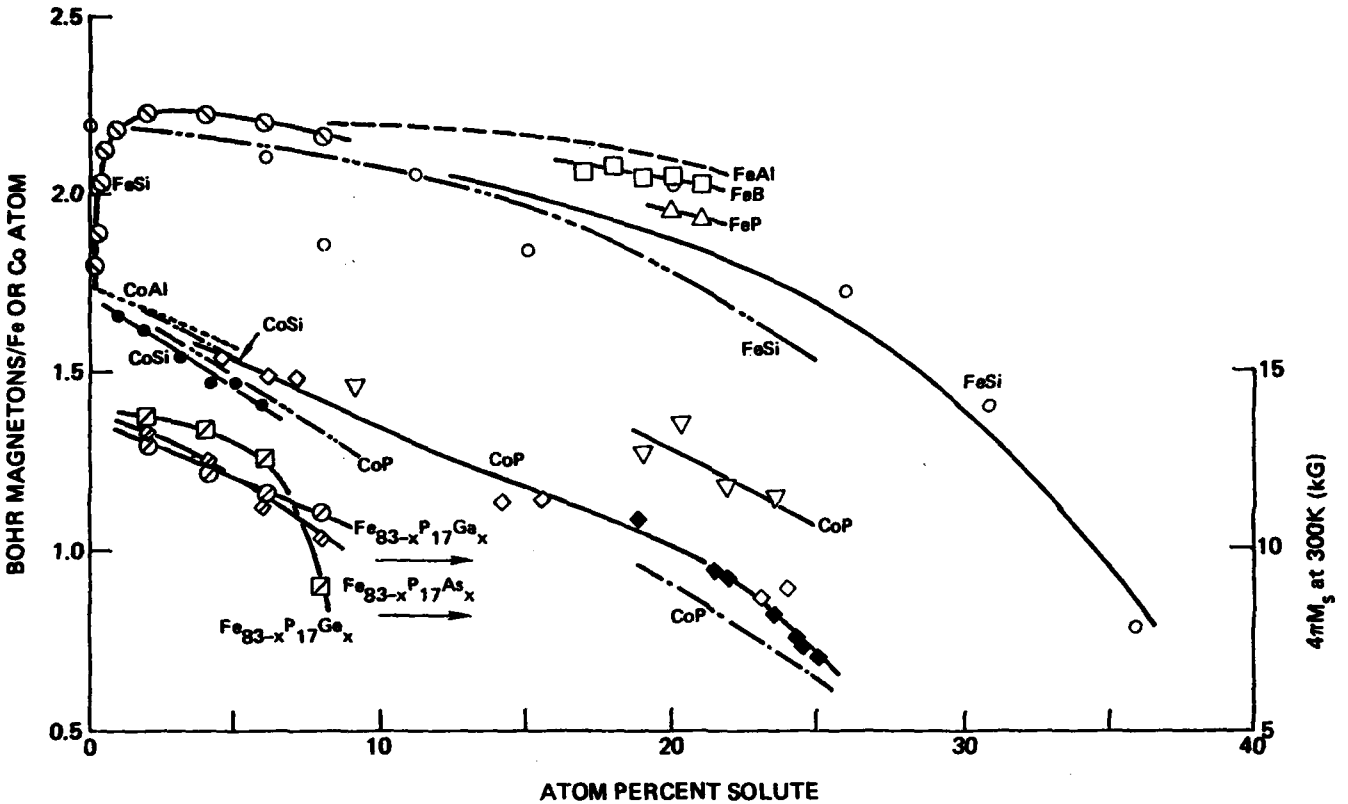

FIGURE 10 Magnetic moments at *O K* as a function of solute concentration. Crystalline alloys are shown by curves with no data points: FeAl, CoAl, CoSi, (Parsons et al., 1958); FeSi (Shimada and Kojima, 1976); CoP (Pan and Turnbull, 1974; Simpson and Brambley, 1971). Amorphous alloys are shown by solid curves with data points: FeSi ⊘ (Shimada and Kojima, 1976; Flesch, 1970); Co P ◊ (Karabe and Kanematsui, 1968), ◆ (Pan and Turnbull, 1974),▽ (Cargill and Cochrane, 1974),▼ (Simpson and Brambley, 1971); FeB ■ and FeP △ (Durand and Yung, 1977); CoSi ● (Felsch, 1970). Magnetization in $4\pi M_S$ for FePGe, -As, Ga ⊡ ⊘ ⊘ (Wiesner and Schneider, 1974).

metalloids (e.g., up to 20 at.%) have little effect on the moment. This cannot be explained by the simple rigid-band model. Also, the moments of the amorphous alloys decrease in the sequence -B, -P, -Si rather than -B, -Si, -P. The rise in moment for very small additions of Si to Fe is also anomalous. However, it is clear that the amorphous alloys have essentially the same moments as the crystalline alloys.

The results for binary transition metal amorphous alloys fortuitously follow the simple rigid-band model somewhat better. Results for Fe-Ni and Fe-Co alloys are shown in Figure 11. The moments of the FeNi amorphous alloys initially decrease approximately linearly with increase in Ni as in crystalline alloys. At an Fe fraction of $\sim$0.3, the moment starts to decrease more rapidly. This has been interpreted as a decrease in the Ni moment (Durand, 1977). The behavior of alloys in the range of 1 to 10 at.% Fe, was explained in terms of a transition from spin glass behavior at low concentrations to superparamagnetic behavior at higher concentrations. Alloys behave as homogeneous ferromagnets only above 10 at.% Fe. The moments of the Fe-Co-B alloys are qualitatively similar to those of crystalline alloys. In crystalline alloys the peak moment occurs at 60 at.% Fe, not near 90 at.%, and the peak moment is 15 percent greater than for pure Fe, not 10 percent, as for the amorphous alloy.

Transition Behavior

Amorphous ferromagnets usually have a well defined magnetic ordering temperature, T_c. This has been confirmed by magnetization, Mössbauer, and specific heat measurements. As in the results for magnetic moments, this Curie temperature behavior reflects the short-range order existing in amorphous alloys. A remarkable demonstration of this retention of short-range order was reported for amorphous Fe-P-B alloys (Durand and Yung, 1977; Durand, 1976). The same change in slope of the T_c vs. composition curve occurred for both the crystalline and amorphous alloys due to the change in phase of the crystalline alloys. Thus, the T_c of amorphous alloys is always significantly lower than that of crystalline alloys as a result of chemical composition, not structural disorder. Results for T_c of crystalline and amorphous alloys on addition of metalloids are shown in Figure 12. The CoP amorphous alloys appear to be a reasonable extension of the crystalline CoSi and CoAl results. The results for the amorphous Fe alloys are more complicated, showing, in fact, an increase in T_c with increase in solute for most of the reported alloys considered (Durand and Yung, 1977; Durand, 1976). This increase has been discussed (Durand and Yung, 1977) by comparing the amorphous Fe to face centered cubic Fe but is not really understood. It may arise, for example, from changes in the average Fe-Fe distance in the alloy as P and B are added.

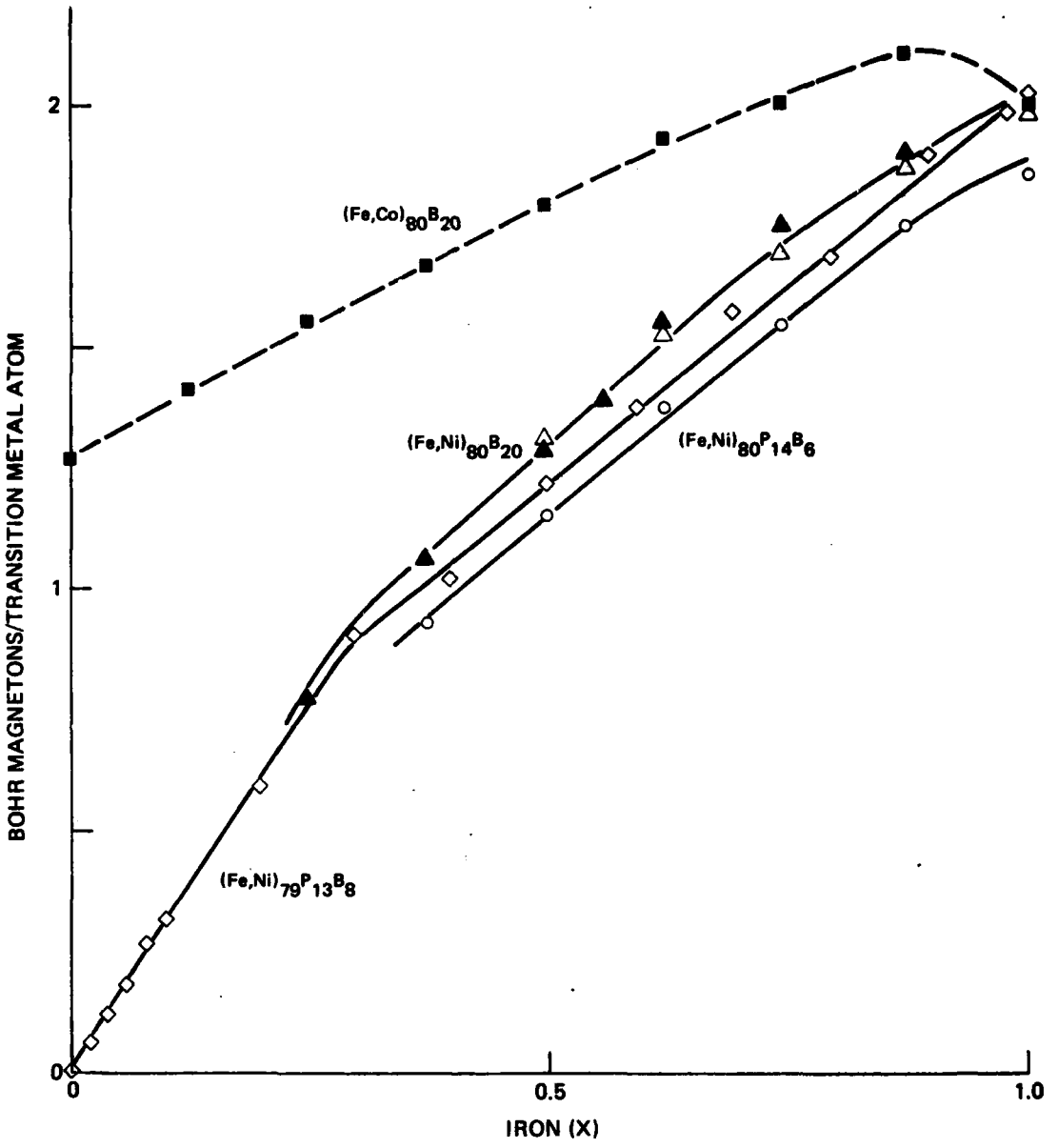

FIGURE 11 Moment per transition metal atom at O K for some amorphous alloys as a function of iron content: FeCoB (O'Handley et al., 1976); FeNiB△ (Becker et al., 1977),▲ (O'Handley et al., 1976); FeNiPB◊ (Durand, 1977),○ (Becker et al., 1977).

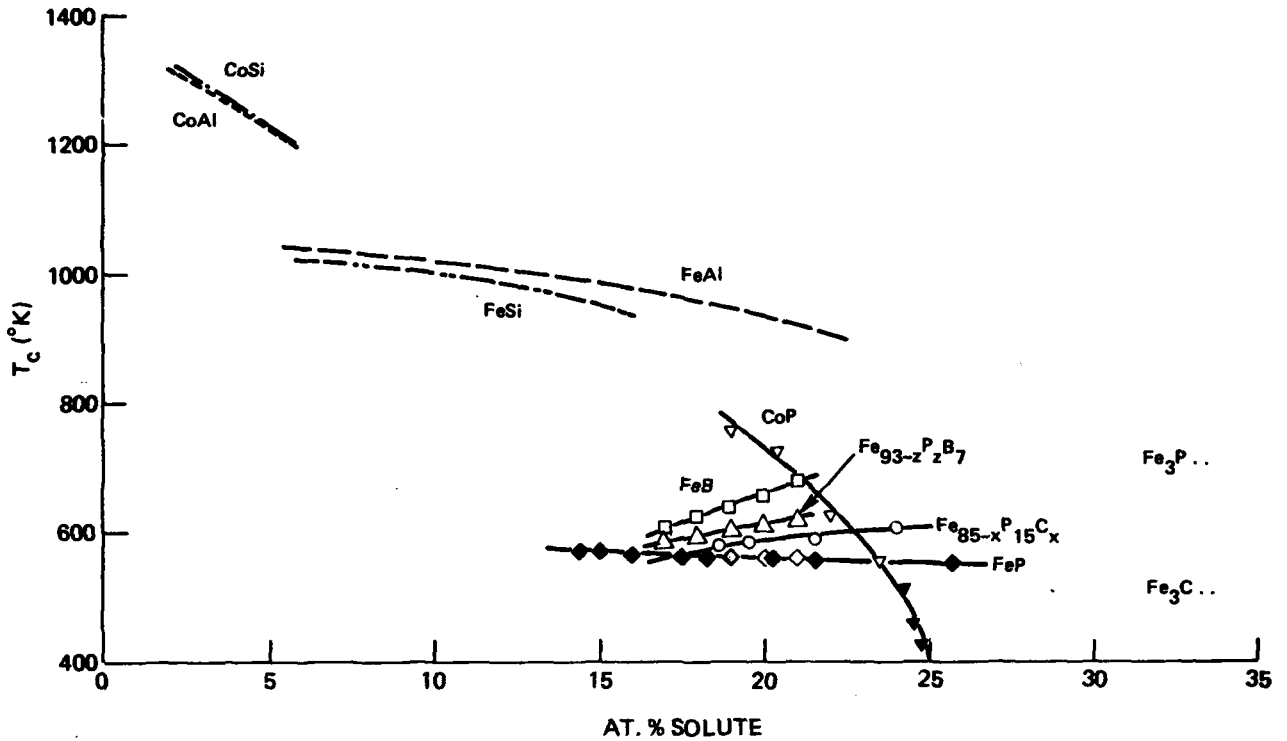

FIGURE 12 Curie temperatures as a function of solute concentration. Crystalline alloys are shown by the broken curves without data points: FeAl, FeSi, CoAl, CoSi (Parsons et al., 1958) Fe_3P, Fe_3C (Chen, 1973). Amorphous alloys are shown by solid curves with data points: ▼ CoP (Pan and Turnbull, 1974), ▽ CoP (Cargill and Cochran, 1974); □ FeB and ◊ FeP (Durand, 1976 and 1977); ◆ FeP (Logan, 1975); ○ FePC (Chen, 1973) where at .% solute = 15 + X; △ FePB (Durand and Yung, 1977) where at .% solute = 7 + Z, typical of a family of reported curves.

Curie temperatures for FeNi alloys vary with transition metal composition for fixed metalloid concentrations (Figure 13). This type of variation of T_c may be systematized by using the phenomenological model described by Kouvel (1969). The molecular field model, modified so that the individual atomic moments vary in magnitude with their local environment is used. For disordered crystalline alloys, an explicit expression is derived that contains the interaction temperatures. The solid curves in Figure 13 were fitted (Luborsky, 1978) using this model normalized at x = 1. Below approximately x = 0.4, the results could not be fitted because of the large change in moment not allowed for in the model. The dashed curves simply follow the data points.

Magnetostriction

Magnetoelastic properties also depend directly on short-range atomic interactions. Magnetostriction coefficients have been reported for a variety of FeNi- and CoNi-metalloid amorphous alloys (Brooks, 1976; Arai, et al., 1976; O'Handley, et al., 1976; Fujimori, et al., 1976; unpublished information from P.J. Flanders and F.E. Luborsky). The significant points to note are that: (1) the saturation magnetostrictions, λ_s, in Fe-rich alloys are large and opposite in sign to values for polycrystalline Fe; (2) the λ_s in Co-rich glasses is negative and comparable in sign to that in crystalline cobalt; (3) the negative λ_s of the cobalt-rich FeCo glasses is also observed in the Ni-rich CoNi glasses reported by Simpson and Clements (1975). O'Handley, et al., (1976) has shown that the λ_s for the FeNiB glasses varies as M_s^2 but that the FeCoB behavior is considerably different. The difference in behavior has not yet been clarified (Cargill and Cochrane, 1974). The discrepancy in the λ_s between amorphous and polycrystalline alloys in the Fe-rich region is most probably related to the differences in short-range order.

Directional Order

In the case of magnetic ordering (Slonczewski, 1963), the magnitude of K_u is expected to be a function of the anneal temperature, θ; the magnetization at the anneal temperature, M_θ, at the measurement temperature, M_T, and at 0 K, M_o; the concentrations of the ordering atoms, C_A and C_B as given by:

$$K_u = Af(c)\ (M_T/M_o)^2 (M_\theta/M_o)^{2/\theta} \quad , \tag{11}$$

where A is a constant that depends on the atomic arrangement and the range of interactions considered. For dilute solutions for monatomic directional order, f(c) = c is the concentration of the ordering species.

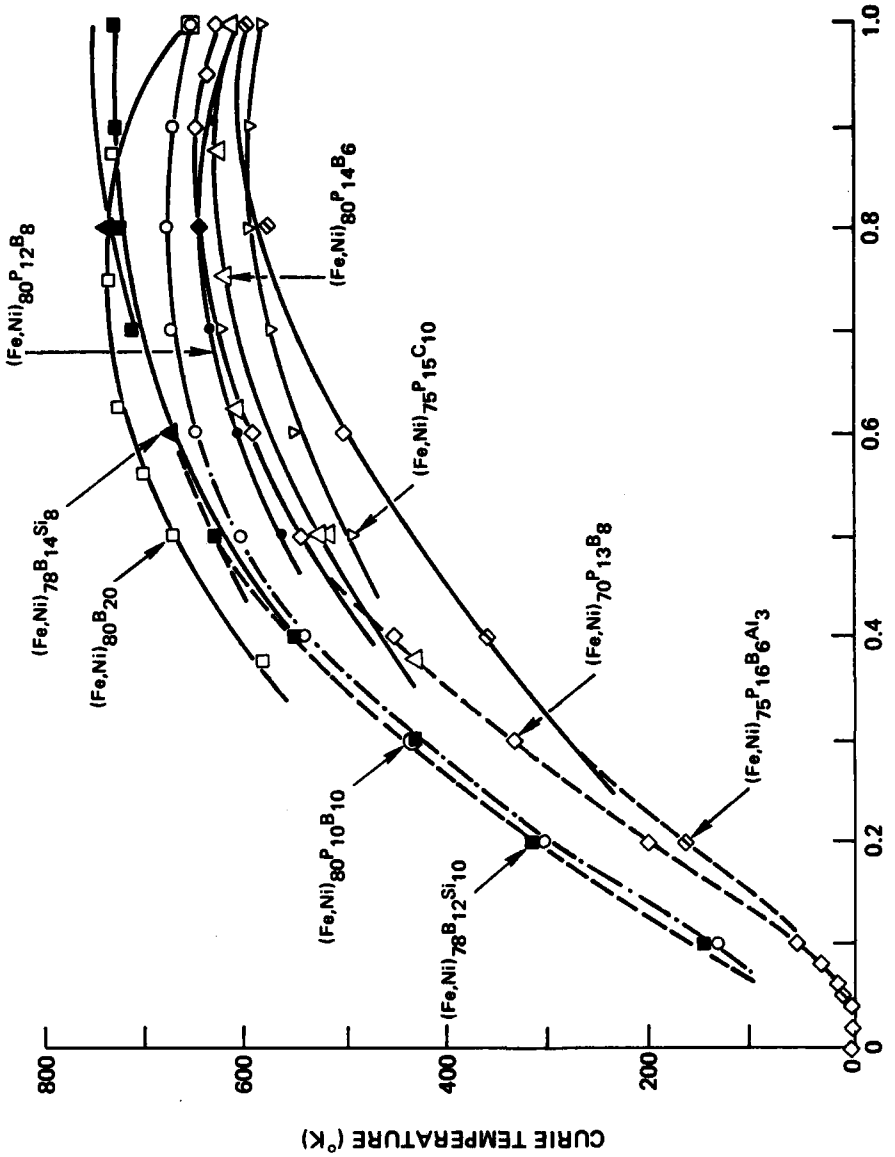

FIGURE 13 Curie temperatures of amorphous FeNi alloys. Solid lines were calculated using phenomenological model and dashed lines follow data: FeNiB and FeNiPB (Becker, et al., 1977; Durand, 1977; Mizoguchi, et al., 1973); FeNiSIb (Masumoto, et al., 1977); FeNiPC (Hasegawa and Dermon, 1973); FeNiPBAl (Gyorgy, et al., 1976).

For diatomic order, $f(c) = c_a^2$ where c_a is the concentration of the dilute species. If neither constituent is dilute, but assuming ideal solutions (i.e., for negligible nonmagnetic interaction energy), then:

$$f(c) = Nn\, c_a^2 c_b^2/2, \qquad (12)$$

where N is the number of atoms per unit volume and n is the number of possible orientations of each pair referred to a crystal lattice. For nonideal solutions, the effective nonmagnetic interaction energy must be included in the expression for f(c) as described by Luborsky and Walter (1977). In amorphous alloys, the interaction energy is expected to be negative (i.e., leading to precipitation). These relations for amorphous Fe-Ni-B alloys were studied in detail by Luborsky and Walter (1977). The reported values of K_u are shown in Figure 14. The direction and magnitude of K_u can be changed reversibly by changing the field direction and anneal temperature. The nonzero value of K_u at x = 1 is interpreted as being due to ordering of the boron. The temperature dependence observed fits the theoretically expected dependence on anneal temperature. The dependence of K_u on Fe-Ni composition follows the theoretical dependence for nonideal solid solutions with a negative interaction energy (i.e., of the type leading to precipitation as expected).

Fujimori, et al. (1977) studied the magnetically induced anisotropy in $(Fe_xCo_{1-x})_{78}Si_{10}B_{12}$ amorphous alloys. Their results for the maximum values of K_u obtained by annealing in a field for 15 minutes at increasing temperatures are shown by the solid circles in Figure 14. The same values were obtained by cooling in a field at a rate of 1.6 degrees per minute as shown by the solid squares. Although these results are of interest from a practical viewpoint, they are difficult to interpret quantitatively in terms of directional order theory because of the uncertainty concerning the anneal temperature and whether equilibrium was achieved at any temperature. Directional order theory predicts a decrease in induced anisotropy as the anneal temperature increases. The decrease in K_u as the anneal temperature is decreased further is the result of the slower kinetics of orientation at low temperature, suggesting that equilibrium was not achieved. The general requirement that two different metal atoms are necessary to obtain a large K_u was further demonstrated by Fujimori, et al. (1977) by adding small amounts of Pd, Ni, or Cr as well as the Fe to CoSiB (Figure 15).

Reorientation Kinetics

There have been a few studies of the kinetics of the reorientation of the directional order anisotropy, K_u. The time constants for this reorientation for various amorphous alloys are shown in Figure 16 as are those for similar crystalline alloys without the metalloid additions.

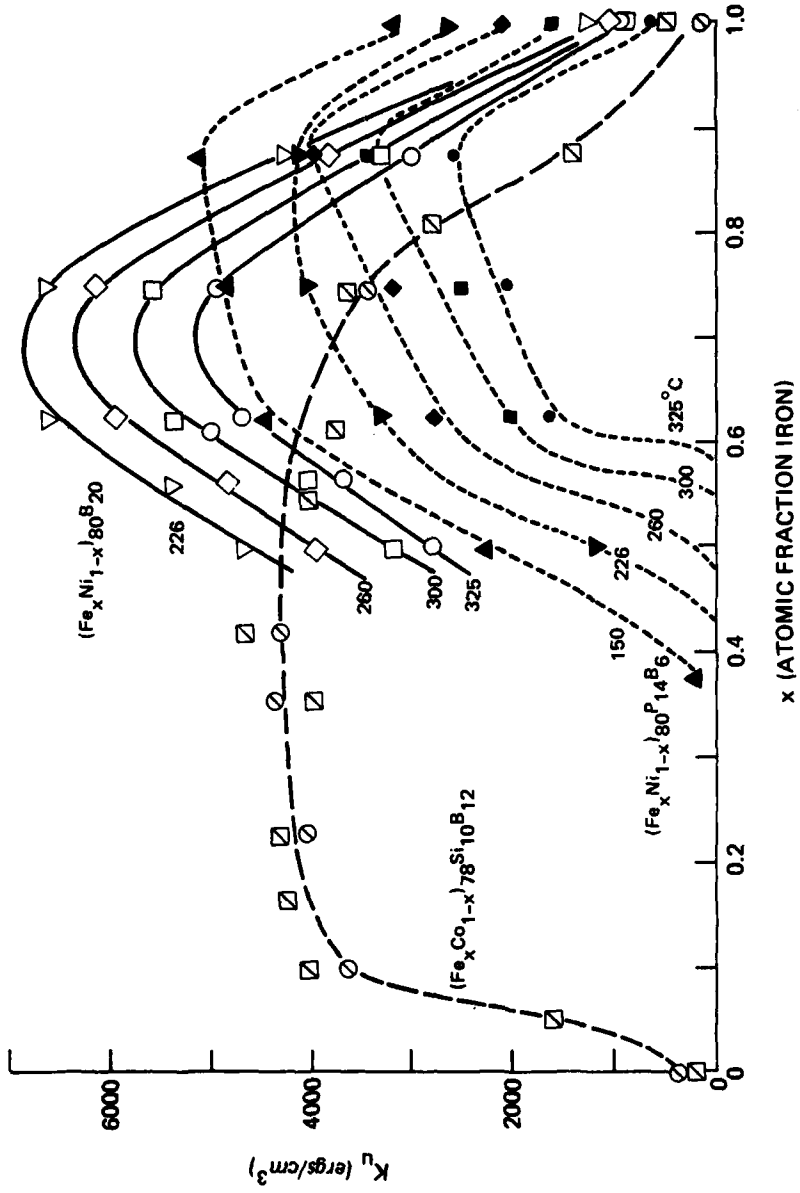

FIGURE 14 Magnetically induced anisotropy as a function of composition. Open symbols are used for FeNiB (Luborsky and Walter, 1977), and solid symbols, for FeNiPB (Luborsky and Walter, 1977), both annealed to equilibrium at each temperature. Slashed symbols are used for FeCoSiB for ⊘ maximum values obtained by heating 15 min. at successively higher temperatures and for ⊡ cooling from 380°C at 1.6 deg/min calculated from (Fujimori et al., 1977).

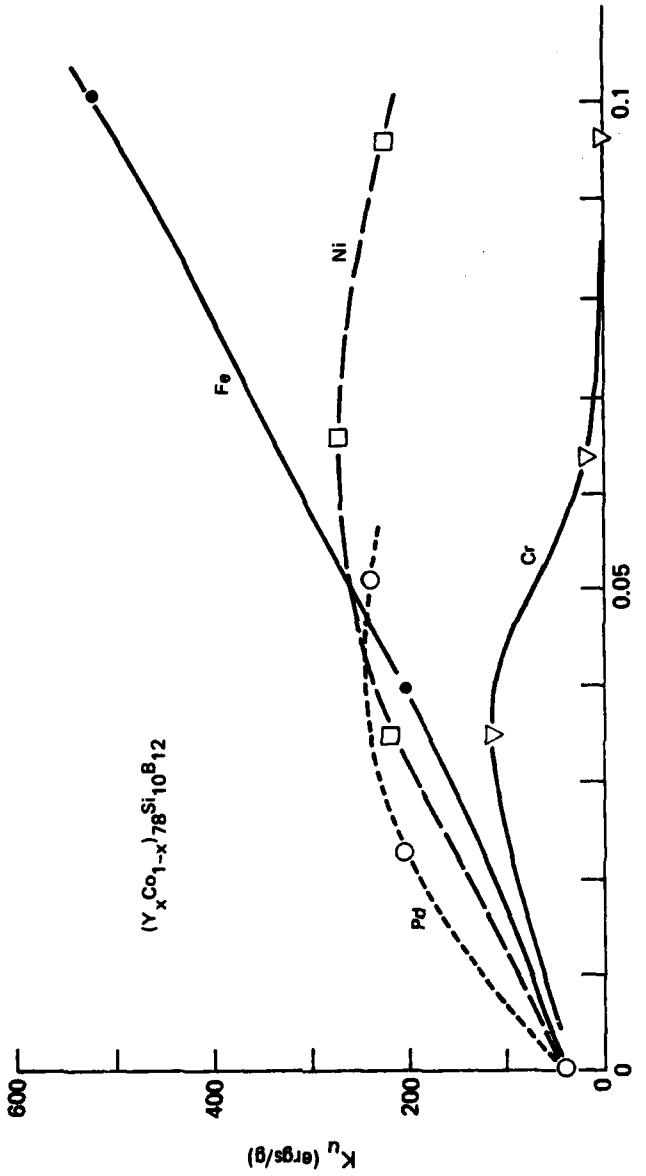

FIGURE 15 The maximum magnetically induced anisotropy for small additions of Fe, Ni, Pd, or Cr to CoSiB (Fujimori, et al., 1977). Maximum values from heating 15 minutes successively higher temperatures

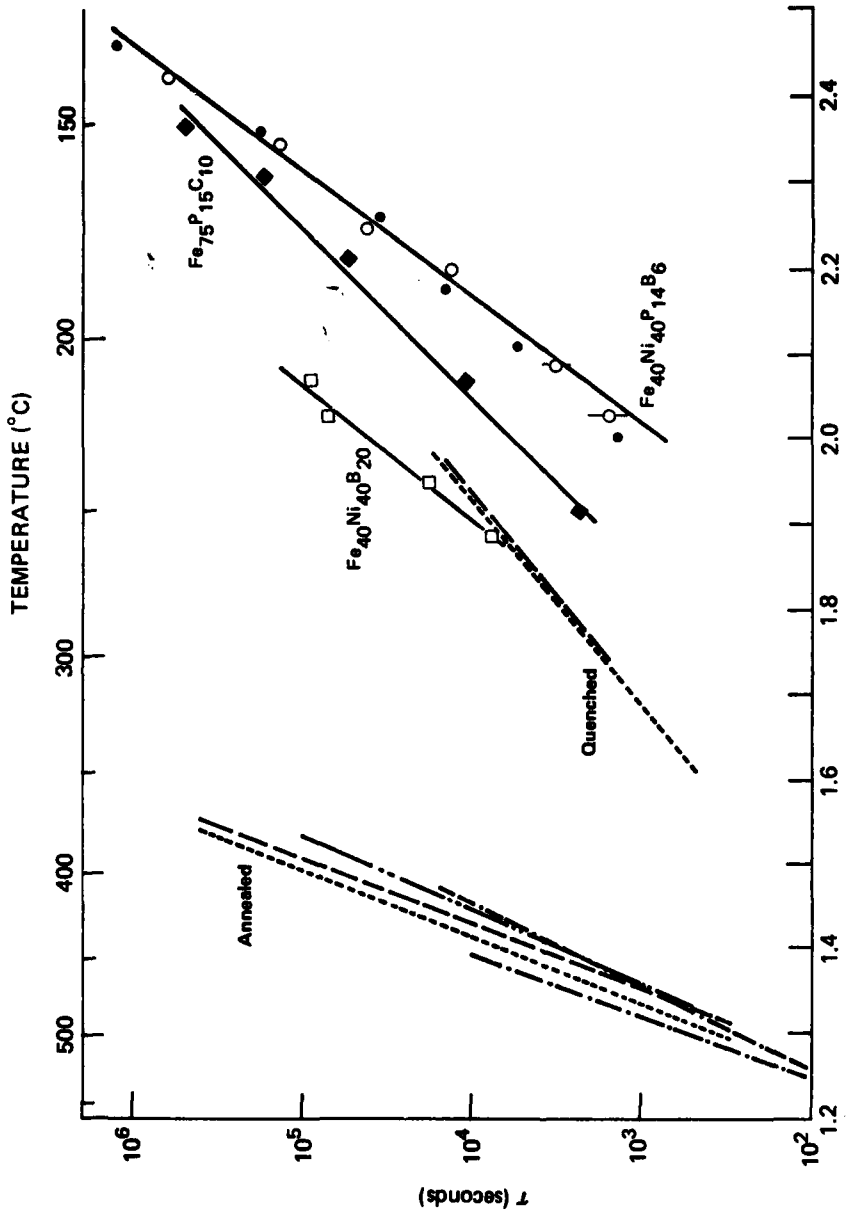

FIGURE 16 Time constants for the reorientation of the induced anisotropy in some amorphous alloys shown by the solid curves with data points: FeNiPB O Luborsky (1976), ● Berry and Pritchet (1976); FePC Berry and Pritchet (1976); FeNiB Luborsky and Walter (1977). Crystalline alloys shown by broken curves---40Fe-60Ni, ...15Fe-85Ni; -.-.20-50Fe-Ni, -.-.-.16 Fe-84Ni; --.--20Fe-20Ni-60Co. References given in Luborsky (1977).

It is clear that the behavior of the amorphous alloys is more closely related to that of the quenched crystalline alloys rather than to that of the annealed crystalline alloys. In the quenched alloys, the rate-determining step in the reorientation has been associated with the excess vacancies present. Thus, it has been suggested that the disordered structure of the amorphous alloys has produced a similar atomic environment and similar kinetics for the reorientation. The $Fe_{40}Ni_{40}P_{14}B_6$ alloy surprisingly exhibited simple first-order kinetics in the reorientation of its anisotropy as measured by the changes in its remanent magnetization ratio, M_r/M_s. This suggests that a uniform atomic environment exists around the reordering species. On the other hand, the reorientation kinetics of the $Fe_{40}Ni_{40}B_{20}$ alloy did not exhibit simple first-order kinetics; the kinetics could be fit with a distribution of time constants or by second-order kinetics with equal concentrations of the two species. Note that the time constants obtained for the $Fe_{40}Ni_{40}P_{14}B_6$ alloy by Lubo[illegible]rsky (1976) using magnetic measurements and by Berry and Pritchet (1976) using measurements of the ΔE effect using a vibrating reed agree.

Stress-Induced Order

These alloys also are susceptible to stress-induced ordering as studied by Berry and Pritchet (1976) using internal friction measurements. As in crystallizing alloys, this ordering presumably occurs via the interactions of the strain-produced with the magnetostriction. The activation energy for stress induced ordering, determined from the internal friction measurements, for $Fe_{75}P_{15}C_{10}$, $Fe_{40}Ni_{40}P_{14}B_6$, and $Fe_{80}B_{20}$ was 2.2, 2.6, and 2.6eV (210, 250 and 250kj/mole), respectively. These activation energies are about twice as large as the values for magnetic ordering. It is, therefore, concluded that stress-induced directional ordering involves different atomic species of motions than those involved in magnetically induced ordering. In addition, the final state produced by the two ordering processes must be different. Table 7 summarized some of these activation energies by comparing the stress-induced with the magnetically induced changes.

TABLE 7 Activation Energies[a] for Various Reversible Anneal Processes in Amorphous Alloys

Alloy	Pretreatment Temp. (°C)	Pretreatment Time (min)	ΔE_s eV	ΔE_s kcal/mole	ΔE_m eV	ΔE_m kcal/mole	Reference
$Fe_{40}Ni_{40}P_{14}B_6$		none	2.6	60	1.35	31	Berry and Pritchet, 1976
	360	120	–	–	1.4	32	Luborsky, 1976
$Fe_{80}B_{20}$		none	2.6	60	–	–	Berry and Pritchet, 1976
$Fe_{75}P_{15}C_{10}$		none	2.2	51	1.0	23	Luborsky, 1976
$Fe_{40}Ni_{40}B_{20}$	325	120	–	–	0.7-1.7	16-39	Luborsky and Walter, 1977c
$Fe_{80}P_{13}C_7$	250	60	1.6-2.0	37-46	–	–	Soshiroda et al., 1976
$Fe_{80}P_{13}C_7$	340	10	1.4-2.7	33-61	–	–	Soshiroda et al., 1976

[a] ΔE_s from internal friction by frequency change method; ΔE_m from magnetic annealing.

Coercive Force, Losses, and Permeability

The extrinsic properties of an amorphous ferromagnet depend on anisotropy, magnetization, exchange energy, inclusions and other defects, surface roughness, sample thickness, strain, and fluctuations in properties in the same manner as in conventional crystalline soft materials (Luborsky, 1977 and 1978; Gyorgy, et al., 1976). The optimum coercive forces (H_c), losses (w), and permeabilities (μ) achieved to date in various amorphous alloys have been summarized (Luborsky, 1977 and 1978). In all cases, the best properties are obtained after minimizing the contribution of the stress-magnetostriction anisotropy by a stress-relief anneal (Luborsky, et al., 1975). Full stress relief can be achieved in most alloys before crystallization starts; however, the stress relief rate depends on the original melting and quenching conditions. The available results for losses in amorphous alloys are shown in Figure 17 for alloys after stress relief. No attempt was made to minimize surface roughness effects or to evaluate the contribution of inclusions or fluctuations in M_S or K. The properties still depend on magnetostriction (Luborsky, 1977). Conventional soft magnetic alloys show essentially the same induction and frequency dependence. For comparison, the losses of some typical crystalline alloys are shown by the letters only for 1 kHz and 1000 G. The amorphous alloys, to date, do not have quite as low losses as the best NiFe alloys but are much better than the FeSi and FeCo alloys. In addition, the amorphous alloys already have higher M_S values than most of the available NiFe alloys and promise to be much less expensive to produce. Similar results are obtained on comparing H_c or μ (Luborsky, 1977 and 1978).

ELECTRICAL PROPERTIES

In a structurally ordered metal, deviations from perfect periodicity in the atomic arrangement govern the transport mechanism for conduction electrons. Among many such disturbances, thermal vibration and impurity potentials are known to be the major ones that contribute to the electrical resistivity of the material. In metallic glasses, on the other hand, conduction electron mean free paths are short due to their highly disordered structures. The major contribution to the resistivity originates from the structural disorder rather than from thermal vibration, impurity potentials, etc. Many metallic glasses are based on transition metals which, in some cases, introduce additional scattering processes involving d-electrons.

The room temperature resistivity values, ρ(RT), thus far reported for metallic glasses range from about 80 $\mu\Omega$-cm (for $Pd_{80}Si_{20}$) to about 330 $\rho\Omega$-cm (for $Mn_1Ti_{49}Be_{40}Zr_{10}$). For nonmagnetic metallic glasses such as Pd-Si, the resistivity varies as T^2 at low temperatures (T<100K) and as T at higher temperature (100K<T>crystallization temperature). The temperature coefficient ($d\rho/dt$) near room temperature changes from positive for low resistivity materials to negative for high resistivity materials, having a zero temperature coefficient near ρ (RT) $\sim$150 $\mu\Omega$. It is relatively easy to design metallic glasses with ρ (RT) $\sim$150 $\mu\Omega$-cm.

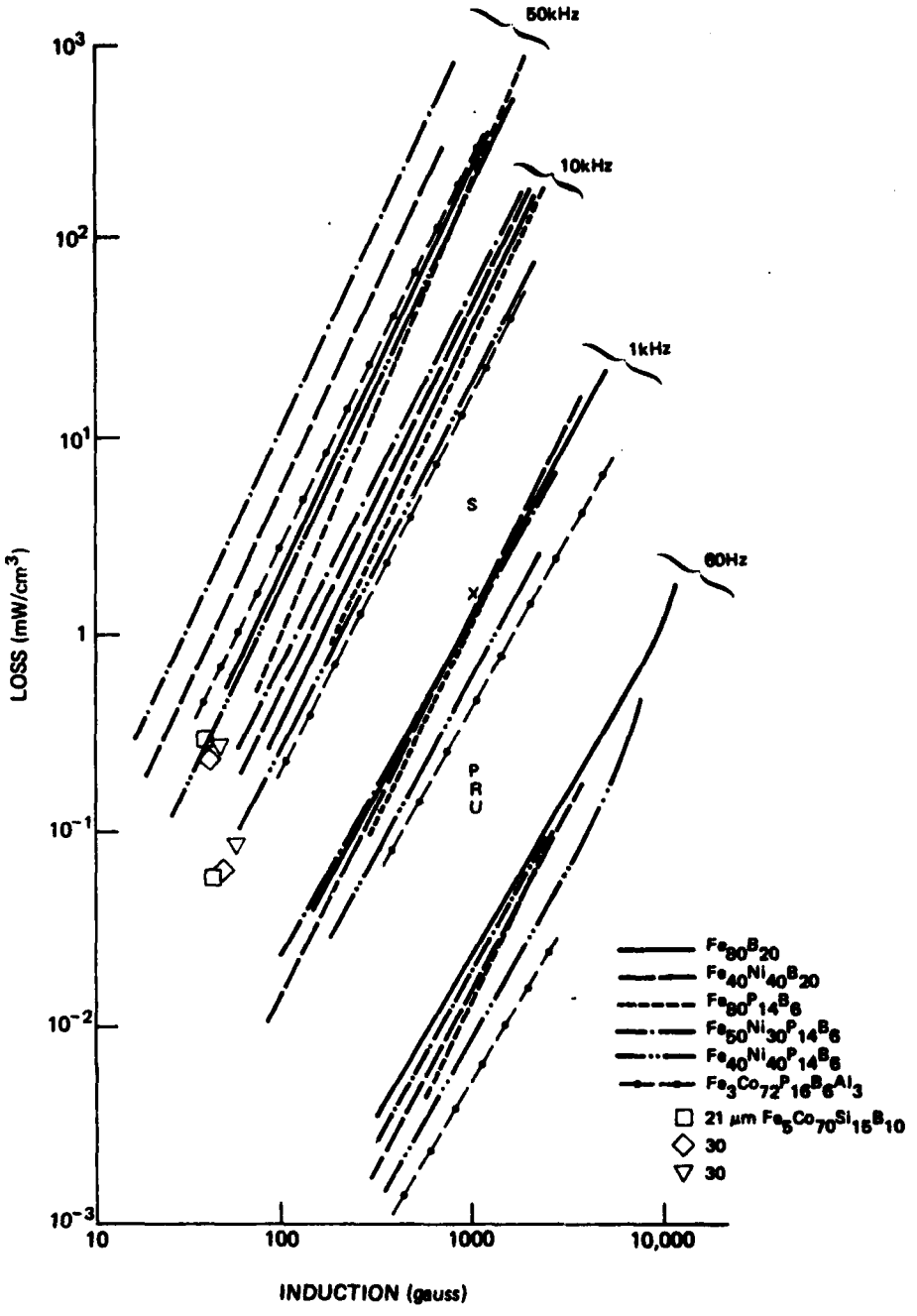

FIGURE 17 Core loss vs. induction for amorphous alloys at various frequencies after a stress-relief anneal. Samples 25-50 μm thick (Luborsky, 1977). Conventional commercial alloys of same thickness shown only at 1000 G and 1 kHz P = 4-79 Permalloy, R = Square Permalloy, S = Silectron, U = Supermalloy, X = Deltamax.

AD-A086 000 NATIONAL MATERIALS ADVISORY BOARD (NAS-NAE) WASHINGTON DC F/G 11/6
AMORPHOUS AND METASTABLE MICROCRYSTALLINE RAPIDLY SOLIDIFIED AL--ETC(U)
MAY 80 N J GRANT, C F CLINE, L A DAVIS MDA903-78-C-0038
UNCLASSIFIED NMAB-358 NL

2 OF 2
AD A086000

END
DATE FILMED
8-80
DTIC

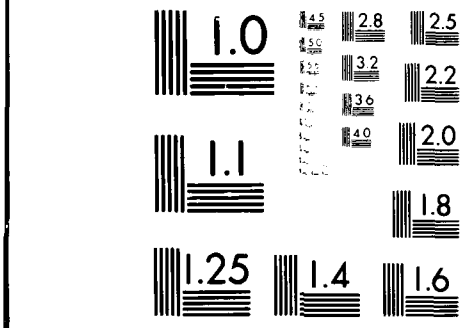

MECHANICAL PROPERTIES

Strength

Among the many unique physical properties of a metallic glass, none is more striking than its strength at temperatures well below T_g where the E/σ_y ratio is about 50. Glasses have been identified, (e.g., $Fe_{80}B_{20}$) that exhibit remarkable strengths ($\sim$370 Kg/mm^2). Since metallic glasses do not work harden, their tensile strengths must be equal to or less than their yield strengths; yielding and failure occur simultaneously. One is able to uniquely identify this occurrence from the mode of failure of the sample. According to plasticity theory (Hill, 1967), a thin sheet will yield (following von Mises' criterion) in a zone whose normal makes an angle θ = 35.3 degrees with the tensile axis and 90 degrees with the thickness vector. Accordingly, the included angle (90 - θ) measured on a wide face at the fracture tip of a specimen which fails coincident with yielding should be $\sim$55 degrees. Failure geometry closely approximating this has been reported for glassy $Ni_{49}Fe_{29}P_{14}B_6Si_2$ strips (Davis, 1975). It also was observed for those alloys (Davis, et al., 1976; unpublished data from S. Takayama) whose tensile yield strengths are listed in Table 8 (except for $Pd_{77.5}Cu_6Si_{16.5}$, where the tensile results are for wires)(Davis, 1975); σ_y values observed range from $\sim$147 Kg/mm^2 for $Pd_{77.5}Cu_6Si_{16.5}$ to $\sim$370 Kg/mm^2 for $Fe_{80}B_{20}$. Similar high-strength behavior, relative to the elastic moduli and in selected cases on an absolute scale, is expected for metallic glasses that contain no metalloids. Although direct measurements of the true yield strengths of such glasses generally are not available in the literature, the yield strength can be estimated from the measured microhardness. Alloys containing large amounts of refractory metals can have yield strengths well above that listed in Table 8 for $Fe_{80}B_{20}$.

In order to observe the 55 degree mode of failure at $T<<T_g$, one must test specimens with a reduced area gauge section with a width to thickness (w/t) ratio of the order of 8:1. If smooth, uniform cross section ribbons are tested, failure typically is initiated at the grips and occurs by tearing (mode III, antiplane strain) (Tetelman and McEvily, 1966). If a reduced section specimen with w/t>>8 is pulled, failure will occur by tearing across the gauge section but at a somewhat higher stress due to elimination of the grip constraint. One therefore has the sequence of failures shown schematically in Figure 18 for Ni-Fe base metallic glasses (Davis, 1975). Tensile strength data in the literature (except as noted in Table 8) invariably pertain to mode III failure on straight strips. If the specimen edges are ragged, one may expect, of course, even lower relative strength than indicated by Figure 18. For composite reinforcement applications, uniform cross section ribbons (or wires) will be used. In this case, the lateral constraint of the matrix may be sufficient to prevent mode III failure, allowing the full intrinsic strength of ribbons to be realized.

TABLE 8 Mechanical Properties of Metallic Glasses

Alloy	H (Kg/mm^2)	σ_y (Kg/mm^2)	H/σ_y	E (10^3 Kg/mm^2)	E/σ_y
$Ni_{36}Fe_{32}Cr_{14}P_{12}B_6$ (METGLAS® 2826A)[a]	880	278 tension (12)	3.16	3.16 (12)	52
$Ni_{49}Fe_{29}P_{14}B_6Si_2$ (METGLAS 2826B)[b]	792	243 tension (11)	3.26	13.2 (53)	54
$Fe_{80}P_{16}C_3B_1$ (METGLAS 2615)[a]	835	249 tension (12)	3.35		
$Fe_{80}B_{20}$ (METGLAS 2605)[c]	1100	370 tension (9)	2.97	16.9 (9)	45
$Pd_{77.5}Cu_6Si_{16.5}$[d]	498	157 comp. (51)	3.17	8.97 (53)	57
		147 tension (13)	3.39		
$Pd_{64}Ni_{16}P_{20}$[e]	452	158 comp. (52)	2.86	9.37 (54)	59

NOTE: H and σ_y have uncertainties of the order of ±5 percent.
[a]Takayama, S. unpublished data.
[b]Davis, L. A., Scripta Met. Vol. 9, 1975, p. 339.
[c]Davis, L. A. et al. Scripta Met. Vol. 10, 1976, p. 541.
[d]Davis, L. A. and Kavesh, S. J. Mat. Sci. Vol. 10, 1975, p. 453.
[e]Chen, H. S. et al. J. Non-Cryst. Solids Vol. 18, 1975, p. 157.

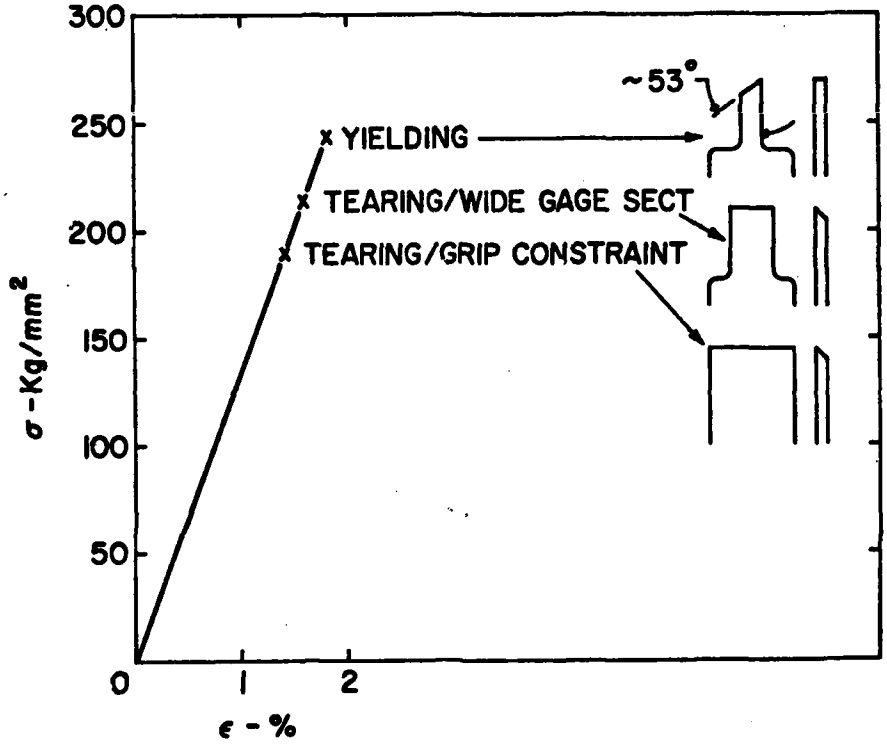

FIGURE 18 Tensile strength and failure mode for Ni-Fe base metallic glasses (Davis, 1975).

Figure 18 is shown with the σ-ε curve linear to failure. Curves often reported in the literature show considerable curvature (reduced slope) prior to separation. This curvature is either an artifact associated with the nature of the specimen, grip, and machine interaction (Davis and Kavesh, 1975) or, perhaps, a nonlinear elastic response at high stress as exhibited, for example, by Fe single-crystal whiskers (Brenner, 1956). Accordingly, often reported (Chen and Wang, 1970; Masumoto and Maddin, 1971 and 1975, Leamy, et al., 1972) yield stresses predicted from the onset of nonlinearity and occasionally carefully labeled "apparent" σ_y are misleading.

Tensile Failure

a. Axial Symmetry or Plane Stress

Tensile failure of glassy alloy wires and strips (plane stress) is accompanied by intense plastic shear deformation. This is true whether the macroscopic mode of failure is brittle (tearing, antiplane strain, mode III failure) or ductile (yielding). In the former case, the shear deformation is localized at the tip of a crack, which propagates across a ribbon in the manner of a screw dislocation (i.e., on a plane of maximum shear stress in a direction perpendicular to the shear direction and the tensile axis). In the case of yielding, the shear deformation zone develops over the entire cross section of the specimen (ribbon or wire) before, or coincident with, failure. In both cases, tearing and yielding, failure occurs by shear rupture through the intense shear zone. Hence, in the microscopic sense, the failure mode is ductile and the fracture surface features observed are identical.

An example is shown in Figure 19 for a $Pd_{77.5}Cu_6Si_{16.5}$ glassy alloy wire that failed coincident with yielding at ambient temperature and pressure (Davis and Kavesh, 1975). The fracture topography includes a featureless shear offset zone, which lies in an arc to the right of the fracture surface (the brush markings in this region are an artifact associated with handling), and a ridge or vein pattern. The observation of this pattern was first noted by Leamy, et al. (1972) who used stereo pair scanning electron micrographs to demonstrate that the veins are hills, not steps, on a smooth background. They also found, after allowing for the relative shear of the specimen, that the opposing fracture surfaces are essentially mirror images of one another; this finding was confirmed by Pampillo and Reimschuessel (1974).

As separation occurs through the shear zone, it is apparent (Figure 19) that failure is initiated by shear disk cracks (i.e., cracks with extended dimensions in the shear zone and minimal thickness to the zone). These cracks expand like dislocation loops and their intersections produce the system of veins observed. As noted by Leamy, et al. (1972), the effects of adiabatic heating may be significant near the terminus of failure. This would lead to viscous necking of the material remaining

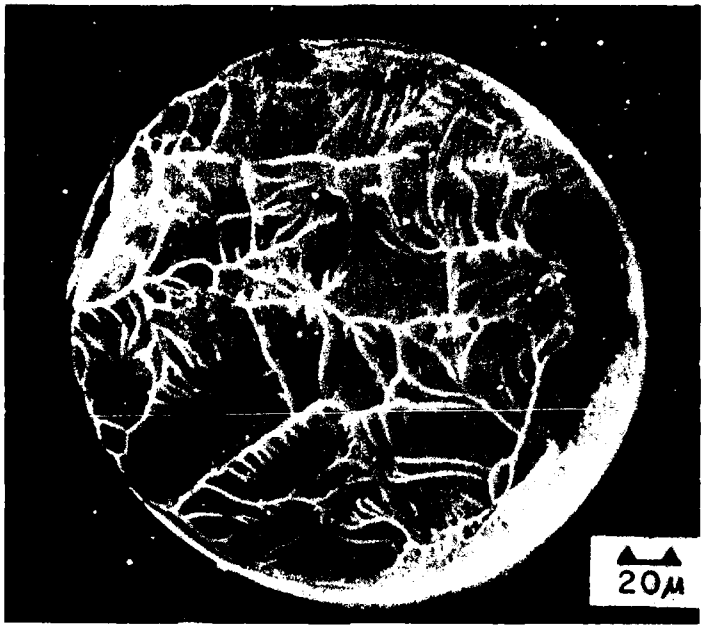

FIGURE 19 Fracture surface of $Pd_{77.5}Cu_6Si_{16.5}$ wire fractured at 1 atm. The fracture surface is inclined at ≈45°, sloping down from left to right (Davis, 1978).

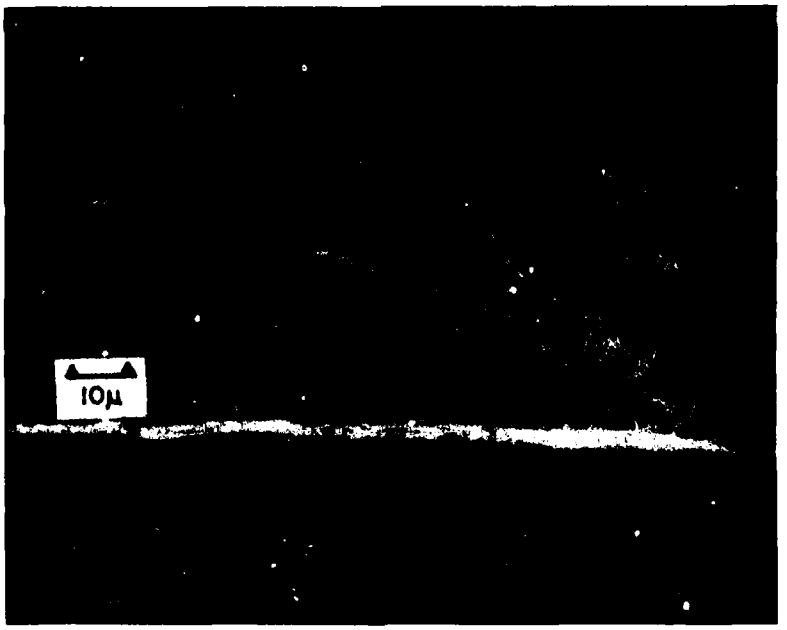

FIGURE 20 A portion of the failure surface of a $Ni_{39}Fe_{39}P_{14}B_6Al_3$ strip. The crack propagation direction is to the left.

between the closely approaching cracks, rather than cracking through, thereby producing the smoothly rounded veins observed (Pampillo and Reimschuessel, 1974).

b. Plane strain

Plastic instability (yielding) and tearing are the favored modes of failure of nominally notch-free glassy alloy wires or ribbons at ambient temperature. At low temperature (Pampillo, 1975; Pampillo and Polk, 1974) or in the presence of a sharp crack in a thick specimen at ambient temperature, crack propagation and failure may occur under plane strain conditions. For example, by means of electric discharge machining (EDM) one may place a small hole (~0.1mm diameter) at the center of a glassy alloy "panel." When this panel is subjected to cyclic loading, fatigue cracks will nucleate at either side of the hole and propagate until catastrophic failure occurs.

Figure 20 shows a section of a failure surface so produced (Davis, 1975). The edge of the EDM hole lies at the extreme right of the micrograph (the fracture features are symmetric about the center of the hole). Adjacent to the hole, the surface is marked by a series of fatigue striations apparently associated with periodic oscillations of the direction of fatigue crack propagation at ±45 degrees from horizontal. Near the center of the micrograph, a sharp boundary marks the onset of catastrophic failure, and to its left, the surface markings tend to approach horizontal. In larger sections it is apparent that these markings have a V-shaped conformation with the apex of the V pointing towards the origin of the crack. This pattern may be recognized as classical chevron markings of the type observed in the failure of steel sheets (Cottrell, 1964).

Creep Strength

Creep strengths of two alloys (with aligned grain structure) are shown in Table 9.

TABLE 9 Creep Rupture Results of RSR 185 and Mar-M200 Alloys Having Aligned Grain Structures

	Temperature		Stress				
ID	°F	°C	ksi	MPa	1% (hr)	Life (hr)	El (%)
RSR-185	1400	760	100	689	176.4	787.5	6.9
RSR-185	1800	982	50	345	14.5	22.2	2.9
RSR-185	2000	1093	30	207	29.9	34.6	4.4
Mar-M200	1400	760	95	655	120	170	14
Mar-M200	1800	982	31.5	217.2	19	55	25
Mar-M200	2000	1093	11	75.8	70	100	30

NOTE: Data from Bernard H. Kear—personal communication Nov. 7, 1978.
Composition: RSR-185-Ni, 6.8 Al, 14.4 Mo, 6.1 W, 0.4 C.
Mar-M200-Ni, 9 Cr, 10 Co, 2 Ti, 5 Al, 12.5 W, 1 Cb, 0.015 B, 0.05 Zr, 0.15 C.

Embrittlement

A variety of amorphous metallic alloys with the general composition of $(Fe, Ni, Co)_{\sim 80}$ $(P, C, B, Si, Al)_{\sim 20}$ have been reported in the literature. These alloys, if quenched rapidly enough when prepared, are extremely strong and deform plastically on bending without fracturing. The stability of these glasses and the influence of composition on stability have been discussed by many authors. The atomic mobility in the amorphous phase is expected to scale roughly as T/T_g where T_g is the glass transition temperature. Hence, any compositional changes that increase T_g should increase the stability of the glass phase. This increased resistance to short-range structural rearrangements is seen in increased resistance to crystallization. However, a number of authors have noted that these amorphous alloys become brittle when heated for relatively short times at temperatures several hundred degrees below their glass transition temperature. Gyorgy, et al. (1976) gives a boundary line for embrittlement in the amorphous alloys in the series $(Co, Ni, Fe)_{75}P_{16}B_6Al_3$ for various binary combinations of transition metal elements. In studies of $Fe_{40}Ni_{40}P_{14}B_6$, it was found that annealing at temperatures up to a few degrees of the initiation of crystallization caused no significant change in the heat of crystallization, in the x-ray or electron diffraction pattern, or in the structure as revealed in high resolution electron microscopy in both bright and dark field. Increased small-angle x-ray scattering was observed as was a small increase in micro-hardness, stress-relief, and the embrittlement described above. Examination of fractured surfaces of annealed samples, by Auger spectroscopy, revealed the presence of regions of high phosphorus concentration. It was concluded that the embrittlement was the result of the diffusion of phosphorus at these low temperatures. Very recently, it was reported that iron-nickel alloys with only boron as the glass former were more stable than alloys with both phosphorus and boron. Based on results of Luborsky and Walter (1976), it was suggested that the increased stability is the result of the removal of the phosphorus. Typical curves of fracture strain as a function of annealing for P-containing and P-free alloys are shown in Figure 21. Chen (1976) has examined the embrittlement of $Fe_{40}Ni_{40}P_{20-x}B_x$ alloys and concluded that only alloy glasses containing both P and B show enhanced embrittlement and that there exists no unusually fast diffusive processes connected with phosphorus which cause embrittlement of glasses.

The kinetics of embrittlement, stress relief, and crystallization of $Fe_{40}Ni_{40}B_{20}$ metallic glassy ribbons obtained by different melt spin quenching processes also were investigated. Ribbons made with higher rates of quenching exhibit better mechanical stability than those made with lower quenching rates. The thermal stability, temperatures, and activation energies for crystallization of all ribbons, however, are identical. The rates of stress relief are higher for ribbons made with higher quenching rates. Values of activation energy for stress

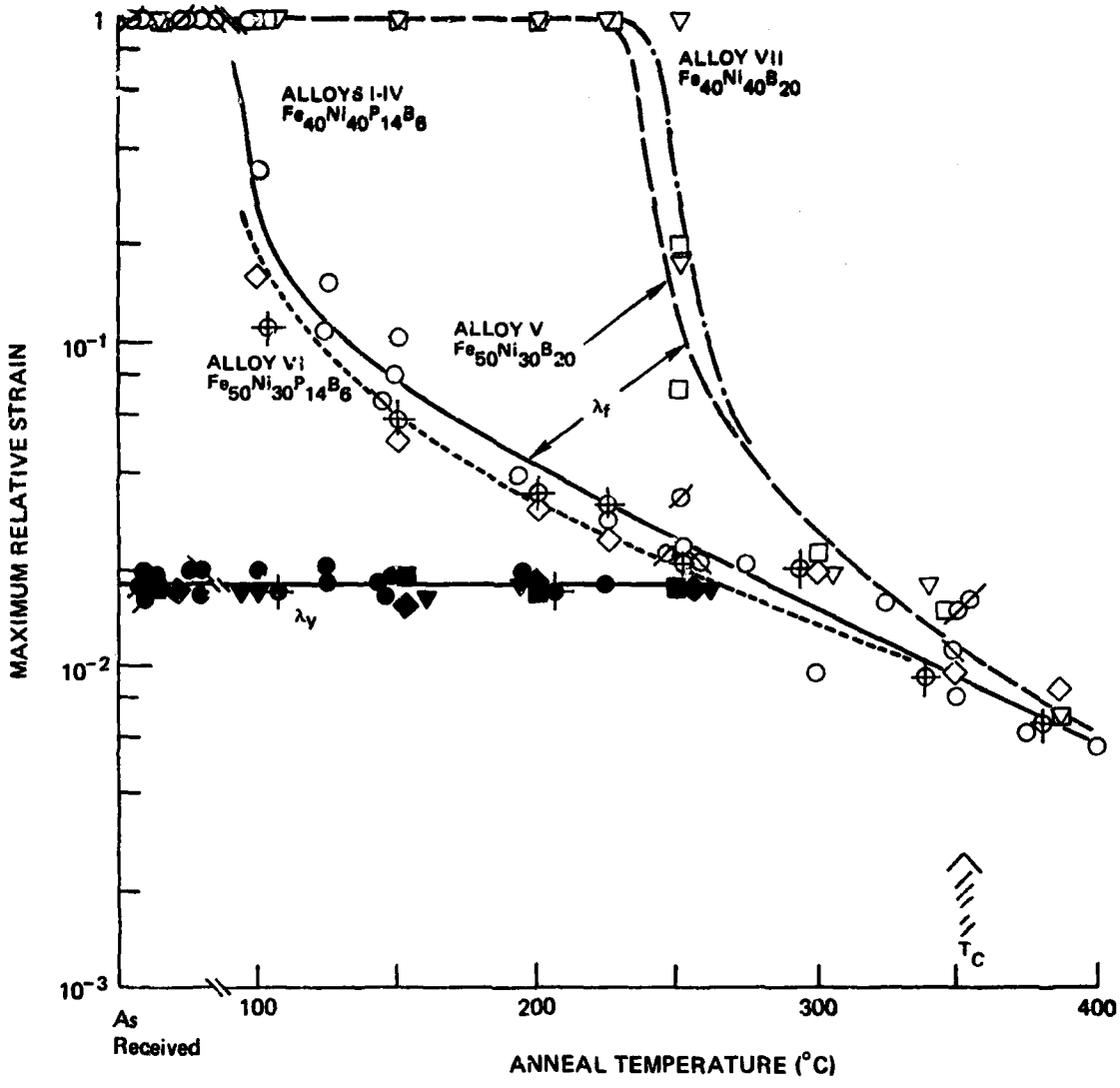

FIGURE 21 Maximum relative strain to fracture λ_f and to yield λ_y for various amorphous alloys as a function of annealing temperature. Annealing time is 2 hours.

relief are about the same for all ribbons. These activation energies for stress relief also are close to those values reported for structural relaxation. Chen (1976) noted that the embrittlement temperature differs by 100 K for Fe-based glasses obtained under different quenching conditions. Typical results are shown in Figure 22.

Hardness

An indication of the strength of a ductile material is provided by measurement of its microhardness (Gilman, 1973). For example, the ratio of hardness (Vickers/136 degree diamond pyramid) to yield stress (H/σ_y) for crystalline metals typically is $\sim$3 (Tabor, 1951). This value is predicted approximately (for the two-dimensional case) by slip-line field analysis (Hill, 1967) in which a basic assumption is that the material underlying the indentation will act rigidly. Material adjacent to the indentation is expected to behave plastically, moving along slip lines and heaving up around the sides of the indenter to form a "coronet." Precisely such behavior has been observed for hardness indentations in metallic glasses (Leamy, et al., 1972; Davis, 1975). Accordingly, the average H/σ_y observed (Table 8) for metallic glasses ($\sim$3.2) is close to the theoretical value; the hardness of an ultra-high-strength alloy such as $Fe_{80}B_{20}$ is then a remarkable 1100 kg/mm^2. In principle, because the hardness test is done under compression conditions, one should use the compression yield stress to calculate H/σ_y when σ_{yc} and σ_{yt} differ. If the results for $Pd_{77.5}Cu_6Si_{16.5}$ are typical (Table 8), σ_{yc}/σ_{yt} for metallic glasses is approximately 1.05. Hence, H/σ_{yc} for glassy alloys is $\simeq$3.

The metalloid-free metallic glasses have microhardnesses that range from 150-200 kg/mm^2 for Ca-based glasses (St. Armand and Giessen, 1978) to 400-650 kg/mm^2 for binary Zr-Cu glasses to 1100 kg/mm^2 for $Ta_{55}Ir_{45}$ (Davis, 1978). The addition of metalloids to the alloys which also contain refractory metals will lead to even higher hardnesses, for example, 1500 kg/mm^2 for alloys such as $Mo_{48}Ru_{32}B_{20}$ (Johnson and Williams, 1979). Such alloys will have remarkably high yield strengths and, when ductile, corresponding tensile strengths.

It also is noted that, unlike crystalline metals, a correlation is found between the microhardness of the metallic glass and its Young's or shear modulus. Further, the elastic moduli of the metallic glass generally scale with those of the corresponding crystalline phases. Thus, the high hardness of metallic glasses containing significant amounts of refractory metals, which have high elastic moduli in their crystalline phases, is not unexpected.

The indentation behavior of metallic glasses is distinctly different from that of nonmetallic glasses (e.g., silicate glasses) which, due to their covalent bonding, exhibit plastic-elastic rather

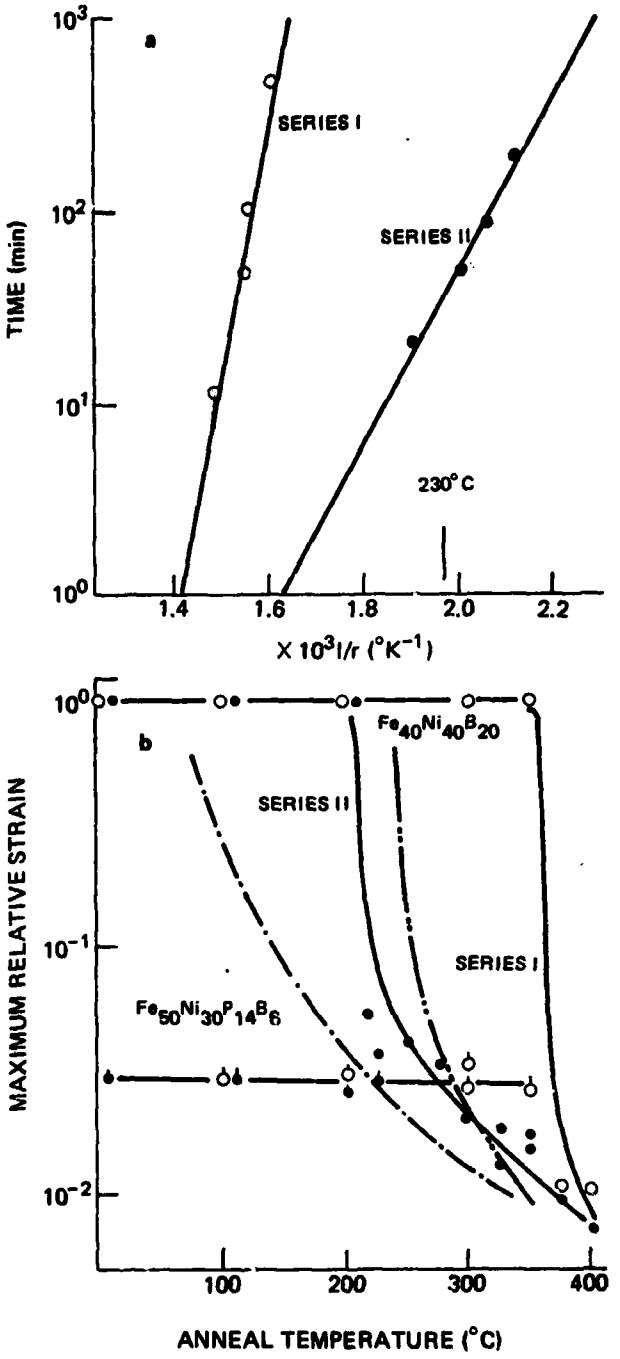

FIGURE 22 a) the rates of transformation for both series ribbons at $\lambda_f = 10^{-1}$. b) relative strain for yield (ȯ, ȩ) and for fracture (o, •) as a result of 2h isochronal annealing, as well as results for $Fe_{50}Ni_{30}P_{14}B_6$ and $Fe_{40}Ni_{40}B_{20}$.

than plastic-rigid behavior when indented. This results in a "sinking in" impression. Marsh (1964) developed a theory for such behavior that predicts a decrease of H/σ_y with increasing σ_y/E and yields $H/\sigma_y \simeq 1.6$ for silicate glasses. This, then, leads to a realistic estimate of σ_y, which is unmeasurable for such glasses; using the ratio $H/\sigma_y \simeq 3$, one makes the unreasonable prediction that σ_y is <u>less</u> than the observed <u>brittle</u> fracture strength. As noted above, an analogous situation occurs with metallic glasses (i.e., when the mode of tensile failure is brittle [tearing] it should be recognized that one <u>cannot</u> look to the σ-ε curve to define a yield stress).

<u>Anelastic Behavior of Metallic Glasses</u>

In his recent review Berry (1978) has identified three major mechanisms that can lead to anelastic effects and internal damping in metallic glasses. These are the magnetostrictive effect, the thermoelastic effect, and the inherent viscoelasticity of metallic glasses. Of these, the first is present only in ferromagnetic alloys, and the second is present only in nonhomogeneous strain fields incorporating important gradients of pressure since the effect is only a result of the dilational part of the stress tensor. On the other hand, the third mechanism is inherent to any glassy state and is present in all alloys and in all strain fields. Its strength, however, decreases sharply at low temperatures.

a. <u>*The magnetostrictive effect*</u>.

In alloys, particularly those with large ferromagnetic components, an important magnetostrictive effect can be present. In such alloys under an applied magnetic field, the application of a stress can evoke, in addition to the normal small strain elastic response, a substantial magnetostrictive strain response that comes from stress-induced displacement of domain walls and rotations of domains. The magnitude of such additional strains usually is measured by a fractional change of modulus $\Delta E/E$. If ε_e, ε_{m1}, and ε_{m2} are out-of-phase magnetostrictive strain, respectively, the fractional change of in-phase modulus is:

$$\frac{\varepsilon_{m1}}{\varepsilon_e} = \frac{\Delta E}{E} = \frac{E_e - E}{E} , \qquad (13)$$

where E_e is the normal Young's modulus and $E = \sigma/(\varepsilon_e + \varepsilon_{m1})$ is the in-phase total modulus that incorporates the in-phase magnetostrictive contribution. Berry (1978) reports that such fractional changes in moduli are normally of the order of 0.1 in as-quenched glasses but can be coaxed to become as high as 0.92 by magnetic annealing treatments that enhance domain wall anisotropy. Additional delayed

rearrangements of domain walls and domain rotations result in out-of-phase strains ε_{m_2} that then produce magnetostrictive damping. The logarithmic decrement δ that results from this effect,

$$\delta = \pi\left(\varepsilon_{m_2}/(\varepsilon_{m_1} + \varepsilon_e)\right) , \qquad (14)$$

is proportional to the fractional change in modulus and can be coaxed together with the latter to show substantial changes due to magnetic annealing treatments. Both $\Delta E/E$ and δ reach their maximum value under well defined levels of magnetizing force. For example, in metallic glass $Fe_{75}P_{15}C_{10}$, $\Delta E/E$ and δ values of 0.1 and 5×10^{-3} exhibited at very small and very large magnetizing force, can be increased by fully one order of magnitude to values of 0.92 and 45×10^{-3} under a magnetizing force of about 10 Oersteds.

b. Viscoelasticity as a source of anelasticity.

In a glassy material, the local disorder that has been widely characterized by a distributed free volume permits local shear relaxations in very small volume elements. The studies of Argon and Kuo (in press) on an analog structure of a glass consisting of a disordered bubble raft not only have elucidated how free volume may be distributed in a hard sphere glass but also have clarified the mechanism of inelastic deformation in glassy solids. These analog studies have demonstrated that free volume in the form of intersitial cavities is continuously distributed with a peak value somewhat larger than the intersitial in a corresponding close packed structure and a rapidly decaying tail that goes to much larger interstitial cavity sizes. Shearing experiments of such disordered bubble rafts have demonstrated that a large fraction of the local shear transformations that produce relaxation under stress are triggered at sites of large free volume and involve cooperative rearrangements between a large number of bubbles—with the transforming regions being usually of about 5 sphere diameters. Such observations have lent support to, and provided mechanistic understanding of, the continuously distributed relaxation processes that are common in all glassy substances. Many investigators have noted that, in addition to a few weak characteristic damping peaks at low temperatures that glasses exhibit, they show a smoothly rising "background damping" that increases monotonically with increasing temperature and dominates by far any characteristic peak at temperatures nearing T_g. The available information on this behavior is consistent with the existence of a continuous density distribution of $f(\Delta F)$ of free energies ΔF of thermally activated internal rearrangements in small volume elements Ω_f that can undergo shear transformations of magnitude γ_o under an applied shear stress σ. Thus, in a constant stress creep experiment, after a time t of application of the stress, this distribution of transformable sites produces a shear strain rate

$\dot{\gamma}$ that can be given by:

$$\dot{\gamma} = (\sigma\Omega_f\gamma_o/2kt)\int_0^\infty \Omega_f\,(\Delta F)\,\dot{\psi}\,(t,F,T)\,d\Delta F, \qquad (15)$$

where $\psi = 1 - \exp\,[\,-2\nu_G t \exp\,(-\Delta F/kT)\,]$ is the characteristic creep function that operates on the distribution function $f(\Delta F)$ of free energy barriers of the transformable complexes (Argon, 1968). Thus, under a given stress at a given temperature T as time goes on, a certain portion of the continuous distribution of shearable sites can be transformed to a relaxed form with the help of thermal agitation. This transformed portion depends on the level of temperature that governs the rate of advance of the creep function ψ. Clearly, by dimensional considerations, the free energy ΔF_o of the shearable sites that contributes most strongly to the strain rate after a time t of the inception of the experiment is:

$$\Delta F_o \simeq kT\,\ell n\,(2\nu_G t)\,, \qquad (16)$$

where ν_G is the characteristic normal mode frequency of the relaxing complexes. By similar considerations, the activation free energy of the relaxation process that makes the principal contribution to damping in air oscillatory experiment carried out at a frequency ν will be given also by Equation 13 where t is to be replaced by ν^{-1}. Clearly, then, the level of damping under those conditions will depend on $f(\Delta F_o)$.

In a series of recent creep and step-wise recovery creep experiments, Argon and Kuo have measured the distribution functions $f(\Delta F)$ of five different metallic class alloys consisting of three Cu_xZr_{1-x} alloys where x = 0.4, 0.56, 0.6, an alloy of $Al_{20}Cu_{25}Zr_{55}$, and finally the often investigated alloy of $Pd_{80}Si_{20}$. In all of these metallic glasses, Argon and Kuo have found that the functions $f(\Delta F)$ rise monotonically from very low values at $T_g/2$ to quite substantial values at a temperature of T_g-100 where the viscous flow component begins to rapidly dominate. The high end cut-off activation energies in these distributions have been found to vary from 45.8 Kcal/mole for $Pd_{80}Si_{20}$ to 55 Kcal/mole for the $Al_{20}Cu_{25}Zr_{55}$ glass, which represents almost exactly the measured activation free energies of isostructural viscous flow in these glasses in initially stabilized forms.

Berry (1978) has shown further that prolonged annealing of metallic glasses at temperatures that stabilize the glass but do not result in crystallization establishes a nearly unique distribution $f(\Delta F)$. On the other hand, Berry goes further and demonstrates that, once crystallization

sets in, the lower energy positions of the distribution are rapidly eliminated and that this modification continues unabated until the spectrum is nearly completely eliminated resulting in very low levels of background damping when crystallization is complete.

Fracture Toughness

Fracture toughness values for metallic glasses have been determined from shear tear tests (Kimura and Masumoto, 1975) and from single-edge-notch (SEN) and center-cracked-panel (CCP) tension tests (Davis, 1975). In the first case, the tearing energy, G, is given by G = 2F/t, where F is the force required to extend the tear and t is the specimen thickness (Rivlin and Thomas, 1952). The fracture toughness, K_{IIIc} (critical stress intensity for mode III crack propagation), is computed as:

$$K_{IIIc} = (G\mu)^{1/2} \quad . \tag{17}$$

In the case of tension (Knott, 1974):

$$K_c \simeq \sigma_f \sqrt{\pi a} \quad , \tag{18}$$

where σ_f is the nominal tensile failure stress and a is the half length (CCP) or total length (SEN) of the so-called "notional" elastic crack (Knott, 1974).

It has been demonstrated that the fundamental fracture mechanics relation given by Equation 18 holds for the dependence of fracture stress on crack half length (CCP) for ∿43 -μm-thick ribbons of glassy $Ni_{39}Fe_{38}P_{14}B_6Al_3$ (Davis, 1975). Fracture toughness values for ∿25 -μm-thick $Ni_{48}Fe_{29}P_{14}B_6Al_3$ ribbons and ∿75 -μm-thick $Ni_{49}Fe_{29}P_{25}B_6Si_2$ ribbons also were determined and are shown along with those for the alloy in Figure 23. The minimum toughness observed (∿30 $kg/mm^{3/2}$) is the plane strain (mode I) fracture toughness, K_{Ic}. With decreasing thickness, the state of mechanical constraint changes from plane strain toward plane stress with a corresponding increase in toughness. The shear tear toughness for the Ni_{39} alloy (Davis, et al., 1976) is plotted as the peak toughness in a thickness range (4 to 8 μm) equivalent to two times the shear lip thickness observed (∿2 to 4 μm) adjacent to a plane strain failure (Davis, 1975). The value cited for comparison for $Fe_{80}P_{13}C_7$ is a factor of 1.36 less than that reported by Kimura and Masumoto (1975) because more appropriate values of E(≃14 x 10^3 Kg/mm^2) and ν(0.4) were used to calculate μ and hence, K_{IIIc} from their value of G.

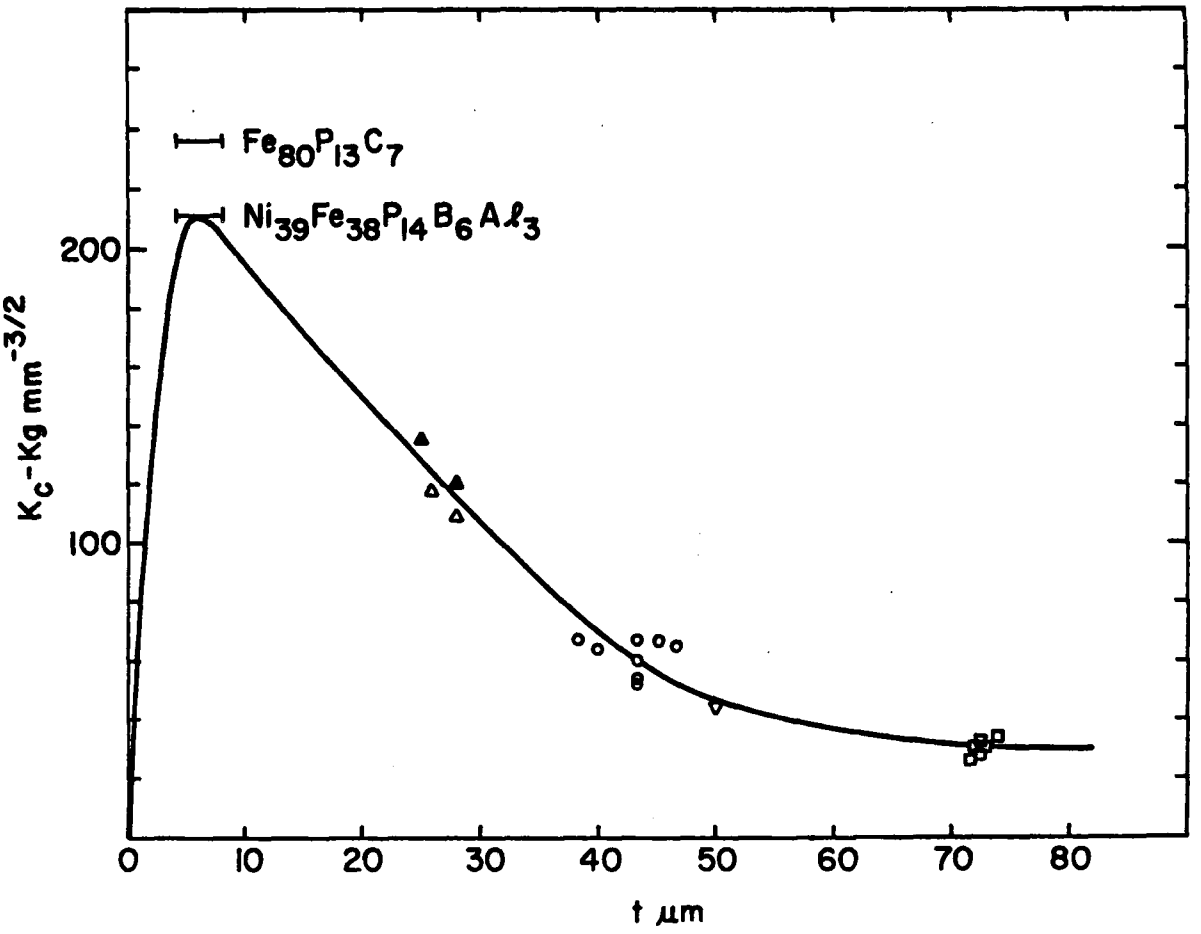

FIGURE 23 Fracture toughness as a function of thickness for Ni-Fe-P-B metallic glasses. The inverted triangle at t = 50 μm is the data of Ast and Krenitsky (1976) for $Ni_{40}Fe_{40}P_{14}B_6$. The horizontal bar (K_{IIIc}) for $Fe_{80}P_{13}C_7$ was obtained from tear tests by Kimura and Masumoto (1975); K_{IIIc} for the Ni_{39} alloys was determined by Davis (1978).

More recently, fracture toughness values have been determined for two high-strength alloys (Davis, 1978), $Fe_{80}B_{20}$ and $Fe_{78}Mo_2B_{20}$ (METGLAS 2605A). The data are collected in Figure 24. For the stronger TM-B alloys ($\sigma_y \simeq 370$ kg/mm^2), plane strain conditions can be obtained in 51-μm-thick sheets; it is evident, then, that K_{Ic} for these alloys is $\sim$40 kg/mm$^{3/2}$, which is slightly larger than that for the Ni-Fe-P-B (Si,Al) alloys. Examination of the figure also indicates K_c is no longer a unique function of thickness; for t = 51 μm, K_c varies by a factor of $\sim$3.5. For both alloys, the higher toughness values (solid symbols in Figure 24) are obtained for specimens that fail by shear rupture. The intermediate and low values (open symbols) are obtained for samples that fail with a partial or complete square fracture. These results are considered to arise from sample inhomogeneity (Davis, 1978).

It is of interest to compare the toughness of metallic glasses with those of other materials, such as steels. When doing so, it is appropriate to consider minimum toughness values. Accordingly, plane strain toughness values for commercial 4340 and 18 percent Ni maraging steels, are shown in Figure 25 as a function of yield strength, along with representative values for ferrous metallic glasses. The areas indicated by the parallelograms are those given by Zackay, et al. (1974). It appears likely, however, that the K_{Ic} vs σ_y behavior is curvilinear (Hahn and Rosenfield, 1968), and this is suggested by the schematic dashed curves. Given the chemical similarities of these materials, it seems reasonable to suggest that the lower K_{Ic} values of the glasses are largely a natural consequence of their considerably increased yield strengths. It is also of interest to compare the toughness of metallic glasses with the toughnesses of other high-strength reinforcement materials, such as oxide glass fibers; K_{Ic} values for the latter filaments are a factor of $\sim 10^2$ less (Hahn, et al., 1972) than those for glassy metal alloys. Oxide glasses are, accordingly, sensitive to surface defects, a factor of 10^4 smaller. In addition, at ambient temperature they are invariably brittle; shear failures are never observed. Such failures may be commonly expected in thin ($\sim$25μ) metallic glass filaments with realization of an additional factor of 3 to 4 improvement in fracture toughness. Glassy alloy filaments should prove useful for the fabrication of matrix-reinforced-composites with improved impact resistance.

Fatigue

Using center-cracked-panel geometry, one may conveniently monitor the advance of a propagating fatigue crack with an optical microscope. One may then deduce da/dn, the cyclic rate of crack advance, as a function of ΔK, the cyclic stress intensity. Davis (1975) found that da/dn (mm/cycle) $\simeq 2 \times 10^{-8}\ \Delta K^{2.25}$, where ΔK has units of Kg/mm$^{3/2}$, for a $Ni_{39}Fe_{38}P_{25}B_6Al_3$ metallic glass (43 μ thick). Making due allowance for the difference in moduli, these data may be compared with those for steels by plotting da/dn vs (ΔK/E); on such a plot the data for the Ni_{39}

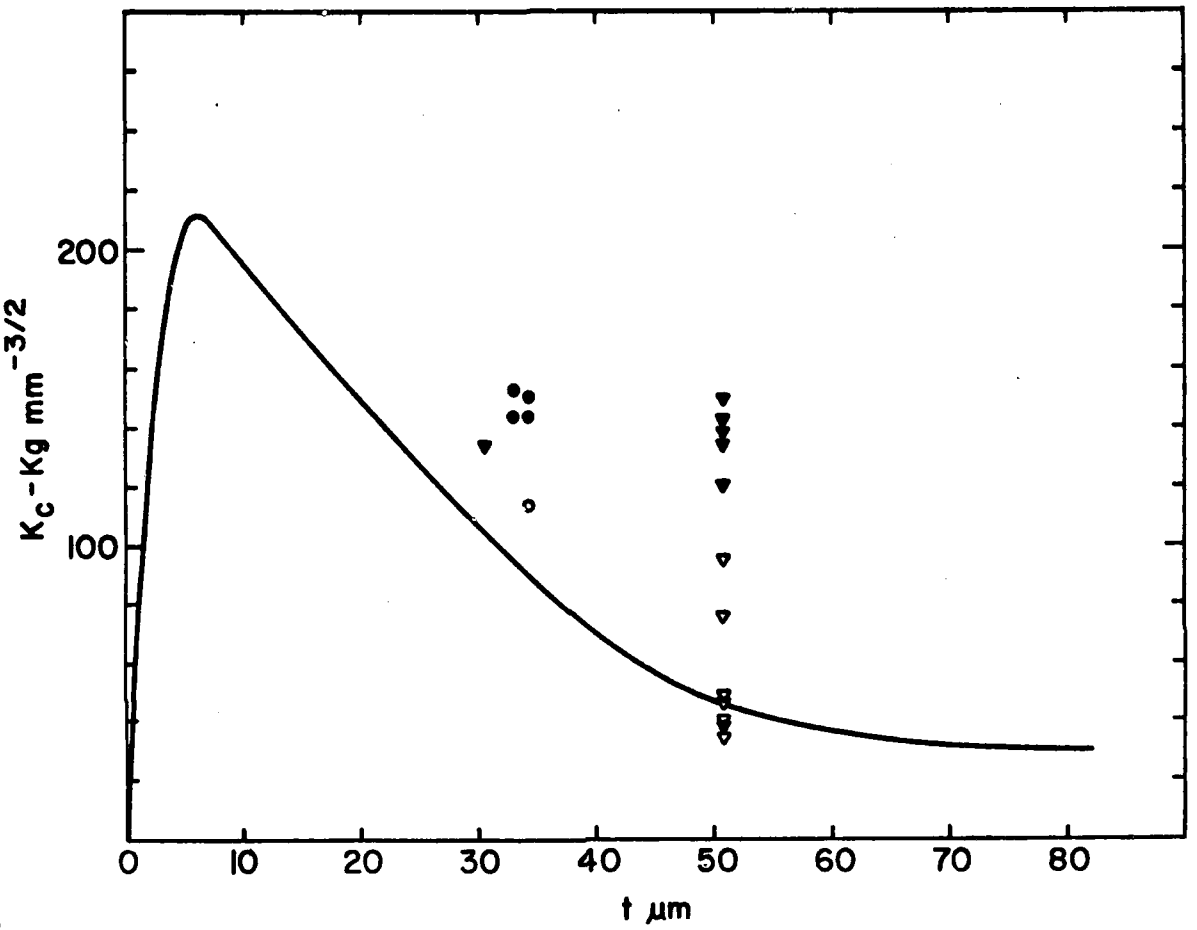

FIGURE 24 Fracture toughness as a function of thickness for Ni-Fe base metallic glasses (Davis, 1978).

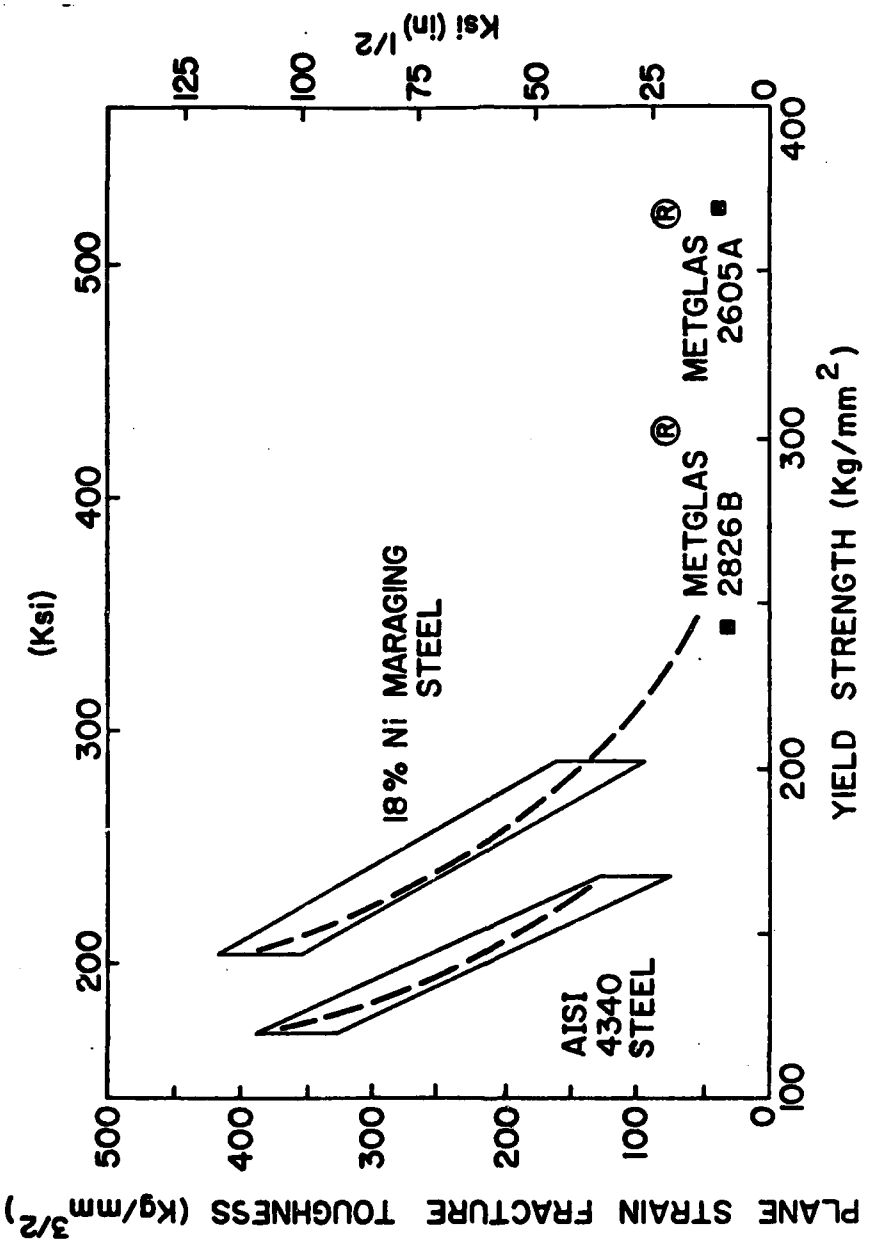

FIGURE 25 Plane strain fracture toughness vs. yield stress for ferrous materials (Davis, 1978).

glass fall within the scatter band of data for various steels (Clark, 1974).

Figure 26 shows a compilation of fatigue lifetime data for Ni-Fe-base metallic glasses. Cyclic loading frequencies of the order of 0.5 to 30 Hz were employed. Since notched samples will sustain static loads of, for example, 0.8 σ_y indefinitely (s = 0.8), it is apparent that the fatigue behavior of metallic glasses is cycle dependent, not time dependent like that of hard nonmetallic glasses.

As one would expect, sample lifetimes are minimized for notched samples (triangles), somewhat better for straight strips (open circles) that suffer interaction with the grips, and maximized for samples with a polished reduced area gauge section (solid circles). The stress ratio for long life ($>10^6$ cycles) also is maximized for the latter samples. As a practical matter, the endurance limit (σ_a for $\sigma_m = 0$) deduced for notched samples from Figure 26 is comparable to that for notched steels.

It is intriguing to note that reduced section samples of Ni-Fe glasses will sustain $\sim$600 stress cycles when loaded within $\sim$1 percent of their yield (and fracture σ_f) stress. By comparison, high-strength steels [$S = (2N_f)^{-0.06}$] (Landgraf, 1970) will sustain only a few cycles when loaded close to their fracture stress, which, in fact, is about the same (i.e., $\sim$245 kg/mm^2) as for the metallic glasses. This comparison reflects the high elastic limit of the metallic glasses. At stresses close to σ_f, glassy alloys behave elastically, and hence, crack initiation is difficult. Steels cyclically loaded to the same absolute stress level experience gross plastic deformation because their yield stresses are well below σ_f. For lower stress ratios (e.g., of the order of 0.4), the lifetime for steels is longer. In this regime, metallic glasses suffer because no mechanism for work hardening exists to effect crack tip blunting. Qualitatively similar behavior was observed for $Pd_{77.5}Cu_6Si_{16.5}$ wires. These data also were in reasonable agreement with the low stress fatigue data presented by Ogura, et al. (1975) for $Pd_{80}Si_{20}$.

RADIATION STABILITY

Metallic glass alloys are the subject of a great deal of metallurgical research, but little has been done to explore the limits of their radiation stability. A brief study by Leseur (1968) on Pd-Si using U^{235} fission fragments indicated no effect detectable by electrical resistivity or large-angle x-ray studies. In 1973, Cline and Pompillo (unpublished) in collaboration with Tom Blewitt at Argonne National Laboratory irradiated an $Fe_{40}Ni_{40}P_{14}B_6$ metallic glass with neutrons at 4K to a fluence of $\sim 10^{18}$ using electrical resistivity as the damage probe. Results of pulse heating experiments indicated no apparent

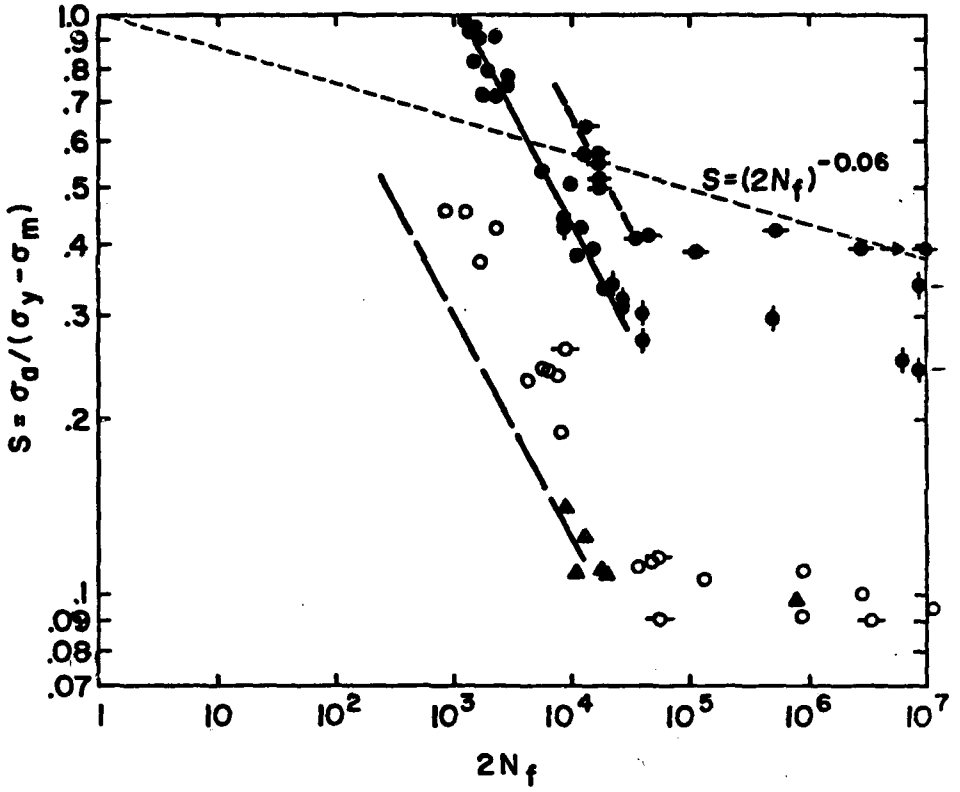

FIGURE 26 Stress vs. reversals to failure ($2N_f$) for Ni-Fe metallic glasses. Stress is given in terms of the parameter $S = [\sigma_a/(\sigma_y - \sigma_m)]$ where σ_a = stress amplitude (one-half the difference between max and min stress), σ_m = mean stress and σ_y = yield stress. The solid line for the Ni_{49} alloy (σ_m 140 Kg/mm^2) is given by $S = 16.9\ (2N_f)^{-0.4}$. The dotted line given by $S = (2N_f)$ is the upper limit of fatigue life-times observed for high strength steels.

change in the electrical resistivity. More recently, work on neutron irradiated (5 x 10^{20} n/cm^2) Pd-Si (Kayano, et al., 1977; Doi, et al., 1977) and $Nb_{40}Ni_{60}$ (Rechtin, et al., n.d.) using neutrons and Ni^{+3} ions indicated no major effects of the irradiation although an increase in the small-angle x-ray scattering was noted (Doi, et al., 1977). Chang and Li (1977) reported the first evidence for radiation where an $Fe_{40}Ni_{40}P_{14}B_6$ alloy ribbon was irradiated by 60 MeV nickel ions and swelling reported. However, a repeat of the experiment by Walters and Johnston (unpublished) indicated that no swelling took place.

Recent studies by Cline, et al. (1978) indicate no effect of neutron radiation to thermal or mechanical properties and no change in the large angle x-ray profiles for fluences $\sim 10^{19}$ at ambient temperatures. $Fe_{80}B_{20}^{10}$ glasses were irradiated with thermal neutrons to carry out the n,α reaction to generate helium. No swelling took place during the generation of $\sim$400 ppm He^4 at a temperature of $\sim 40^{o}C$. Additional studies on metallic glasses $Fe_{80}B_{20}$, $Ti_{50}Be_{40}Zr_{10}$, and $Ni_{40}Fe_{40}P_{14}B_6$ are under way with fission fragment irradiation to a fluence of $\sim$10 DPA with expectation of no swelling or change in properties. Electron irradiation by Kiritani, et al. (1978) indicated that considerable crystallization was occurring but that the dose rate was very high and heating effects were suspected.

CORROSION

Amorphous metal structures may be characterized chemically as thermodynamically metastable and can be considered to be chemically homogeneous owing to their single-phase nature; they are without the crystalline defects (e.g., grain boundaries, dislocation faults, segregates) that act as chemically active sites. However, the addition of large quantities of metalloidal elements is necessary for the formation of the amorphous structure in certain glassy alloy systems, and these additive elements affect chemical properties. Crystalline metals containing such large amounts of metalloids are, perhaps without exception, brittle and chemically unstable because of a mixture of several phases containing compounds. Certain amorphous metals, on the other hand, include metalloidal elements in the matrix in a solid solution state. This fact helps to explain the effects of metalloids on the chemical behavior of metals with the single-phase nature.

Studies of the chemical properties of amorphous metals so far have been confined to their corrosion behavior. Much of this work has been conducted by Masumoto and his co-workers.

First Observations of Corrosion Behavior of Amorphous Iron-Base Alloys

The primary investigation concerning the chemical properties of amorphous alloys was carried out on the corrosion behavior of amorphous

iron-base alloys with phosphorus and carbon by Naka, et al. (1974). They demonstrated that the addition of chromium to amorphous Fe-13P-7C alloy gave rise to an extraordinarily high corrosion resistance. The amorphous iron-base alloys with various compositions were prepared in ribbons about 20 μm thick and 0.7mm wide by the centrifugal quenching method. Crystalline high-purity iron, Fe-Cr alloys, 18Cr-8Ni stainless steel (Type 304), and 17Cr-14Ni-2.5Mo stainless steel (Type 316L) were used for comparison. Figure 27 illustrates the variation of corrosion rates estimated from the weight loss in 1 N NaCl at 30 $\pm$ 1°C. The corrosion rates of the crystalline Fe-Cr alloys are hardly affected by the addition of chromium in a nonoxidizing corrosive sodium chloride solution whereas those of the amorphous Fe-Cr-13P-7C alloys are rapidly lowered as the chromium content becomes higher. Although the amorphous Fe-13P-7C alloy is significantly corroded (exhibits a corrosion rate much higher than crystalline pure iron), the corrosion rates of the alloys containing more than 2 at.% chromium are lower than those of the crystalline Fe-Cr alloys, and at about 8 at.% or more chromium it becomes so small that the weight change could not be detected by a microbalance after immersion for 168 hours.

Corrosion Behavior as a Function of Type of Metalloid

In amorphous iron-, nickel- and cobalt-base alloys, the addition of large quantities of metalloid elements such as phosphorus, boron, silicon, and carbon is necessary for the formation of the amorphous structure by rapid quenching from the melt. These additive elements affect the corrosion behavior of amorphous alloys. Figure 28 shows the effect of metalloid X on the corrosion rate (estimated from the weight loss) of amorphous alloys of Fe-10Cr-13B-7X and Fe-10Cr-13P-7X systems in 0.1 N H_2SO_4 at 30°C. Similar behavior is observed in 3 percent NaCl. It is clear that the corrosion rates of the alloy system containing phosphorus as a major metalloid are more than two orders of magnitude lower than those of the alloy system with boron as a major metalloid in neutral and acidic solutions. Furthermore, the corrosion rate of the amorphous Fe-Cr alloy in 0.1 N H_2SO_4 is progressively decreased by the addition of silicon, boron, carbon, and phosphorus; the progression is boron, carbon, silicon, and phosphorus in 3 percent NaCl. The addition of chromium without phosphorus to the amorphous alloys is ineffective in improving corrosion resistance properties as seen in examples of Fe-10Cr-13B-7C and Fe-10Cr-13B-7Si alloys. On the other hand, the amorphous Fe-Cr alloys with phosphorus reveal a negligible corrosion rate in all cases except for the alloy containing silicon. Similar results have been obtained by electrochemical measurements.

Thus, phosphorus is the metalloid element among phosphorus, carbon, silicon, and boron most effective for improving the corrosion resistance

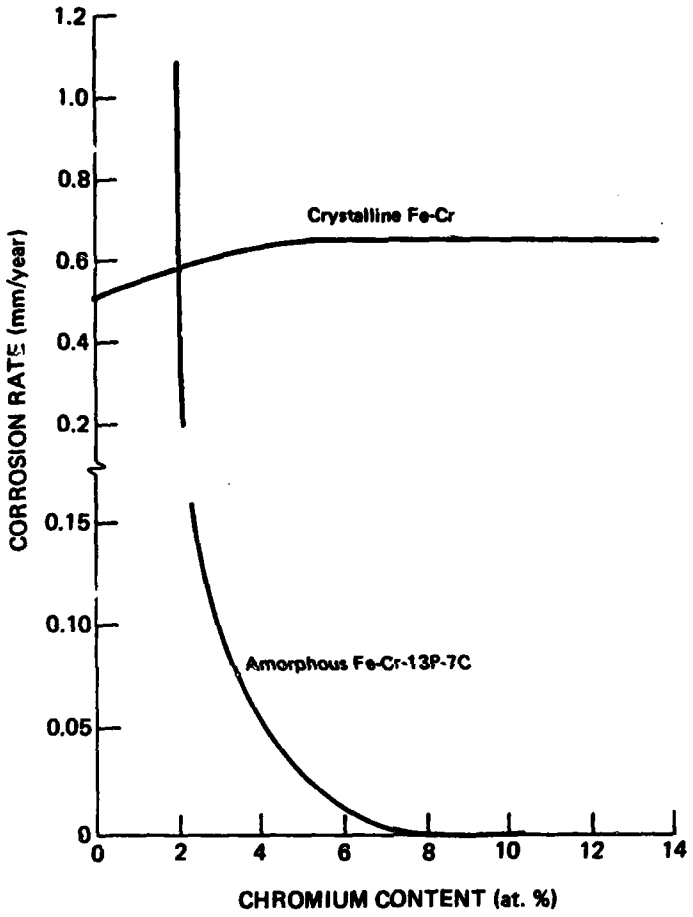

FIGURE 27 Comparison of corrosion rates of amorphous Fe-Cr-13P-7C alloys and crystalline Fe-Cr alloys in 1 N NaCl at 30± 1°C. Weight change of amorphous Fe-10Cr-13P-7C alloy was not detected by a microbalance after immersion for 168 hr.

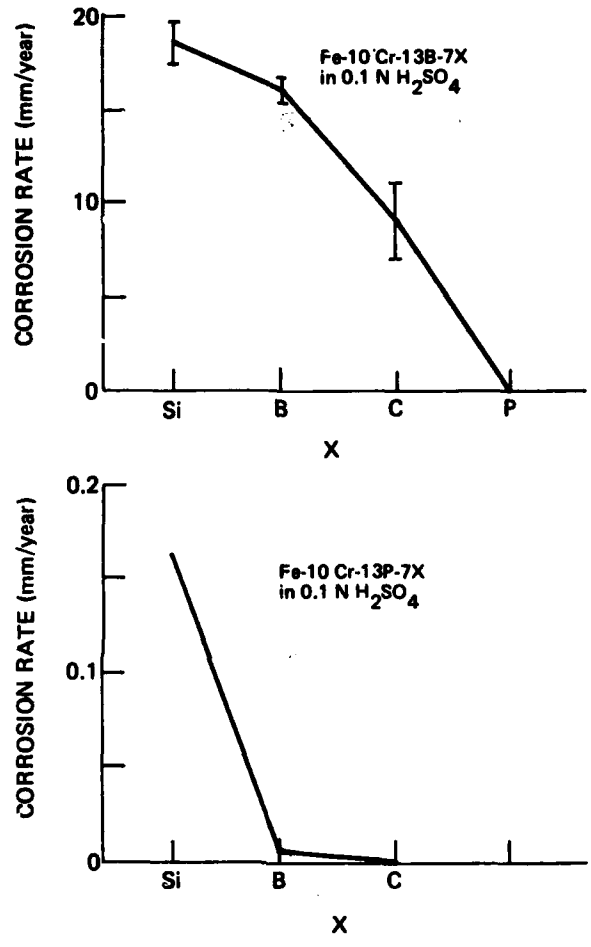

FIGURE 28 Average corrosion rates estimated from the weight losses of amorphous Fe-10Cr-13B-7X and Fe-10Cr-13P-7X alloys in 0.1 N H_2SO_4 at 30 ± 1°C. X is a metalloidal element denoted on the abscissa.

of amorphous iron-base alloys containing chromium, and a significant increase in the corrosion resistance of the amorphous iron-base alloys by the addition of chromium cannot be attained unless phosphorus is present as a major metalloid. Consequently, the combination of metalloids that produces superior corrosion resistance in amorphous Fe-Cr alloys is phosphorus and carbon.

Corrosion Behavior as a Function of Additive Metallic Elements

The addition of various metallic elements such as Ni, Mo, and W to amorphous Fe-P-C alloys definitely improves the corrosion resistance of the alloys. Figure 29 shows the effect of change in the nickel content of the amorphous Fe-Ni-13P-7C alloys on the potentiodynamic polarization curves measured in 1 N NaCl; for comparison, the polarization curve of the crystalline binary Fe-20 at percent Ni alloy also is presented. The crystalline binary Fe-Ni alloy exhibits a high dissolution current owing to pitting corrosion. The amorphous Fe-Ni-13P-7C alloys, however, are passivated in 1 N NaCl, and an anodic current of the amorphous alloys in the passive region decreases with an increase in the nickel content. The corrosion potentials of the amrophous Fe-Ni-13P-7C alloys are elevated 100 mV or more as compared with that of the crystalline Fe-Ni alloy. Since the oxygen reduction current of the amorphous alloys in the cathodic polarization curves is not higher than that of the crystalline Fe-Ni alloy, the rise in the corrosion potential of the amorphous alloys is attributable to the reduction of anodic reaction. Consequently, the addition of nickel to the amorphous iron-base alloys improves their corrosion resistance in neutral chloride solution.

The effects of additive metallic elements in improving corrosion resistance are especially remarkable when a small amount of chromium exists in amorphous Fe-P-C alloys. Thus, extra metallic elements interact synergistically with chromium.

The corrosion rate decreases definitely with the addition of extra metallic elements; molybdenum, tungsten, titanium, and vanadium are particularly effective. The addition of nickel to amorphous Fe-Cr-P-C alloys also is effective in improving corrosion resistance.

Dominating Factors in Corrosion Behaviors

The great corrosion resistance of amorphous alloys can be attributed partly to the formation of a passive film with a high protective quality due in part to the presence of chromium and a large amount of phosphorus. High chemical homogeneity also is a characteristic of amorphous alloys.

In order to examine the effect of crystallinity on corrosion resistance, a perfect single crystal and an amorphous alloy having

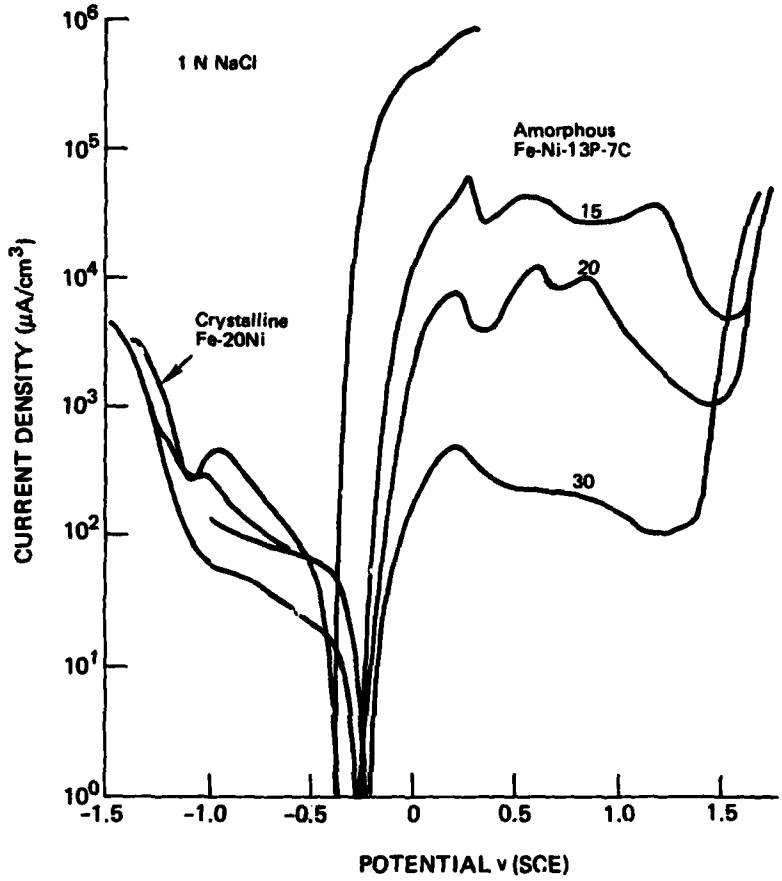

FIGURE 29 Potential dynamic polarization curves of amorphous Fe-Ni-13P-7C alloys and crystalline Fe-20N alloy measured in 1 N NaCl. Atomic percent of Ni is indicated by the number in the Figure.

the same composition must be prepared as specimens. This attempt has been made by crystallizing amorphous alloys. Pitting in crystalline alloys occurs not by a change in the protective quality of the passive film but by the presence of crystal defects on which it is difficult to form a stable passive film. Pitting of amorphous alloys is avoided by the formation of highly uniform continuous passive films.

When the passive hydrated chromium oxy-hydroxide film is formed on alloys containing a certain amount of chromium, the corrosion resistance of the alloys is determined by the rate of film formation and the homogeneity of the passive film. This indicates that without surface films the amorphous alloy itself is more reactive than the stainless steel. After cessation of abrasion, the amorphous alloy exhibits a higher rate of current decrease and a lower stationary current density than the 304 stainless steel. The sharp decrease in current density with time corresponds to the rapid decrease in the reactivity of bare surface (i.e., the rapid formation of the protective film).

Concluding Remarks

Amorphous alloys that contain adequate (large) amounts of chromium and phosphorus posses extremely high corrosion resistance, especially against pitting. The chemically homogeneous single-phase nature of amorphous alloys provides for the formation of a uniform protective film without weak points with respect to corrosion. The admixture of large amounts of phosphorus facilitates active dissolution of alloys prior to the formation of the passive film and leads to the rapid enrichment with chromium of the alloy/solution interface. This results in the rapid formation of a uniform passive hydrated chromium oxy-hydroxide film with high protective quality.

REFERENCES

Alben, R., et al. 1971. In Metallic Glasses, Chap. 12. Edited by H.J. Leamy and J.J. Gilman. ASM, Metals Park, Oh.

Argon, A.S. 1968. "Delayed Elasticity In Inorganic Glasses." J. Appl. Phys., Vol. 39, p. 4080.

Argon, A.S., and H.Y. Kuo. In press. J. Noncrys. Solids.

Arai, K., et al. 1976. In Proc. Second Int. Conf. on Rapidly Quenched Metals, p. 489. Edited by N.J. Grant and B.C. Giessen. MIT Press, Cambridge, Ma.

Ast, D.G., and D. Krenitsky. 1976. In Proc. Second Int. Conf. on Rapidly Quenched Metals, p. 241. Edited by N.J. Grant and B.C. Giessen, MIT Press, Cambridge, Ma.

Becker, J.J., et al. 1977. IEEE Trans. Magnetics, Vol. 13, p. 988.

Berry, B.S. 1978. In Metallic Glasses, p. 161. Edited by H.J. Leamy and J.J. Gilman. ASM, Metals Park, Oh.

Berry, B.S., and W.C. Pritchet. 1976. AIP Conf. Proc., No. 34, p. 292.

Brenner, A. 1956. J. Appl. Phys., Vol. 27, p. 1484.

Brooks, H.A. 1976. J. Appl. Phys., Vol. 47, p. 344.

Cargill, G.S., III. 1975. Solid State Physics, Vol. 30, p. 227.

Cargill, G.S., III, and R.W. Cochrane. 1974. J. Phys., Vol. 35, p. C4-269.

Chang, B., and J.C.M. Li. 1977. Scripta Met., Vol. 11, p. 933.

Chen. H.S. 1973. Phys. Stat. Sol., Vol. 17, p. 561.

Chen, H.S. 1976. Appl. Phys. Lett., Vol. 29, p. 12.

Chen, H.S., and T.T. Wang. 1970. J. Appl. Phys., Vol. 41, p. 5338.

Chen, H.S., et al. 1975. J. Non-cryst. Solids, Vol. 18, p. 157.

Clark, W.G., Jr. 1974. ASM Metals Eng. Quart., August, p. 16.

Cline, C., et al. 1978. Paper presented at the Third Int. Conf. on Rapidly Quenched Metals, University of Sussex, England, July 3-7.

Cottrell, A.H. 1964. The Mechanical Properties of Matter. John Wiley, N.Y., N.Y.

Davis, L.A. 1975. Scripta Met., Vol. 9, pp. 339 and 431 and J. Mat. Sci., Vol. 10, p. 1557.

Davis, L.A. 1978. In Metallic Glasses, p. 190. Edited by J.J. Gilman and H.J. Leamy. ASM, Metals Park, Oh.

Davis, L.A., and S. Kavesh. 1975. J. Mat. Sci., Vol. 10, p. 453.

Davis, L.A., et al. 1976. Scripta Met., Vol. 10, pp. 541 and 937.

Doi, K., et al. 1977. Appl. Phys. Lett., Vol. 31, p. 421.

Durand, J. 1976. IEEE Trans. Magnetics, Vol. MAG-12, p. 945.

Durand, J. 1977. In Amorphous Magnetism, Vol. 2, paper AB.12. Edited by R.A. Levy and R. Hasegawa. Plenum Press, N.Y.

Durand, J., and M. Yung. 1977. In Amorphous Magnetism, Vol. 2. Edited by R.A. Levy and R. Hasegawa. Plenum Press, N.Y.

Egami, T., et al. 1975. AIP Conf. Proc., No. 24, p. 697.

Felsch, W. 1970. Z. Angew. Phys., Vol. 29, p. 218.

Fujimori, H., et al. 1976. Sci. Repts. Res. Inst. (Tohoku Univ.), Vol. A26, p. 36.

Fujimori, H., et al. 1977. In Amorphous Magnetism, Vol. 2. Edited by R.A. Levy and R. Hasegawa. Plenum Press, N.Y.

Gilman, J.J. 1973. In The Science of Hardness Testing and Its Research Applications, p. 51. Edited by J.H. Westbrook and H. Conrad. ASM, Metals Park, Oh.

Gyorgy, E.M., et al. 1976. AIP Conf. Proc., No. 29, p. 198.

Hahn, G.T., and A.R. Rosenfield. 1968. ASTM Stp #423, 5.

Hahn, G.T., et al. 1972. Ann. Rev. Mat. Sci., Vol. 2, p. 381.

Hasegawa, R., and J.A. Dermon. 1973. Phys. Lett., Vol. 42A, p. 407.

Hasegawa, R., et al. 1976. AIP Conf. Proc., No. 34, p. 298.

Hill, R. 1967. The Mathematical Theory of Plasticity. Oxford Univ. Press, London.

Johnson, W.L., and A.R. Williams. 1979. Calif. Inst. of Tech. Rpt. CALT-822-107.

Kanabe, T., and R. Kanematsui. 1968. J. Phys. Sol. (Japan), Vol. 24, p. 1396.

Kayano, H., et al. 1977. Sci. Rep. Inst. (Tohoku Univ.), Vol. A-26, p. 240.

Kimura, H., and T. Masumoto. 1975. Scripta Met., Vol. 9, p. 211.

Kiritani, M., et al. 1978. Paper presented at the Third International Conf. on Rapidly Quenched Metals, Univ. of Sussex, England, July 3-7.

Knott, J.F. 1974. Fundamentals of Fracture Mechanics, pp. 114, 246. Butterworth, London.

Kouvell, J.S. 1969. Magnetism and Metallurgy, p. 523. Edited by A.E. Berkowitz and E. Kneller. Academic Press, N.Y.

Landgraf, R.W. 1970. In Achievement of High Fatigue Resistance in Metals and Alloys, Vol. 3, ASTM.

Leamy, H.J., et al. 1972. Met. Trans., Vol. 3, p. 699.

Leseur, D. 1968. C.R. Acad. Sci. (Paris), Vol. 266B, p. 1038.

Logan, J. 1975. Phys. Stat. Sol., Vol. 32, p. 361.

Luborsky, F.E. 1976. AIP Conf. Proc., No. 29, p. 209.

Luborsky, F.E. 1977. Mat. Sci. Eng., Vol. 28, p. 139, and In Amorphous Magnetism, Vol. 2. Edited by R.A. Levy and R. Hasegawa. Plenum Press, N.Y.

Luborsky, F.E. 1978. In Ferromagnetic Materials, Chapt. 20. Edited by E.P. Wohlfarth, North Holland Publishing Co., Amsterdam.

Luborsky, F.E., and J.L. Walter. 1976. J. Appl. Phys., Vol. 47, p. 3648.

Luborsky, F.E., and J.L. Walter. 1977. IEEE Trans. Magnetics, Vol. MAG-13, and Mat Sci. Engr., Vol. 28, p. 77.

Luborsky, F.E., et al. 1975. IEEE Trans. Magnetics, Vol. MAG-11, p. 1644.

Marsh, D.M. 1964. Proc. Royal Soc., Vol. A 279, p. 420, and Vol. A 282, p. 33.

Masumoto, T., and R. Maddin. 1971. Acta Met., Vol. 19, p. 725.

Masumoto, T., and R. Maddin. 1975. Mat. Sci. Eng., Vol. 19, p. 1.

Masumoto, T., et al. 1977. In Amorphous Magnetism, II. Edited by H.O. Hooper and A.M. deGraff. Plenum Press, N.Y.

Mizoguchi, T. 1976. AIP Conf. Proc., No. 34, p. 286.

Mizoguchi, T., et al. 1973. In Amorphous Magnetism, p. 325. Edited by H.O. Hooper and A.M. deGraff. Plenum Press, N.Y.

Naka, M., et al. 1974. J. Japan Inst. Met., Vol. 38, p. 835.

O'Handley, R.C., et al. 1976. Appl. Phys. Lett., Vol. 29, p. 330.

Ogura, T., et al. 1975. Scripta Met., Vol. 9, p. 109.

Pampillo, C.A. 1975. Scripta Met., Vol. 6, p. 915.

Pampillo, C.A., and D.E. Polk. 1974. Acta Met., Vol. 22, p. 741.

Pampillo, C.A., and A.C. Reimschnuessel. 1974. J. Mat. Sci., Vol. 9, p. 718.

Pan, D., and D. Turnbull. 1974. J. Appl. Phys., Vol. 45, p. 1406.

Parsons, D., et al. 1958. Phil. Mag., Vol. 3, p. 1174.

Rechtin, M.D., et al. (n.d.). Paper presented at 35th Annual EMSA Meeting.

Rivlin, R.S., and A.G. Thomas. 1952. J. Polymer Sci., Vol. 10, p. 29.

St. Amand, R., and B.C. Giessen. 1978. Scripta Met., Vol. 12, p. 1021.

Shimada, Y., and H. Kojima. 1976. J. Appl. Phys., Vol. 47, p. 4156.

Simpson, A.W., and W.A. Clements. 1975. IEEE Trans. Magnetics, Vol. MAG-11, p. 1338.

Simpson, A.W., and D.R. Brambley. 1971. Phys. Stat. Solids, Vol. 43, p. 291.

Slonezemski, J.C. 1963. In Magnetism, Vol. I, Chapt. 5. Edited by G. Rado and H. Suhl. Academic Press, N.Y.

Soshiroda, T., et al. 1976. J. Noncryst. Solids., Vol. 22, p. 173.

Tabor, D. 1951. The Hardness of Metals. Oxford Univ. Press, London.

Tetelman, A.S., and A.J. McEvily, Jr. 1966. Fracture of Structural Materials, p. 94. John Wiley, N.Y.

Tsuei, C.C. 1976. In Proc. Second Int. Conf. on Rapidly Quenched Metals, p. 441. Edited by N.J. Grant and B.C. Giessen. MIT Press, Cambridge, Ma.

Weisner, H., and J. Schneider. 1974. Phys. Stat. Sol., Vol. 26, p. 71.

Wright, J.G. 1976. IEEE Trans. Magnetics, Vol. MAG-12, p. 95.

Zackay, V.F., et al. 1974. Mat. Sci. Eng., Vol. 16, p. 201.

SECTION II

METASTABLE CRYSTALLINE MATERIALS

Chapter 9

HETEROGENEOUS NUCLEATION

It is well known that crystallization of a melt on cooling does not begin exactly at the equilibrium melting point but at some lower temperature and after some time lapse. The purer the system and the faster the quench, the greater is the undercooling. The first crystals generally begin at surfaces, either by homogeneous or by heterogeneous accidental nucleation at the coldest points; and subsequent crystal growth, with associated heat evolution and/or density changes, results in large crystals, voids, and changes in shape of the crystalline solids.

More finely grained homogeneous aluminum castings and other alloys have been made by purposely introducing insoluble carbide crystals into the melt. These act as independent growth sites, or heterogeneous nuclei, as the melt cools. Many cases of purposeful heterogeneous nucleation can be cited in controlled crystallization of silicate glasses. Introduction of the foreign nuclei into the viscous glass melt and its uniform dispersion are difficult or impossible; therefore, the usual technique involves making a homogeneous melt of glass containing the ingredients of nuclei in solution and precipitating a uniformly dispersed insoluble colloid (the nuclei) of a minor ingredient that is soluble in the melt at high temperature but insoluble at lower temperature. The atomic lattice spacing of the crystal structure of the nuclei is chosen to match that of the desired crystal phase within 15 percent. Cooling and subsequent controlled reheating produces, first, a controlled uniform dispersion of nuclei pre-existing at temperatures below crystal growth temperatures and, then, controlled growth of crystals of other minor phases or of the major constituents of the piece of material when the glass is reheated.

The higher viscosity silicate glasses allow more freedom for this technique than do metals. In the photosensitive glasses, for example, small concentrations of ions of gold, silver, or copper remain in the transparent rigid glass at room temperature. Irradiation with ultraviolet light initiates a localized chemical reduction to insoluble colloidal metal, and reheating of the glass can initiate epitaxial growth of nonmetallic crystals on the individual metal crystals. Possibly, localized application of high-energy radiation can produce patterns of controlled crystallinity in glassy metals as ultraviolet light does in transparent silicate glasses.

Chapter 10

ALUMINUM ALLOYS

In the search for improved properties for aluminum alloys, a variety of techniques that involve direct quenching from the liquid state have been investigated. These techniques, referred to as rapid solidification processing (RSP), are aimed at achieving beneficial microstructural modifications through the use of a highly efficient dissipation of heat away from the liquid-solid interface so that a substantial increase in undercooling and the corresponding interface velocity can be obtained. This objective usually implies an improved heat-transfer coefficient at the casting-quenchant surface and an increase in the surface-area-to-volume ratio of the casting. The overall effect is the achievement of cooling rates estimated at from 10^3 to 10^{10} K/s. A second guideline in RSP is to obtain a great enough degree of supercooling prior to nucleation so that the liquid will act as the main sink for the heat of fusion; the solidification then proceeds in an essentially adiabatic manner. Solidification under the increasingly higher cooling rates—and conceivably higher undercoolings—typical of atomization, splat cooling, and other related techniques commonly results in progressive departure from the regular microstructures produced by conventional casting.

MICROSTRUCTURES OF RAPIDLY SOLIDIFIED ALUMINUM ALLOYS

Rapid solidification of aluminum alloys commonly results in one or more of the following microstructural modifications:

1. Microstructural refinement manifested as smaller grain size, dendrite arm and eutectic spacings.
2. Extension in terminal solid solubility of alloying elements in the primary α-Al phase and change in segregation patterns eventually leading to the reduction or elimination of the second phase.
3. Morphological changes of the eutectic or the primary phase.
4. Formation of metastable phases.
5. Coupled eutectic growth at off-eutectic compositions.
6. Vacancy supersaturation.

Although all these effects have been observed in aluminum alloys, some even at the moderate cooling rates of 10 to 10^3 K/s, only the first four, which are important in terms of improving the properties of the final product, are well understood, and hence, only these are discussed below.

Microstructural Refinement

In general, the fineness of microstructure during dendritic solidification of aluminum alloys, as in most other alloy systems, can be correlated to average cooling rate during solidification, ε_{Avg}, or local solidification time (i.e., time available for coarsening), t_f, by:

$$DAS = a\varepsilon_{Avg}^{-m} = bt_f^{m} \quad , \tag{19}$$

and

$$\varepsilon_{Avg} = \frac{(T_L - T_S)}{t_f} \quad , \tag{20}$$

where $(T_L - T_S)$ is the solidification temperature range, DAS is the dendrite arm spacing, and a, b and m are constants.

Experimental relationships between average cooling rate and dendrite arm spacing are available for several aluminum alloys (Bower, et al., 1966; Spear and Gardner, 1963). For example, dendrite arm spacings for an Al-10.5% Si alloy versus average cooling rates are reported for cooling rates of up to 10^5 K/s (Armstrong and Jones, 1977). Dendritic spacings of 0.01 to 0.5 μm (Ramachandrarao, et al., 1972; Matyja, et al., 1968; McComb, et al., 1964; Suryanarayana and Anantharaman, 1970) and eutectic spacings in the same order of magnitude (Davies and Hull, 1974) have been reported for electron-transparent areas of Al alloy gun splats on Cu substrates. However, in most studies, experimental difficulties have limited the range of accurately measured cooling rates to less than $\sim 10^5$ K/s.

Figure 30 illustrates the capabilities of various solidification techniques in terms of microstructural refinement expected from the estimated achievable cooling rates and a relationship of the type given by Equation 19 for aluminum alloys. It should be noted that caution must be exercised when the exponential correlation in Equation 19 is used to estimate cooling rates in RSP from the dendrite spacings since the reliability of extrapolating this relationship over many orders of magnitude is probably poor, especially if the microstructures examined do not exhibit typical dendritic morphologies. Furthermore, the constants in Equation 19 vary with alloy composition. Studies on the effect of alloy composition on structure at a fixed average cooling rate for Al binary alloys with Cu, Mg, Si, or Zn have shown that increasing the solute content refines the dendrite arm spacings, especially at low solute concentrations (Spear and Gardner, 1963; Horwath and Mondolfo, 1962).

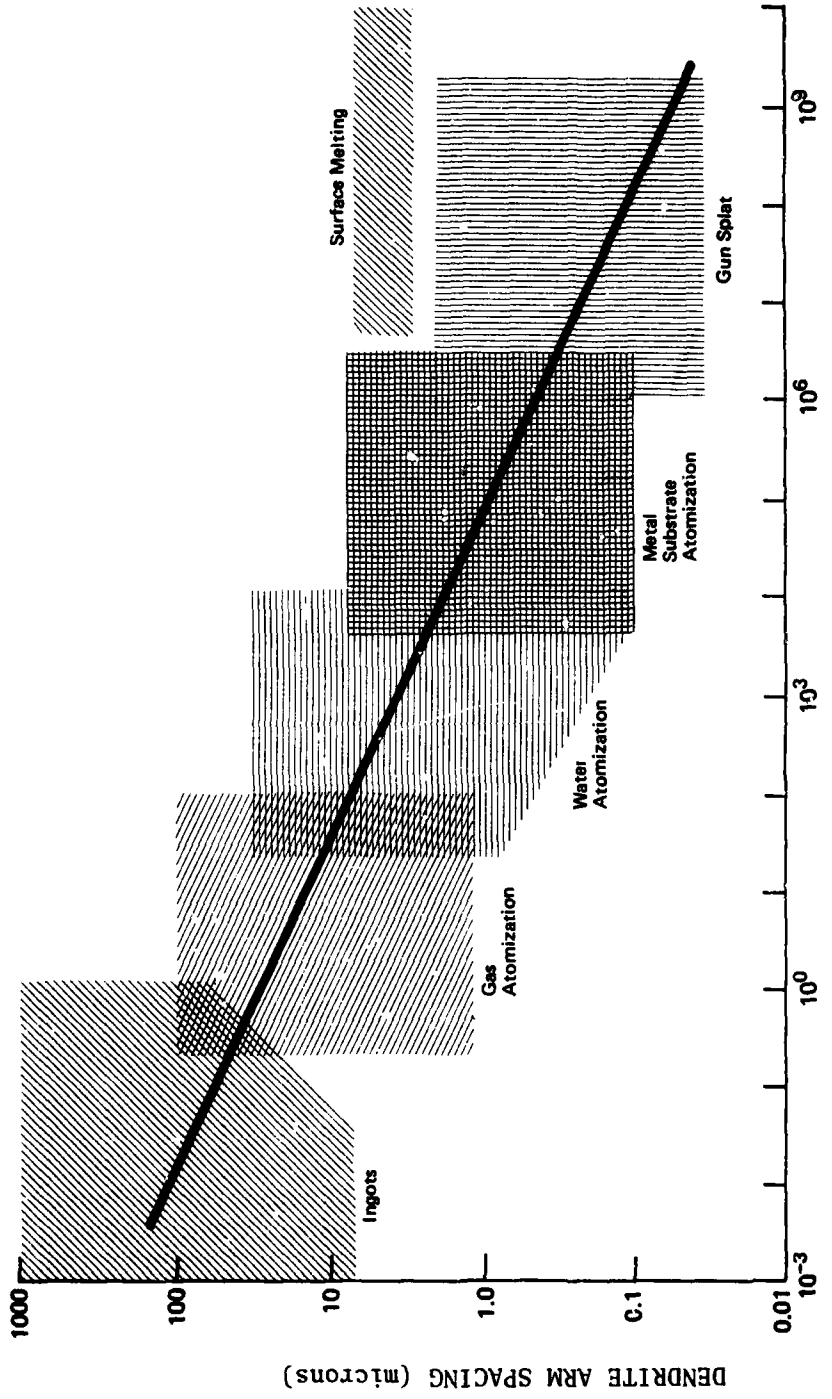

FIGURE 30 Dendrite arm spacing as a function of cooling rate for aluminum and aluminum alloys (Grant, 1970).

Refinement of secondary phases including eutectic constituents also occurs with increasing cooling rate during solidification. Dispersion hardening associated with this effect has been reported in Al-Si (Dixon and Skelly, 1971) and Al-Fe (Town, 1958; Thursfield and Stowell, 1974; Panseri and Paganelli, 1967) base alloys.

RSP also is able to produce grain sizes of $\sim 1\mu m$ which are significantly smaller than those developed in conventional casting. A quantitative analysis of the grain refinement resulting from solidification at the high cooling rates ($>10^5$ K/sec) obtained by splat quenching has been made by Boswell and Chadwick (1977), and good agreement was obtained between observed and predicted grain sizes for rapidly quenched aluminum.

Extension in Solid Solubility

Terminal solid solubility extension has been obtained at sufficiently high cooling rates in almost all aluminum alloy systems investigated, Al-Zn being the only notable exception (Anantharaman and Suryanarayana, 1971). The increased solid solubility permits higher alloying levels resulting in superior strength-ductility combinations in a number of systems. Table 10 shows the maximum reported solid solubilities for a number of binary aluminum alloys of practical interest.

TABLE 10 Extension of Solid Solubility in Binary Aluminum Alloys Quenched from the Melt

Element	Max. at Equil. at %	Max. at Equil. Temp. °K	Reported Maximum, at - %
Cr	0.44	934	>5 - 6
Cu	2.5	821	17 - 18
Fe	0.025	928	4 - 6
Mg	18.9	723	36.8 - 40
Mn	0.7	923	>6 - 9
Ni	0.023	913	1.2 - 7.7
Si	1.59	850	10 - 16
Zn	66.5	655	38 ?

NOTE: From Jones, 1978.

There are indications that the extent of solute solubility increases with severity of the quench (Jones, 1978) and increased initial alloy composition (Krishnanand and Cahn, 1976) and that it is not necessarily bounded by the eutectic composition. Furthermore, it has been shown that additions especially susceptible to solubility extension in binary alloys (e.g., Mn) can be used in ternaries to increase the solubility limit of less susceptible elements (e.g., Fe, Co, and Ni) (Jones, 1978).

Morphological Modifications

Both conventional dendritic (columnar and equiaxed) and modified dendritic morphologies have been reported in alloys solidified at high cooling rates (Linde, 1966; Wood and Honeycombe, 1974; Brown and Adams, 1966). The primary phase in the latter tends to assume a cellular or rod-like configuration with progressively faster cooling rates (Matyja, et al., 1968; Brown and Adams, 1966). Similar observations have been reported in bulk specimens of nickel- and iron-base alloys with increasing supercooling prior to nucleation of the solid phase (Kattamis and Mehrabian, 1974). High cooling rates sometimes can suppress primary formation of an equilibrium phase from the melt. For example, formation of α-Al dendrites instead of equilibrium $FeAl_3$ phase in hypereutectic Al-Fe alloys both in chill-cast (Jones, 1970) and splat-cooled specimens (Jones, 1969) has been reported.

Sufficiently rapid cooling rates during solidification can alter the composition range of cooperative eutectic growth, the eutectic constituents, and their morphologies. Relatively rapid solidification of Al-Fe alloys in the range of 10 to 10^4 K/s has resulted in eutectic morphologies changing from irregular Al-$FeAl_3$ to regular Al-$FeAl_6$ as well as coupled eutectic growth at noneutectic compositions (Jones, 1970). In addition, degenerate and radial eutectic structures in Al-17.3 at.% Cu and structural changes as a function of Cu content have been studied via splat cooling (Williams and Edington, 1976).

Formation of Metastable Phases

Departure from the phase equilibria predicted by the phase diagram of aluminum alloys is not as common as the effects noted above. Nevertheless, a certain number of cases are reported in the literature and have been classified by Jones (1978) as:

Type I - phase present at equilibrium but not stable at the temperature and alloy compositions in which they were observed;

Type II - phases not formed from the melt but appearing, normally transiently, on further heat treatment or precipitated during quenching through the solid state; and

Type III - phases present in the rapidly quenched specimen but not known to exist under equilibrium conditions at any composition within the alloy system.

A summary of the reported observations in binary aluminum alloy systems is given in Table 11. It should be noted that the only report of a noncrystalline structure in an aluminum alloy (Davies and Hull, 1974), splat cooled Al-17.3 at.% Cu alloy, has not been supported by further investigation (Scott and Leake, 1975).

TABLE 11 Nonequilibrium Phases Detected in Aluminum Binary Alloys Under Rapid Solidification

Alloying Element	Concentration Range, at %	Nonequilibrium Phase Detected	Type	Corresponding Eq. Phases	Reference
Cr	1.6 - 3	Al_4Cr	I	α-Al + Al_7Cr	Varich and Lyukevich, 1970
Cu	45	Al_3Cu_2 (Trigonal)	III	$O + \eta_2$	Ramachandrarao and Lavidjoni, 1974
	17.3	Noncrystalline	III	α-Al + O	Davies and Hull, 1974
Fe	2 - 4	$\gamma, \gamma', \gamma'', O^a$	II	$Al_3Fe + \alpha$-Al	Jacobs et al., 1974
	4	Al_6Fe (Orthorhombic)	II		Jacobs et al., 1974
		Al_6Fe	III		Jones, 1978
Mg	25	$L\ell_2$ superlattice	II	α-Al + β-Al_3Mg_2	Jones, 1978
	40	(α-Mn) like structure	III	α-Al + β-Al_3Mg_2	Jones, 1978
	~10 wt %				
Mn	$\lesssim$6	Al_4 Mn	I	α-Al + Al_6Mn	Varich and Kolesnichenko, 1961
Ni	7.3 - 10.1	η (Orthorhombic)	III	α-Al + β Al_3Ni	Tonejc et al., 1971

[a]Formed transiently during aging following a decomposition kinetics similar to the supersaturated Al-Cu solid solutions.

It is commonly observed that particular nonequilibrium effects do not happen above a critical thickness in splat cooling (i.e., below a given average cooling rate during solidification). For example, Al_6Fe can displace the equilibrium phase Al_3Fe at cooling rates as low as 3 K/s; however, cooling rates of the order of 10^4 K/s are required to displace the equilibrium FCC Al_3Mg_2 phase in Al-Mg alloys (Jones, 1978).

MECHANICAL PROPERTIES OF CONSOLIDATED RAPIDLY SOLIDIFIED ALUMINUM ALLOY POWDERS

The most significant metallurgical factor that influences mechanical properties is the type and distribution of second-phase particles. In commercial aluminum alloys, these have been classified into three types:

1. Constituent particles that are Fe-, Mn-, Co-, Ni-, Si-, and Cu-rich inclusions from 0.1 to 10 μm in diameter that are formed during

casting; Fe and Si are usually impurities, whereas Cu is a deliberate alloying addition.

2. Intermediate particles or dispersoids, rich in Cr, Be, Ag, Mn, or Zr and 0.05 to 0.5 μm in size, that are used to control recrystallization and grain growth.

3. Precipitate particles, rich in Cu, Mg, Zn, etc., and from 0.005 to 0.5 μm in size, that are used to strengthen the matrix.

The role of these different particle dispersions, together with other important parameters such as grain size, will be reviewed separately for each property of interest. The potential beneficial influence of rapid solidification on the microstructure and properties also will be discussed.

Room Temperature Strength

Strengthening of aluminum alloys is achieved by a number of different mechanisms including solid solution strengthening, precipitation hardening, dispersion hardening, work hardening, and use of a fine grain size. Precipitation hardening is the most effective mechanism and is achieved by solution heat treatment, quenching, and aging to precipitate coherent G-P zones, partially coherent intermediate precipitates, or incoherent equilibrium precipitates, depending on the aging conditions. In the 2000 series aluminum alloys, Cu is the principal alloy element and gives precipitation strengthening by zones, intermediate precipitates, or the equilibrium precipitate $CuAl_2$. In the 7000 series alloys, Zn and Mg are the principal alloying elements and provide zones and precipitates of the $MgZn_2$ type. In addition to direct strengthening, which is achieved by precipitates interacting with dislocation movement, alloy elements can provide indirect strengthening by the formation of fine stable dispersoids that stabilize a fine grain structure.

Rapid quenching of aluminum alloys can result in significant strength increases, first, as a result of increasing the solid solubility and thereby increasing the volume fraction of precipitate which forms on aging and, second, as a result of the very fine grain size (∿1μm) that is well below the size (∿5μm) at which significant strengthening starts to occur. Increased solid solution hardening and dispersion strengthening after aging have been reported for Al-Cu compositions beyond the equilibrium solubility limit (Krishnanand and Chan, 1976). Moreover, the possibility of precipitation hardening in Al-Fe base alloys has been demonstrated (Thursfield and Stowell, 1974), and there is considerable interest in the substantial ductilities attainable in high-silicon aluminum alloys (Dixon and Skelly, 1971;

Town, 1958; Thursfield and Stowell, 1974; Panseri and Paganelli, 1967; Boswell and Chadwick, 1977; Anantharaman and Suryanarayana, 1971; Jones, 1978).

Fracture Toughness

Alloy elements affecting fracture toughness in aluminum alloys are predominantly those that form brittle insoluble intermetallic compounds (Hahn and Rosenfield, 1965). These brittle particles fracture at low strains and initiate microcracks that result in failure. The role of various alloying elements in affecting both strength and fracture toughness has been studied by many workers (e.g., in 7178 Al alloy by Piper, et al., 1966, who found that Fe degraded toughness to the greatest extent). Recent work (Low, et al., 1972; Thompson and Levy, 1970) has shown that the most significant elements influencing toughness of aluminum are Fe and Si. This has led to the development of improved alloys having the same nominal chemistry as previous ones but with Fe and Si contents kept to minimum levels (0.03-0.05 percent). Examples are 2124 (the counterpart of 2024) and 7475 (the counterpart of 7075), which have the same strengths as their counterparts but provide increased toughness in conventionally cast products. Both the particle size, shape, and volume fraction of the intermetallics are important and large particles are particularly detrimental. As noted above, RSP usually produces microstructural refinement and reduces the amount of segregation so that the undesirable phases are either eliminated or finely dispersed, which results in an increase in fracture toughness.

The reduction in grain size that is achieved by rapid quenching may be even more important than the reduction in the intermetallic particle size since it represents a unique opportunity by which the material may be both strengthened and toughened. This is particularly attractive in view of the generally observed inverse relationship between strength and toughness. The stability of this fine-grained structure also will be improved by the fine dispersion of intermetallic particles. Data reported by Hahn and Rosenfield (1975) and by Thompson (1975) show that significant increases in fracture toughness occur with a decrease in grain size for a number of 7000 series alloys in both the underaged and overaged conditions. Similar data are presented by Nes (1978) for Al-Zn-Mg alloys in the naturally aged and peak aged conditions. If the fine grain sizes produced by the splat cooling technique ($\sim$1μm) can be retained through subsequent consolidation, it should be possible to achieve a significant improvement in toughness over conventionally cast alloys.

Elastic Modulus

Significant increases in the elastic modulus of aluminum alloys result from the presence of a large volume fraction of a fine dispersion

of second-phase particles of high elastic modulus. Solid solution alloying or texture modifications also can increase the modulus but generally to a lesser extent. The dispersion of second-phase particles can be achieved in two ways, either as precipitates during conventional age hardening of solution treated and quenched material or as a relatively insoluble dispersoid that precipitates during cooling or subsequent processing. The volume fraction is determined by the amount of solute and by the composition and density of the precipitated phase.

The Al-Li system is an example of the first type of system in which there is extensive solid solubility of Li in Al so that the alloy can be solution treated, quenched, and aged in the conventional way, and rapid solidification is not required to achieve a high volume fraction of precipitate. Extensive studies made of this system reveal that it has the highest specific modulus for a given solute content of any aluminum alloy system. The precipitate that forms at low aging temperatures is Al_3Li, and very high volume fractions can be obtained, which gives a high modulus. Difficulties (particularly low toughness at peak strength and segregation in large ingots) have been experienced with the Al-Li system in the conventionally cast and wrought condition. Rapid solidification of powders should permit significant improvements in the strength and toughness of these alloys to be achieved by decreasing segregation and producing a very fine grain size. Table 12 presents comparative data on alloy 2024 in the form of standard ingot product and the same alloy produced-from-roll quenched foils cooling rate 10^6 K/s) and containing at 1 and 3 percent lithium (Sankaran, 1978). Attention is called to the very large increases in the modulus-to-density ratio for the rapidly quenched lithium-alloyed product compared to standard 2024. Similar increases in the strength-to-density ratio of the rapidly quenched metal with increasing lithium are observed.

TABLE 12 Roller Quenched[a] Al-Li Alloys 2024 Base Composition

Property	2024-T4, Ingot Product	RQ 2024 - 1% Li		RQ 2024 - 3% Li, T6
		T4	T6	
Y.S (0.2%), ksi	41.5	56.3	63.5	82.8
UTS, ksi	67.4	76.0	77.5	84.5
Elong, %	23.8	20.7	8.2	5.1
R of A, %	23.5	9.2	5.2	2.5
E, $\times 10^6$ psi	10 4	11.2	11.2	12.3
Density, lb/in.^{3}	0.100	0.097	0.097	0.091
YS/Density, $\times 10^4$ in.	41.5	58.0	65.5	91.0
E/Density, $\times 10^7$ in.	10.6	11.5	11.5	13.5
Fatigue Stress (σ fat) for 10^7 cycles, ksi	25.	32.	–	42.
σ fat/UTS (for 10^7 cycles life)	0.37	0.43		0.5

[a]Estimated cooling rate 10^6 K/s.

From Sankaran and Grant, to be published.

The Al-Mn system is an example of the second type of system, with limited solid solubility, in which conventional casting will not achieve sufficient supersaturation to give a large volume fraction of fine precipitate. Rapid solidification is needed to achieve this requirement. This alloy in the cast and wrought condition has shown a higher modulus than most other aluminum alloys (Dudzinski, et al., 1947). Rapid quenching of Al-Mn alloys will give a supersaturated solid solution, and if the precipitation of second phase Al_6Mn can be controlled during consolidation and subsequent processing to give a fine dispersion, high modulus and improved secondary properties should be obtained.

Fatigue Crack Initiation and Propagation

Many studies of fatigue crack growth rates in the intermediate growth rate regime have shown that metallurgical factors such as monotonic yield strength, thermal-mechanical treatment, and preferred orientation do not have a significant effect on the crack growth rate in aluminum alloys. The most significant finding has been that the fatigue crack growth rates in engineering alloys depend on the modulus of elasticity. By normalizing the stress intensity factor range by the modulus, differences in fatigue crack growth rate are largely eliminated (Bates and Clark, 1969). One of the significant benefits of the production of high-modulus aluminum alloys from rapidly solidified powders is the reduction in fatigue crack growth rate that should be achieved.

Results reported by Lebo and Grant (1974) show significantly improved fatigue strengths and fatigue lifetimes in rapidly quenched aluminum alloys. These improvements have been attributed to the decreased crack initiation that results from the refinement or elimination of coarse constituent particles. Table 12 shows the improvement in stress limit for a fatigue life of 10^7 cycles between conventionally cast Al-2024 ingot and roll-quenched 2024 alloy with lithium additions. Note that the ratio σ_{fat}/UTS for this fatigue life increases to 0.5 for the splat quenched 3 percent Li alloy; the usual value of this ratio for ingot product varies between 0.3 and 0.35. This value of 0.5 is probably the highest ever reported for high-strength aluminum alloys (private communication from N.J. Grant).

Environment-Assisted Cracking

The environment-assisted cracking of aluminum alloys recently has been reviewed by Speidel (1975). The main metallurgical factors affecting environment-assisted cracking in aluminum alloys are alloy chemistry, heat treatment, and thermal-mechanical treatment. Many

studies have shown that overaging is the most effective way to improve the environment-assisted cracking behavior of aluminum alloys. Overaging also decreases the yield strength but increases the fracture toughness. The same factors that apply in conventionally cast and wrought materials likely will apply in rapidly quenched aluminum alloys. The resistance to environment-assisted cracking generally improves with decreasing size of constituent particles (Speidel, 1975). The microstructural refinement and reduction of segregation-related second phases produced by RSP should therefore improve these properties. Rapid solidification also allows the production of alloy compositions and microstructures that have improved environment-assisted cracking resistance and that cannot be made using conventional ingot metallurgy techniques (e.g., the aluminum alloys Ma 67 and Ma 87) (Lyle and Cebulak, 1975; Otto, 1976; Cebulak, 1978).

Elevated Temperature Strength

One of the requirements for elevated temperature strength is a fine dispersion of thermodynamically stable, coherent, coplanar precipitates or second-phase particles (Fine, 1975). The intermediate size precipitates that are found in 7075 containing Cr are stable, partially coherent precipitates, and Al_3Zr also is partially coherent with the Al matrix. The volume fractions of both these particles are limited in conventionally cast systems but may be significantly increased by rapid solidification. Al_3Ni also is a very stable phase used to obtain elevated temperature strength and, normally, only small volume fractions can be obtained. The presence of Fe in conventionally cast Al alloys normally has a deleterious effect on properties because of the relatively coarse intermetallic particles that are formed; however, RSP of Al-Fe alloys has been shown to result in a very fine dispersion of stable $FeAl_3$ particles, that results in better high-temperature alloys (Thursfield and Stowell, 1974). In binary Al-Mg alloys, Mg_2Al_3 is a reasonably stable phase and large volume fractions may be formed in conventional casting. Refinement and more uniform distribution of this phase can result from RSP and would be expected to improve elevated temperature strength. Similar effects are possible in the Al-Cu system where the stable $CuAl_2$ phase is used to improve elevated temperature properties in alloys containing Cu in excess of the solid solubility limit (e.g., 2021 and 2219 Al alloys).

To give an indication of the number of alloy systems investigated, the more recently published research results on rapidly solidified aluminum alloys are summarized in Table 13, which indicates the solidification methods used for producing the particulate, the consolidation procedures, and the type of mechanical properties evaluated. Some reported property improvements of particular interest are summarized in Table 14, along with properties obtained from conventionally produced

TABLE 13 Microstructure and Mechanical Property Measurements on Consolidated Material

Alloy System	Quenching Method	Cooling Rate, K/sec	Consolidation Method	Properties Evaluated[a]	Reference
Al-Cu-Mg (2024)	Splat	10^6	Cold compaction, vac. annealing, hot extrusion	1,2,3,4,5	Lebo and Grant, 1974
Al-Zn-Mg (7075)	Splat	10^5-10^6	Vac. annealing, hot extrusion	1,2	Durand et al., 1976
Al-Zn-Mg (7075)	Melt Spinning	10^5-10^6	Cold compaction, vac. annealing, hot pressing, hot extrusion	1,2,3	Mobley et al., 1972
Al-Fe	Splat	10^6	Cold compaction, annealing, hot extrusion	1,2,3,6	Faninger et al., 1976
Al-Fe Al-Fe-Zr,Al-Fe-Mn	Splat	$>10^5$	Cold compaction, hot extrusion	1,2,3,5,6	Thursfield and Stowell, 1974
Al-Mn-Cu Al-Mn-Cr-Mg-Zn	Atomization			1,2,6	Rostoker et al., 1973
Al-Mn	Atomization		Extrusion	1,2	Sheppard, 1974
Al-Cu-Mg-Li (2024 + Li)	Melt Spinning	10^4	Cold compaction, vac. hot pressing, hot extrusion	1,2,4,6	D. Webster, unpublished LMSC independent research work, 1977
Al-Cu-Mg-Li (2024 + Li)	Splat	10^5	Cold compaction, hot extrusion	1,2,4,5,6	Sankaran, 1978
Al-Zn-Mg-Cu-Co (MA67,MA87)	Atomization	10^3-10^5	Cold compaction, vac. annealing, hot pressing, hot extrusion	1,2,4,5,6	Lyle and Cebulak, 1975 Otto, 1976 Cebulak, 1978

[a] 1 = microstructure, 2 = tensile, 3 = elevated temperature tensile, 4 = fatigue, 5 = creep, 6 = corrosion/stress corrosion.

TABLE 14 Selected Examples of Property Improvements Reported for Consolidated Rapidly Quenched Aluminum Alloy Particulate

Alloy	Property	Property Value Reported	Improvement Over Commercial Alloy	Reference
2024-T4	Room Temp. Y.S.	326 MPa	18%	Lebo and Grant, 1974
	Fatigue Life	3.5×10^6 cycles at 207 MPa	Increased by a factor of 7	Lebo and Grant, 1974
	Fatigue Strength	220 MPa at 10^6 cycles	14%	Lebo and Grant, 1974
	Stress Rupture at 423K	Stress for 1000 hours life – 400 MPa	About 50% higher stress	Lebo and Grant, 1974
7075 plus 1.3 wt.% Ni and 0.96 wt.% Fe T6 condition	Room Temp. Y.S.	634 MPa	24% Over 7075-T6	Durand et al., 1976
7075-T6	Room Temp. Y.S.	579 MPa	16%	Mobley et al., 1972
	Elevated Temp. Elongation	200% at 673K	Increased by a factor of 3	
Al-8 wt.% Fe	Room Temp. Tensile U.T.S.	572 MPa	24%, over RR 58	Thursfield and Stowell, 1974
	Elevated Temp. Tensile U.T.S.	234 MPa at 575K	29%, over RR 58	Thursfield and Stowell, 1974
	Elastic Modulus	81 GPa at RT	15%, over 7075-T76	Thursfield and Stowell, 1974
	Creep Resistance		Superior to RR 58	
Al-5Mn-4Cu	Elevated Temp. Y.S.	165 MPa at 523K	70% over 7075	Rostoker et al., 1973
Al-5Mn-0.5 Mg	Room Temp. T.S.	345 MPa		
2024-3 wt.% Li-T6	Specific Modulus	3.4×10^6 m 85 GPa	30% over 2024-T4	Sankaran, 1978; D. Webster, unpublished LMSC independent research work, 1977
	Elastic Modulus	12.3×10^6 psi	18.3% over 2024-T4	Sankaran, 1978
	Density	2.5×10^3 Kg/m^3	9.0% reduction over 2024-T4	Sankaran, 1978
	Room Temp. Y.S.	571 MPa	62% over 2024-T4	Sankaran, 1978
	Fatigue Strength	317 MPa 10^6 cycles	48% over 2024-T4	Sankaran, 1978
MA 87	Short Transverse Room Temp. Y.S.	471 MPa	12% over 7050-T73652	Otto, 1976
	Fracture Toughness K_Q	34.3 MPa m	66% over 7050-T73652	
	Fatigue Crack Growth Rate	1.9×10^{-7} m/cycle at $\Delta K = 11.0$	Decreased by a factor of 4, over 7050-T73652	Otto, 1976
	Stress Corrosion	Alternate immersion Tests	Equivalent to 7050-T73652	Otto, 1976

ingot metallurgy alloys for comparison. The data summarized in Table 14 have been selected from a relatively large body of published results to illustrate some of the more significant property improvements reported for different aluminum alloy systems on consolidated rapidly quenched materials.

REFERENCES

Anatharaman, T.R., and C. Suryanarayana. 1971. J. Mater. Sci., Vol. 6, p. 1111.

Armstrong, G.R., and H. Jones. 1977. "Solidification and Casting." Paper presented at a conference at the University of Sheffield (to be published by the Metals Society).

Bates, R.C., and W.G. Clark, Jr. 1969. Trans. Quart., ASM, Vol. 62, p. 380.

Boswell, P.G., and G.A. Chadwick. 1977. Scripta Met., Vol. 11, p. 459.

Bower, T.F., et al. 1966. Trans. AIME, Vol. 236, p. 624.

Brown, P.E., and C.M. Adams. 1966. Trans. AFS, Vol. 69, p. 879.

Cebulak, W.S. 1978. In Rapid Solidification Processing, p. 324. Edited by R. Mehrabian, et al. Claitor Pub. Div., Baton Rouge, La.

Davies, H.A., and J.B. Hull. 1974. J. Mater. Sci., Vol. 9, p. 707.

Dixon, C.F., and H.M. Shelly. 1971. Int. J. Powder Met., 7, Vol. 3, p. 47.

Dudzinski, N., et al. 1947. J. Inst. Metals, Vol. 74, p. 291.

Durand, J.P.H.A., et al. 1976. Mat. Sci. Eng., 23, Vol. 213, p. 247.

Fanninger, G., et al. 1976. In Proc. Second Int. Conf. on Rapidly Quenched Metals, p. 483. Edited by N.J. Grant and B.C. Giessen, MIT Press, Cambridge, Ma.

Fine, M.E. 1975. Met. Trans. A, 6A, p. 625.

Grant, N.J. 1970. In Rapid Solid. Proc., p. 230. Edited by R. Mehrabian, et al. Claitor Publ. Div., Baton Rouge, La.

Hahn, G.T., and A.R. Rosenfield. 1965. Acta Met., Vol. 13, p. 293.

Hahn, G.T., and A.R. Rosenfield. 1975. Met. Trans. A, Vol. 6A, p. 653.

Horwath, J.A., and L.F. Mindolfo. 1962. Acta Met., Vol. 10, p. 1037.

Jacobs, M.H., et al. 1974. J. Mater. Sci., Vol. 9, p. 1631.

Jones, H. 1969. Mat. Sci. Eng., Vol. 5, p. 1.

Jones, H. 1970. Metallography, No. 3, Vol. 3, p. 307.

Jones, H. 1978. Aluminum, No. 54, Vol. 4, p. 274.

Kattamis, T., and R. Mehrabian. 1974. J. Vac. Sci. Tech., No. 11, Vol. 6, p. 1118.

Krishnanand, K.O., and R.W. Cahn. 1976. In Proc. Second Int. Conf. on Rapidly Quenched Metals, p. 76. Edited by N.J. Grant and B.C. Giessen. MIT Press, Cambridge, Ma.

Lebo, M., and N.J. Grant. 1974. Met. Trans., Vol. 5, p. 1547.

Linde, R.K. 1966. Trans. AIME, Vol. 58, p. 236.

Low, J.R., Jr., et al. 1972. NASA TR 2.

Lyle, J.P., and W.S. Cebulak. 1975. Met. Trans. A, Vol. 6A, p. 685.

Matyja, H., et al. 1968. J. Inst. Met., Vol. 96, p. 30.

McComb, J.A., et al. 1964. J. Phys. Soc. Japan, Vol. 19, p. 1691.

Mobley, C.E., et al. 1972. J. Inst. Metals, Vol. 100, p. 142.

Nes, E. 1978. Z. Metallkd., Vol. 69, p. 35.

Otto, W.L. 1976. Metallurgical Factors Controlling Structure in High Strength Al P/M Products, AFML-TR-76-60. Air Force Materials Laboratory.

Panseri, C., and M. Paganelli. 1967. Alluminio, Vol. 36, p. 179.

Piper, D.E., et al. 1966. Met. Soc. Conf., Vol. 31, p. 227.

Ramachandrarao, P., and M. Lavidjani. 1974. J. Mater. Sci., Vol. 9, p. 434.

Ramachandrarao, P., et al. 1972. Phil. Mag., Vol. 25, p. 961.

Rostoker, W., et al. 1973. AFML-TR-73-36. Air Force Materials Laboratory.

Sankaran, K.K. 1978. J. Mat. Sci., Vol. 13, p. 291.

Sankaran, K.K., and N.J. Grant. "Structures and Properties of Splat Quenched 2024 Aluminum Alloys Containing Lithium Additions." Materials Science & Engineering (to be published).

Scott, M.G., and J.A. Leake. 1975. Acta Met., Vol. 23, p. 503.

Sheppard, T. 1974. In Proc. 15th Int. Machine Tool Des. and Res. Conf. (Birmingham, England), p. 659.

Speidel, M.O. 1975. Met. Trans., Vol. 5, p. 1547.

Spear and Garner. 1963. Trans. AFS, Vol. 71, p. 209.

Suryanarayana, C., and T.R. Anatharaman. 1970. J. Mat. Sci., Vol. 5, p. 992.

Thompson, D.S. 1975. Met. Trans. A, Vol. 6A, p. 671.

Thompson, D.S., and S.A. Levy. 1970. AFML-TR-70-171. Air Force Materials Laboratory. WPAFB, Oh.

Thursfield, G., and M.J. Stowell. 1974. J. Mater. Sci., Vol. 9, p. 1644.

Tonejc, A., et al. 1971. Acta Met., Vol. 19, p. 311.

Town, R.J. 1958. Met. Prog., Vol. 73 (5), p. 70.

Varich, N.I., and K. Ye. Kolesnichenko. 1961. Met. Abs., Vol. 28, p. 715.

Varich, N.I., and R. Lyukevich. 1970. Russ. Met., Vol. 4, p. 58.

Williams, D.B., and J.B. Edington. 1976. In Proc. Second Int. Conf. on Rapidly Quenched Metals, p. 135. Edited by N.J. Grant and B.C. Giessen. MIT Press, Cambridge, Ma.

Wood, J.V., and R.W. Honeycomb. 1974. J. Mat. Sci., Vol. 9, p. 1183.

Chapter 11

HIGHER MELTING ALLOY

NICKEL-BASE AND COBALT-BASE SUPERALLOYS

As demands for higher strength, high-temperature nickel-base alloys developed, efforts to achieve these goals in terms of higher alloy content inevitably led to less-forgiving ingot alloys and more brittle casting alloys, with the net result that alloy development via ingot technology and precision casting has progressed little in recent years. Rapid quenching technology makes it possible to produce fine powders and foils with highly refined structures: fine grain size, sharply decreased segregation, very fine second-phase particles, (e.g., chromium carbides), etc. Quench rates from the melt in excess of 10^2 ^{o}C sec^{-1} and preferably 10^4 ^{o}C sec^{-1} permit these refinements. Even those alloy compositions originally designed as casting alloys when consolidated from rapidly quenched particles are readily hot-workable in the refined, rapidly quenched state, with large increases, compared to cast alloys, in ductility over the entire range of temperatures of interest and accompanying improvements in toughness, fatigue resistance, and, in specific instances, corrosion resistance.

Table 15 presents representative room-temperature tensile properties for nickel-base alloys IN100 and Rene 95 and for cobalt-base Mar-M-509. At room temperature (and up to about 200^{o}C), the very fine-grained, as extruded, quenched-powder extrusions are very much stronger and more ductile (by factors of 4 or 5) than their conventionally cast counterparts. These fine-grained, homogeneous alloys are not useful above about 700 or 800^{o}C, in contrast to the cast, coarse-grained products (Table 16). Recrystallization to coarsen the grain size (uniform coarsening) does recover the high-temperature strength (982^{o}C) with attendant loss of ductility. As fine-grained materials, these nickel-base alloys become attractive disk alloys below about 700^{o}C.

Given the right composition and a two-phase structural mix, these nickel- and cobalt-base alloys exhibit superplasticity or high levels of hot plasticity at relatively slow strain rates. The IN100 alloy with a grain size finer than about 10 μm will attain fracture elongation values greater than 1000. The Mar M-509 alloys, with a similar fine grain size, show ductility levels of 80 percent in slow stress rupture tests at 982^{o}C (Table 16) and values two to three times that level at more appropriate temperatures and strain rates.

The superplastic properties of the extruded, fine-grained materials have been exploited to produce shaped parts by closed-die forging and thin-sheet products by hot rolling. At temperatures above γ' solvus temperature, the fine-grained material experiences rapid grain coarsening (i.e., secondary recrystallization occurs).

TABLE 15 Room Temperature Tension Properties of Representative Superalloys Prepared from Rapidly Quenched Particulates

Alloy	Condition	0.2% Y.S ksi	0.2% Y.S MN/m^2	UTS ksi	UTS MN/m^2	Elong, %	RA, %
IN-100[a]	As-Cast, 1500μ G.S	136	938	143	986	4	8
IN-100[a]	As-HIP'd (PM)	137	945	163	1124	8	10
IN-100[a]	As-Extrud., 8μ G.S(PM)	175	1207	244	1682	21	17
Mar M-509[b]	As-Cast, 4000μ G.S	80	552	115	793	3	4
Mar M-509[b]	As-Extrud., 3-4 G.S(PM)	130	896	192	1324	14	12
René 95[c]	Ingot forging[d]	180	1241	230	1586	10	12
René 95[c]	HIP, roll.[d] (PM)	199	1372	254	1751	15	22

[a]IN-100 composition (%)–10.5 Cr, 3.0 Mo, 5.5 Al, 4.7 Ti, 1.1 V, 0.16 C, 0.015 B, 0.06 Zr, 15.4 Co, balance is Ni.
[b]Mar M-509 composition (%)–22 Cr, 7 W, 3.5 Ta, 0.60 C, 0.7 Zr, 10 Ni, balance is Co.
[c]René 95 composition (%)–13 Cr, 3.5 Mo, 3.5 W, 3.5 Al, 2.5 Ti, 3.5 Cb, 0.08 C, 0.010 B, 0.05 Zr, 8 Co, balance is Ni.
[d]Heat treated.

TABLE 16 Comparison of Values of Stress for 100 Hours Life at 982°C (1255K) for Conventional Ingot As-Cast Coarse Grained and Splat Quenched Fine Grained Structures

Alloy	Condition	Grain Size, μm	Stress for 100 hr Life ksi	Stress for 100 hr Life MN/m^2	Elong, %
IN-100	As-Cast	1500	22	152	10
IN-100	PM. As-Extrud.	8	2	14	43
IN-100	PM. As-Extrud., Recryst.	100	12	83	5
IN-100	PM. As-Extrud., Recryst.	500	17	117	4
Mar M-509	As-Cast	4000	17	117	9
Mar M-509	PM. As-Extrud.	5	2.5	17	80
Mar M-509	PM. As-Extrud., Recryst.	200[a]	12	83	10

[a]Mixed recrystallized grain size; average about 200 μm.

When secondary recrystallization takes place under a steep temperature gradient, the material can develop a relatively coarse-grained, textured columnar structure. Observed texture orientations are primarily of the <100> and <111> types. Any single crystal orientation can be produced by starting the directional recrystallization process from an appropriately oriented seed crystal.

Significant improvements in fatigue properties have been realized in rapidly quenched and processed fine-grained polycrystalline materials. Superior creep strength has been shown in textured columnar-grained material. Some benefits in oxidation and hot corrosion resistance also have been found in homogeneous, recrystallized material. Such structure-property control makes possible some important applications for rapidly quenched and processed alloys in gas-turbine engines. Thus, fatigue-resistant alloys can be exploited for disks, creep-resistant alloys for blades, and corrosion-resistant alloys for vanes.

Another development of some significance is the ability to produce thin sheet by hot rolling. This should make possible the fabrication of air-cooled blades and vanes of unparalleled complexity simply by bonding together stacked arrays of photo-etched wafers. Computations suggest that the improved cooling efficiencies possible in a wafer blade of advanced design, coupled with the higher temperature capability of rapidly quenched powder metallurgy alloys, should permit much higher turbine inlet temperatures and quite possibly make the attainment of a stoichiometric engine a realistic technical goal.

TOOL STEELS

Various grades of high-speed tool steels are commercially produced today from hot-worked powders quenched from the melt at moderate rates. High-speed tool steels produced by ingot technology tend to have coarse carbides at ingot centers due to slow cooling and the high alloy levels that result in high volume content of carbide phases. Ingot cross sections are therefore kept as small as possible to avoid formation of coarse carbides; however, cooling rates must not be too great in order to avoid ingot cracking upon cooling to low temperatures. Subsequent resolution of such carbides for improved hot work leads to grain coarsening. The refractory carbides do not solutionize easily without danger of burning.

By achieving even intermediate quench rates through gas atomization, carbides are distinctly finer, and hot consolidation through hot work proceeds much more readily than with ingots. As a result of having produced fine carbides, solution treatments are simplified, hot working temperatures are lower, and burning is avoided.

Several other major advantages also are realized:

1. Higher volume content of carbides is possible.
2. Totally different combinations of carbide formers become attractive, with resultant different combinations (compositions) and distribution of the phases.
3. Final product size can be significantly larger (cross section as well as total weight) because the coarse grain size and coarse carbides of very large, slowly cooled ingots are no longer controlling. Through hot isostatic pressing, section sizes over 30 inches are possible, and special rolls and other heavy sections are being produced.
4. Powder products that are hot isostatically pressed (HIP) to shape and precision closed die forgings permit new areas of application.

As a successful commercial venture, the tool steels demonstrate the great potential of the wrought powder metallurgy process, using quench rates for the powders that may be as low as 10^2 °C per second and still achieving highly beneficial results. As a further demonstration of the beneficial role of fine grain size, O. Sherby of Stanford University has recently produced superplastic Fe-C alloys containing from about 2.2 to 2.5 percent carbon.

TITANIUM-BASED AND OTHER ALLOYS

Titanium, although not used in large tonnages in aircraft structures, is used extensively in jet engines. Titanium is an extremely important structural metal, and much effort has been directed to making it a more versatile material. Castings, although extensively studied and subjected to major developmental efforts, have not been broadly successful, in part due to contamination, segregation problems, and the need to remove reacted surfaces.

Early developmental efforts with atomized titanium alloy powders have shown great promise for the process. Titanium and its alloys along with other reactives and/or high-melting temperature alloys such as V, Zr, Nb(Cb), Ta, Hf, and Cr cannot be crucible melted in preparation for atomization or splat quenching without encountering undesirable levels of contamination. Thus, for such reactive alloys it is more attractive to use noncrucible (conventional) melting processes. One such method is the rotating electrode process (REP) that uses premelted cast or wrought bar (in preference to electrodes sintered from elemental alloys and masteralloys), which is clean and homogeneous by virtue of its prior preparation by vacuum-arc remelt (VAR), for example.

The powders produced using the REP process tend to be relatively coarse (>200 μm), but they are clean and of uniform size and quench rate. Quench rates typically are not greater than 10^2°C per second.

Obviously, there is great need for variations of the REP process or substitute processes that would:

1. Bypass the use of electrodes prepared from VAR wrought materials.
2. Permit alloy variations more readily while avoiding an intermediate ingot stage.
3. Permit attainment of finer powders subjected to higher quench rates than the maximum of 10^2°C per second attainable by REP (dynamic helium quenching is, of course, one possibility as a variation of the REP).
4. Permit higher production rates.

Only a few titanium alloys have been studied in any important detail, the most common being the well known Ti-6Al-4V alloy. Ti-6-4, in the fine-grained condition due to the atomization and hot consolidation steps, is superplastic by virtue of its two-phase structure. Several other titanium alloys also are superplastic. This permits easy hot or cold forming of the alloys into intricate shapes.

An obvious potential advantage for the rapidly quenched powder process route could be the replacement of the costly double-melting step for ingot production, with attendant product yield losses in processing. The potential for development of a much broader range of compositions, structures, and properties among Ti alloys is of particular interest.

Several aluminum alloys, produced as 1 to 20 μm grain size products from rapidly quenched, atomized powders, have deformed superplastically. The so-called microduplex stainless steels of the Fe-Ni-Cr type, balanced compositionally to have a mixed $\alpha+\gamma$ (ferrite plus austenite) structure and produced as rapidly quenched atomized or roll-quenched foils to have 1 to 20 μm grain size in the hot worked condition, are superplastic on deformation at about 1050 to 1150°C. For structures varying from 30 α - 70γ to 70α - 30γ, ductilities at fracture for strain rates of 10^{-2} to 10^{-6} second^{-1} vary from 200 to 700 percent elongation. These microduplex alloys are much stronger at room temperature than fully austenitic stainless steel.

Through rapid quenching of liquid copper alloys containing small amounts of Zr, Cr, Mg, and other poorly soluble (in the solid state) alloying elements, high-conductivity (thermal), high-strength, high-temperature alloys have been produced. For applications requiring the combination of high temperature strength and stability and high thermal conductivity, these copper alloys are outstanding.

SECTION III

APPLICATIONS

Chapter 12

MAGNETIC APPLICATIONS

In the past two years a variety of magnetic applications using amorphous metallic alloys have been reported. Thus, the early promise of the potential usefulness of amorphous alloys appears to be coming true. Some previous reviews cover the application of amorphous metals in both electronic and power devices (Luborsky, 1977; Luborsky, et al., 1978).

ELECTRONIC DEVICE APPLICATIONS

Until 1976 there were no magnetic devices described in the literature using amorphous alloys. In 1976 two different applications of amorphous metals were reported. The first of these applications was the use of the ribbon for shielding. Large sheets were made by simple weaving and then coating with a polymer. Cylindrical shields made from these woven fabrics were measured at 60 Hz and compared to an equal weight shield wrapped from polycrystalline 80Ni20Fe foil. Neither was annealed. Shielding ratios of the woven glass compared favorably with those of the polycrystalline foils. The woven glass, however, is more flexible and less sensitive to mechanical strain.

The use of metallic glasses for shielding is limited, however. At fields as low as several milli oersteds metallic glasses can have permeabilities (μ) of the order of 10 to 100 K (i.e., similar to those of the permalloys). However, for very low fields (e.g., 10^{-4} to 10^{-3}Oe), μ is likely to be of the order of several hundred. In other words, as opposed to the case for the permalloys, the μ vs. H behaviors of metallic glasses are highly nonlinear. Since shielding effectiveness depends on ease of magnetization (i.e., it is promoted by high permeability), metallic glasses are relatively ineffective for shielding very low fields. The source of the nonlinear μ vs. H behavior of glassy ferromagnets is a subject of great fundamental and technological interest.

The second application reported in 1976 was for delay lines. Electronically controllable acoustic delay lines were built and tested (Arai, et al., 1976; Tsuya and Arai, 1978). These made use of the ΔE effect (i.e., the change in Young's modulus E with applied field H were E is directly related to the sound velocity). The ΔE effect was extremely large in a variety of amorphous alloys tested for the delay lines. $Fe_{80}P_{13}C_7$ had a peak ΔE of 0.8 at 5 Oe (Arai, et al., 1976), and $Fe_{78}Si_{10}B_{12}$ had a peak value of 1.9 (Tsuya and Arai, 1978), the largest ever reported. In these same efforts the magnetomechanical coupling factor, k, also was measured. The value of k is the most important dynamic transducer parameter and gives a measure of the

elastic energy generated by magnetic excitation. The very large values of 0.53 for annealed $Fe_{80}P_{13}C_7$ and of 0.75 for $Fe_{78}Si_{10}B_{12}$ were found. Delay times of ∿2 μs/cm were obtained in zero field; maximum changes of ∿12 percent were obtained in a field of 8 Oe at 100 kHz.

Other applications were reported in 1977. An electronic current transformer used an amorphous metal tape core made from $Fe_{40}Ni_{40}P_{14}B_6$ operating into a virtually zero ohm load by using feedback from an operational amplifier. Due to the very low flux density created by virtually short circuiting the transformer, the nonlinear effects and core losses are reduced substantially. A transformer core of reduced size may be used if such an electronic transformer is provided. Test results have shown that the amorphous metal core using the active load has performance equal to 80Ni20Fe with respect to magnitude error; however, the phase shift is somewhat poorer than for NiFe of the same size. The amorphous core is significantly superior to the FeSi core in both magnitude and phase shift error. The results demonstrated the suitability of this amorphous core material for use as a current transformer with the active load.

Another application reported in 1977 was the use of amorphous cores as tensile-stress transducers in a multivibrator configuration. This makes use of the remarkable sensitivity in magnetic properties and tensile stress of amorphous alloys. A differential type of multivibrator was constructed using two cores wound from $Fe_{40}Ni_{40}P_{14}B_6$. Tension or compression could be applied to the windings of one of the cores. It was made with two types of transducing behavior: an analog type with no zero output but good linearity and sensitivity and no hysteresis, and a threshold type with zero output for tensile stress under a critical stress and maximum output for stress over this critical stress. Conventional crystalline permalloy would be very poor for use in this application because of its soft mechanical behavior.

Presently available powdered cores are made from flake iron or powders of different sizes of iron, Mo-Permalloy (79Ni-17Fe-4Mo), and iron oxides. Basically, the method of producing powdered iron cores consists of first insulating the iron, for example, by tumbling with zinc flake. The zinc then is removed by sieving and binder is added with a lubricant. The material is pressed from 10 to 50 tons/in.^{2} and the core is baked to set the plastic binder. Such cores may be used from 60 Hz to above 250 MHz depending on the particle size. Thus, the flake material with particle sizes of about 80 μm are used from 60-2000 Hz whereas 8 μm powders are used from 40-250 MHz. The oxide powders are used at the highest frequencies.

Compared to metal tape wound cores, powdered cores have a much greater frequency response and may be molded directly to finished size. However, because of the necessary interparticle insulation and

the binder, the saturation flux is reduced and the coercivity and losses are increased as compared to tape wound cores. Using amorphous alloy, which has substantially lower losses, should result in lower loss cores.

The final application reported in 1977 was for the use of amorphous ribbon in transverse filters. These make use of the magnetostrictive waves on the amorphous ribbon. Arbitrary transfer functions were easily realized by adjusting voltages and polarities.

POWER DEVICE APPLICATIONS

The concept of using amorphous alloys in power size transformers has been developed in a series of papers (Luborsky, 1977; Luborsky, et al., 1978). It was first shown (Luborsky, 1977) that the high saturation magnetization alloy $Fe_{80}B_{20}$ exhibited extremely low losses. Losses were down by a factor of four as compared to the best oriented Fe3.2%Si. In a finished transformer this reduction in core loss would result in substantial energy savings over the lifetime of the installation. For example, of the 2×10^{12} kWh of electrical power generated annually in the United States, roughly 0.5 percent is lost as iron losses in the cores of distribution transformers alone. At \$0.03/kWh, a reduction in losses from 1.5 to 0.44 mw/g (i.e., in going from oriented FeSi to amrophous FeB) would save over \$200 million annually now wasted as heat in transformers. Thus, there is a real incentive to push forward the development of amorphous alloys for use in large transformers.

The drawbacks presently under consideration are the lower saturation magnetization, $4\pi M_s$, of the amorphous alloys and the thinner gage of the sheet. The impact of the lower $4\pi M_s$ on the cost of the finished transformer is shown in Figure 31. This figure gives the total cost of a moderate size transformer relative to a transformer of the same rating made from FeSi as a function of the $4\pi M_s$ and as a function of the relative cost/gm of the core material. These costs are based on the construction costs remaining the same with appropriate changes in coil and core dimensions plus a fixed cost equal to approximately half of the total cost. Three data points are shown. The one at 17 kG represents the cost of present transformers made from oriented Fe3.2%Si. The amorphous $Fe_{80}B_{20}$ is shown operating at a conservative 14.5 kG, and a material cost of 1.5 times that of Fe3.2%Si. This cost factor is conservatively high and is based on today's costs for boron and a generous allowance for conversion. The amorphous FeB would increase the total transformer cost to 127 percent of its present level; however, the lower losses would more than offset this initial cost during its operating lifetime. The third data point shown in Figure 31 corresponds to the design of a transformer using Fe3.2%Si operating at the same low losses as the amorphous FeB. This would

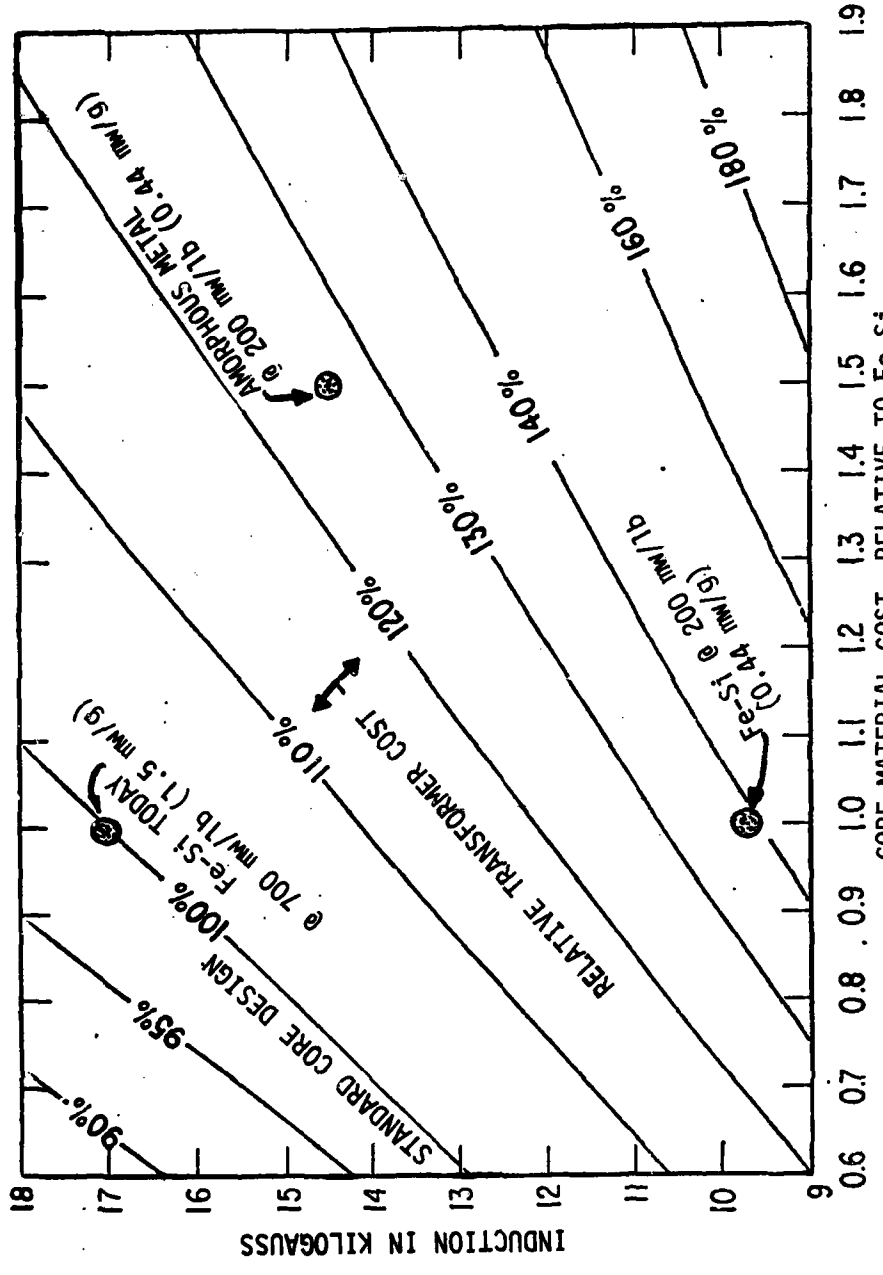

FIGURE 31 Costs of transformers made from amorphous FeB compared to conventional Fe3•2%Si.

require operating the core at 9.7 kG, requiring substantially more material in the core. This would raise the transformer cost to 138 percent. The present thrust of the materials research in this area is to try to raise $4\pi M_s$ of available inexpensive amorphous alloys as already discussed.

The limitation on the thickness of amorphous ribbons is ∿50 μm and is determined by the heat-transfer rate through the solidifying ribbon. The cooling curve must be such as to miss the intersection of the nose of the crystallization curve on the T-t diagram. This thickness is about five to six times smaller than the thickness of conventional Fe3.2%Si. Thin material has the advantage of low eddy current losses, but it is not possible to prepare Fe3.2%Si at thicknesses thinner than ∿300 μm and still achieve the same low losses. Thus, the amorphous alloys have the inherent advantage of low eddy current losses. On the other hand, the thin material will occupy less of the total available space, particularly if interlayer insulation is used. However, the greater resistivity and lower losses of the amorphous alloy might make it unnecessary to insulate all of the layers.

The permeability of the amorphous alloy $Fe_{80}B_{20}$ at 60 Hz is shown in Figure 32 as a B vs. H curve compared to Fe3.2%Si, FeNi, and FeCo alloys. All curves are for 50 to 100 μm thicknesses. Although the amorphous FeB has a higher initial permeability, its permeability at 14.5 kG is lower than FeSi at 17 kG. Thus, higher drive fields will be required unless the permeability can be improved.

A present practical limitation on the uses of glassy alloys in distribution transformers is that ribbon widths of the order of 4 to 6 inches are required. In principle, this is a straightforward extension of present technology; in practice, it is a highly challenging problem. In order to expedite its solution, a substantial program is being funded at Allied Chemical by the Electric Power Research Institute.

Using present prices for materials and processing, a crude comparison can be made of the cost of distribution transformers applications:

	lb/100 lb alloy*	Cost $/lb	Amorphous Alloy $/100 lb
Ferroboron	19	2.15	41
Fe Scrap	81	.04	3
Total			44

Thus, the cost per ton to produce finished tape is:

*Pounds of ferroboron or iron scrap per 100 pounds of alloy.

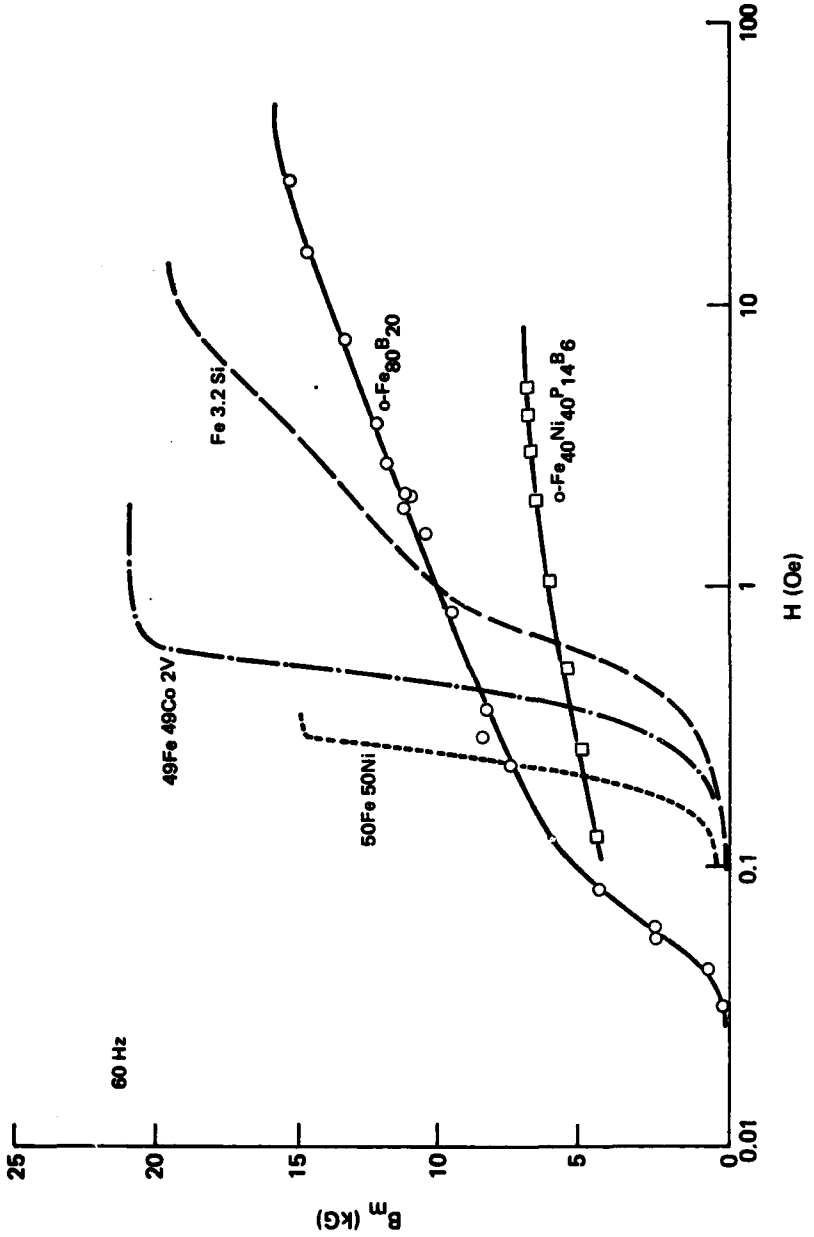

FIGURE 32 Maximum induction vs. applied field at 60 Hz for a variety of conventional crystalline alloys compared to FeB and FeNiPB amorphous alloys.

Raw material	880
Processing	300
	1180 $/ton = $0.60/lb.

This compares favorably with present day costs of high-quality Fe3.2%Si (M-4 grade) of $0.50 to $0.60/lb.

REFERENCES

Aria, K., et al. 1976. In Proc. Second Int. Conf. on Rapidly Quenched Metals, p. 489. Edited by N.J. Grant and B.C. Giessen. MIT Press, Cambridge, Ma.

Luborsky, F.E. 1977. Mat. Sci. Eng., Vol. 28, p. 139, and In Amorphous Magnetism, Vol. 2. Edited by R.A. Levy and R. Hasegawa. Plenum Press, N.Y.

Luborsky, F.E., et al. 1978. J. Magn. Magn. Mater., Vol. 8, p. 318

Tsuya, N., and K.I. Arai. 1978. J. Appl. Phy., Vol. 49, p. 1718.

Chapter 13

ELECTRICAL APPLICATIONS

Inexpensive precision resistance wires could be fabricated mainly from nonstrategic materials such as iron. The large resistivity values generally exhibited by metallic glasses may lead to their usage as low-temperature heating elements. In this type of application, the high mechanical strength and ductility characteristic of metallic glasses also would be advantageous.

Another area of electrical application would be to utilize the large negative temperature coefficients of these materials. Two cases of metallic glasses to be used as elements for resistance thermometers have been considered. They are Pd-Si and Ti-Be-Zr base alloys. The former alloys, containing a small amount of Cr, give a large negative temperature coefficient at low temperatures due to the Kondo effect. The latter alloys utilize negative temperature coefficients arising purely from structural disorder and therefore can be applicable over a wider temperature range. The temperature sensitivities of such elements based on these metallic glasses become larger below about 20K where conventional Pt base thermometers lose their sensitivity due to the vanishing of electron scattering by phonons toward $T = 0^{o}K$.

Chapter 14

ADVANCED STRUCTURAL MATERIALS - REINFORCEMENT IN COMPOSITE MATERIALS

Recent design trade-off studies have identified certain structural elements in missiles, spacecraft, and aircraft that are prime candidates for advanced alloys. These elements are:

- Missiles and Spacecraft

  Pressure vessels and other shell structures
  Support rings and plates
  Missile body interstage assemblies
  Antenna and mirror frames
  Sensor module support structures

- Aircraft

  Wing, fuselage and empennage surface cover, spars, ribs
  Control surfaces
  Bulkheads and frames
  Engine components—blades, rings, disks

These design trade-off studies have identified property improvement goals for advanced aluminum alloys, titanium alloys, and composite materials that would have a significant pay-off in future military systems. To improve range, payload, and/or service life of new aerospace weapons systems, advanced materials must have higher strengths, higher elastic modulii, or have lower densities or a combination of these improvements over currently used materials. For structural applications, aluminum alloys are of particular interest to the aerospace industry as they represent by far the major portion of the total structural weight in present aerospace systems. In addition, extensive manufacturing facilities suitable for this class of alloys already exist.

Because of the very significant anisotropy of unidirectionally aligned fiber reinforced composites, the attainment of planar isotropy can be realized only through multi-axial reinforcement. Complex composite lay-up sequences have been designed to meet these requirements. These compromise lay-ups, although offering the desired isotropy, provide properties far below those of the purely axial configuration.

Another approach to this engineering problem is to choose a form of reinforcement which, because of its geometric shape, provides high composite properties both in parallel with and transverse to the principal axis. A ribbon form achieves this goal and has been investigated for a wide variety of reinforcement materials including B, C, SiC, B_4C, and steel. In each case it was possible to demonstrate that the principles of off-axis reinforcement could be achieved and that transverse composite properties could be improved without the

need for multi-axial lay-up. The fabrication cost of ribbon, however, was found to be excessive and for the high-modulus, brittle materials, the larger cross section forms were weaker due to a pronounced flaw sensitivity.

The recent availability of high-performance amorphous metal ribbons offers the latest avenue of approach to achieving multi-axial reinforcement. Because of their extremely high strength, large width-to-thickness ratios, exceptional toughness and projected low cost, these ribbons provide a unique opportunity to achieve structural application. Also, the relatively low fabrication and use temperatures of resin matrix composites are compatible with the recrystallization temperatures of currently available ribbons although future generations of ribbons, with higher thermal stability, may prove acceptable for metal matrix composite applications. In addition to the structural desirability of amorphous metal ribbons, there also are several other environmental stability aspects that make a metallic reinforcement particularly attractive. The current concern for graphite fiber contamination of the environment and its concomitant disruptive effects on electrical equipment is a primary example. Potentially large-scale applications (e.g., in sheet body panels, both the tension and compression faces of honeycomb filled structures, and the fabrication of high-pressure tubing) can be reconsidered in light of these new forms of amorphous ribbon reinforced composites.

The properties of two amorphous metal ribbon alloys are presented for comparison with other high strength or high modulus fibers used in advanced composite materials. The amorphous alloys selected were $Ti_{50}Be_{40}Zr_{10}$ (METGLAS Alloy 2204), a relatively high-specific-strength and high-specific-modulus alloy, and $Fe_{78}Mo_2B_{20}$ (METGLAS Alloy 2605A), a very-high-strength and relatively-high-modulus alloy.

Properties of unidirectional composites, where the reinforcing fibers are aligned parallel to one another, and quasi-isotropic composites, where composite laminates are layed-up with fibers at 0, 45, and 90 degrees, are summarized in Table 17 for epoxy matrix composites. The composite properties given in Table 17 were calculated using the rule-of-mixtures with the following assumptions:

- The composites contain 60 percent fiber by volume.
- The density of the epoxy matrix is 0.044 lb/in.^{3}.
- The strength and stiffness of quasi-isotropic laminates are one-half those of the unidirectional composite when the reinforcing fibers have nearly round cross section. This is a conservative assumption as properties of actual quasi-isotropic composites are often greater than 50 percent of the longitudinal properties of the unidirectional composite.

- For the amorphous ribbon reinforcements the width-to-thickness ratio and the strength of the interface bond between the ribbon

TABLE 17 Typical properties of Bare Fibers Used in Advanced Composite Materials and Calculated Properties of Unidirectional and Quasi-Isotropic Composite Laminates

Reinforcing Fiber Designation	Manufacturer	Bare Fiber				Unidirectional Composite				Quasi-Isotropic Composite Laminate			
		Modulus (10^6 psi)	UTS (10^3 psi)	Density (lb/in.^{3})	Density (lb/in.^{3})	Longit. Mod. (10^6 psi)	Longit. UTS (10^3 psi)	Spec. Mod. (10^8 in.)	Spec. UTS (10^6 in.)	Modulus (10^6 psi)	UTS (10^3 psi)	Spec. Mod. (10^8 in.)	Spec. UTS (10^6 in.)
T50	Union Carbide	57	350	0.065	0.057	34	210	6.1	3.7	17	105	3.0	1.9
T300	Union Carbide	33	390	0.062	0.055	20	234	3.6	4.3	10	117	1.8	2.1
VSB-32	Union Carbide	55	250	0.073	0.061	33	150	5.4	2.4	17	125	2.7	1.2
VSB-0054	Union Carbide	100	331	0.075	0.063	60	199	9.6	3.2	30	160	4.8	1.6
GY-70	Celanese	75	270	0.071	0.060	45	162	7.5	2.7	23	131	3.8	1.3
C-1000	Celanese	34	360	0.064	0.056	21	216	3.7	3.9	11	108	1.8	1.9
C-3000	Celanese	34	400	0.064	0.056	21	240	3.7	4.3	11	120	1.8	2.1
Kevlar	DuPont	19	525	0.052	0.049	12	315	2.4	6.5	6	158	1.2	3.2
SiC	AVCO	62	400	0.103	0.079	37	240	4.7	3.0	19	120	2.4	1.5
Boron	CTI	59	400	0.088	0.070	36	240	5.1	3.4	18	120	2.5	1.7
FP(Al_2O_3)	DuPont	50	217	0.143	0.103	30	130	2.9	1.3	15	115	1.4	0.6
2204[a]	Allied Chemical	15.3	270	0.149	0.107	9	162	0.9	1.5	9	162	0.9	1.5
2605[a]	Allied Chemical	25	470	0.267	0.178	15	282	0.9	1.6	15	282	0.9	1.6

[a]Amorphous metal ribbon alloys.

and the epoxy is assumed to be sufficient to result in full load transfer into the ribbon reinforcement under transverse load so that the transverse properties of the composite are fully equal to the longitudinal properties.

The amorphous metal alloy 2605A has one of the highest strengths, exceeded only by Kevlar; however, the densities of the amorphous alloys are from three to five times greater than the conventional reinforcing fibers resulting in relatively low strength to density ratios. For many aerospace applications, the density-corrected properties (e.g., specific strength and specific modulus) are of prime consideration in the final selection of a material.

Table 18 summarizes the properties for the quasi-isotropic composite materials in terms of specific strength and specific modulus listing them in order of merit. The two amorphous ribbon alloys placed 8th and 10th on the specific strength ranking and last, 12th and 13th, on the specific modulus ranking. The amorphous ribbon alloys were not considered for use in metal matrix composites such as an aluminum matrix because the required processing temperatures would be above the recrystallization temperature of the amorphous alloy. Special applications for amorphous ribbon alloys in composite materials might exist where certain unique characteristics of the amorphous alloys would be applicable and where the higher density would be acceptable.

TABLE 18 Calculated Properties of Quasi-Isotropic Composite Laminates

Specific Strength Ranking			Specific Modulus Ranking		
Reinforcing Fiber Designation	Specific Strength (10^6 in.)	Specific Modulus (10^8 in.)	Reinforcing Fiber Designation	Specific Modulus (10^8 in.)	Specific Strength (10^6 in.)
Kevlar	3.2	1.2	VSB-0054	4.8	1.6
T300	2.1	1.8	GY/70	3.8	1.3
C3000	2.1	1.8	T50	3.0	1.9
T50	1.9	3.0	VSB-32	2.7	1.2
C1000	1.9	1.8	Boron	2.5	1.7
Boron	1.7	2.5	SiC	2.4	1.5
VSB-0054	1.6	4.8	T300	1.8	2.1
2605A[a]	1.6	0.9	C3000	1.8	2.1
SiC	1.5	2.4	C1000	1.8	1.9
2204[a]	1.5	0.9	FP	1.4	0.6
GY/70	1.3	3.8	Kevlar	1.2	3.2
VSB-32	1.2	2.7	2605A[a]	0.9	1.6
FP	0.6	1.4	2204[a]	0.9	1.5

[a]Amorphous metal ribbon alloys.

Chapter 15

DIFFUSION BRAZING APPLICATIONS

Diffusion brazing is a method of joining materials that combines the essential features of both conventional brazing and diffusion bonding. Typically, the process employs a filler material that closely matches the composition of the workpiece except for the addition of an appropriate melt depressant to form a low melting point eutectic. The filler material is placed between the mating surfaces of the workpiece and is permitted to alloy with it at a temperature where only the eutectic melts. Under isothermal conditions, the melting point of the filler material gradually rises as the melt depressant diffuses away into the workpiece. Bonding is judged to be complete when no melt remains. Subsequent heat treatment is employed to erase all traces of the original junction. Excellent joints have been produced in a variety of materials by this means, including the difficult to bond nickel-base superalloys. Furthermore, bond strengths comparable with base metal strengths have been achieved in the superalloys, even in high-temperature stress rupture tests.

Success in diffusion brazing depends not only on good design of filler material, but also on the ability to produce the material in a useable form. A particular problem is encountered in the preparation of thin sheet material, ∿1 to 2 in. in width x 0.001-2 in. in thickness, which is very difficult, and frequently impossible, to produce using conventional processing methods (e.g., hot rolling) owing to the limited ductility of the eutectic alloys. An interesting solution to this problem has been to prepare the sheet stock directly from the melt by such techniques as melt spinning or melt extraction. The resulting thin sheet product is particularly useful when the cooling rates are sufficient to give an amorphous metallic solid. This is because in this condition all the eutectic alloys exhibit some ductility, which facilitates subsequent handling of the materials (e.g., cutting, bending, or otherwise shaping) which may be necessary properly to dovetail filler material and workpiece. Considerable success has been achieved in utilizing amorphous nickel-base alloys (boron added as melt depressant) for diffusion bonding of superalloy components in gas-turbine engines.

Standard brazing alloys (e.g., those based on Ni) contain substantial quantities of metalloids, such as P, B, or Si, that have been added to suppress the melting points of the alloys. Since the solubilities of such metalloids in Ni are essentially nil, equilibrium phases present include phosphides, borides and silicides, the presence of which renders the crystalline material exceedingly brittle. Such materials are unamenable to typical metal working processes; hence, they typically are available in the form of powders or powder-binder (e.g., plastic tape) composites. The use of such materials for brazing complex joints often is physically awkward and burn-off of the

polymer binder can be a considerable problem.

The amounts of P, B, or Si added are typically of the order of 20 at.%. Such additions yield near-eutectic alloys, which, for the purposes of brazing, minimizes melting points. It is, of course, well known that transition metal (TM)-metalloid (M) alloys with an 80/20 at.% ratio tend to be amenable to glass formation by rapid quenching. This proves to be the case for the Ni brazing alloys designated BNi-1a, 2, 3, and 6 by the American Welding Society (AWS). Glassy foils of such alloys currently are being produced for sale. Their primary virtues are convenience of form, chemical uniformity, and cleanliness (no binder to pyrolyse). They, of course, crystallize prior to melting in the brazing process. However, once the foil has been fitted in the joint, the need for ductility no longer exists as the brazing process proceeds. In addition, it is well known that the volume shrinkage on devitrification is only about 1 percent; hence, shrinkage of the filler metal on crystallization is inconsequential. It appears that the only technical or economic limitation of metallic glass brazing materials is that not all the standard AWS alloys are amenable to rapid solidification processing. In some cases, moderate changes of alloy composition may render a standard alloy processable, but such changes dictate that the use of the material must be "requalified" for critical joining applications.

SECTION IV

CONCLUSIONS AND RECOMMENDATIONS

CONCLUSIONS AND RECOMMENDATIONS

CONCLUSIONS

1. Amorphous and glassy rapidly solidified alloys have exhibited considerable developmental and commercial potential. Some alloy systems have been well defined but others require further study to clearly establish their potential.

2. The magnetic and electrical glassy alloy systems have received considerable attention, but there are, as yet, no commercial applications.

3. A number of microcrystalline alloy systems have demonstrated unusually high-strength values and show promise of making major contributions to advanced military aerospace structures.

4. Fine-grained superalloys (e.g., ASTM 8 and finer) have been developed, tested, and used in jet engine disks, and a number of nonsuperalloy systems also show potential for such applications. Some of the superalloys are superplastic, which permits near-net-shape forging, but other ultra-fine-grained alloys, not superplastic, are expected to exhibit high levels of hot and cold plasticity, making them suitable candidates for disk, sheet, and strip applications.

5. Directionally recrystallized, coarse-grained turbine blades are a major development. Current work in this field focuses primarily on the familiar nickel-base alloy compositions (e.g., IN-100 and Mar M200) and not on the identification of totally new alloys that would be more suitable to rapid quenching.

6. Rapid solidification technology has demonstrated a capability for broadly extending compositional limits. Cast brittle alloys, lacking in toughness, can be made highly ductile, readily hot and cold formable (even superplastic), and tough through extreme structural refinement by rapid solidification. Nevertheless, development efforts to formulate new compositions and structures that take full advantage of the uniqueness of rapid solidification technology are lacking.

7. Improved corrosion resistance, sometimes to unexpected levels, has been demonstrated for a fair number of glassy alloys; however, the microcrystalline alloys have received little attention in this regard and the mechanisms associated with improved corrosion resistance are not well understood since both composition and structure appear to be important variables. Any improvements in stress corrosion cracking because of the benefits associated with rapid quenching from the melt would have profound benefits in the total DoD effort as well as in the commercial area.

8. A self-quenching technique for surface alloying using directed energy beams (laser, electron beam, plasma-arc, etc.), in conjunction with prealloyed feed (wire, powder, vapor deposit, etc.) has been developed. The fabrication of a bulk rapidly solidified article by fusing one deposited layer to another in a sequential and continuous manner, so-called Layerglase process, has also been demonstrated.

RECOMMENDATIONS

1. Time-temperature-creep deformation studies and research on consolidation techniques should be initiated with the goal of converting particulate glasses into bulk bodies. Near-term study and development of glassy alloy powders should be given special attention. In order to preserve the fine metallurgical microstructures characteristic of rapdily solidified material (powders, splats, or ribbons), further work should be done on the consolidation of fine particulates by high-energy-rate forming techniques. In this regard, the process known as dynamic compaction appears to hold great promise. Not only has it been employed successfully to compact rapid solidification rate superalloy powders, tool steel powders, and amorphous Metglas® ribbons, but also to produce unique mixed phase compacts.

2. High-strength microcrystalline alloy studies should be given adequate support since 500,000 psi fracture stresses could be attained in splat quenched materials. One approach would be to develop and produce glassy alloys that can be crystallized into microsrystalline structures with grain sizes of .01 to 1.0 micron.

3. Alloy systems that do not follow the conventional nickel-base γ-γ' hardening method should be investigated for jet engine disk and turbine blade applications.

4. Efforts to develop new alloy compositions and structures that take full advantage of rapid solidification technology should be initiated immediately and given major support. Higher specific strength amorphous or microcrystalline ribbons, e.g., Al-, Mg-, Ti-base alloys, need to be developed for applications in composite structures.

5. A major effort to seek out new superplastic (or highly ductile), fine-grained, strong, and tough alloys for jet engine, transportation, power generation, landing gear, and aircraft structure applications should be initiated immediately.

6. Efforts to improve stress corrosion cracking resistance should be initiated immediately and should include study of the mechanisms.

7. Maintain or extend programs which show potential for developing or improving rates of solidification while increasing yield of useful particulates with close control of final structure of the particulates.

8. Work on consolidation techniques, to provide greater bulk, is needed, as are investigations to sharpen compositional boundries and to check alloy structure and property stability.

9. More effective quenching techniques should be studied, to produce thicker amorphous tapes for magnetic applications.

10. The production of bulk articles or self-quenched layers through the use of intense energy beams needs further investigation. A potential exists for continuous grading of composition and properties.

11. Refinements in the production of rapidly solidified particles such as the use of crucible-less melting could improve the quality and economics of the process.

12. Applications in composite structures will require the development of higher specific strength and/or higher specific modulus alloys.

THE NATIONAL ACADEMY OF SCIENCES was established in 1863 by Act of Congress as a private, non-profit, self-governing membership corporation for the furtherance of science and technology, required to advise the federal government upon request within its fields of competence. Under its corporate charter the Academy established the National Research Council in 1916, the National Academy of Engineering in 1964, and the Institute of Medicine in 1970.

THE NATIONAL ACADEMY OF ENGINEERING was founded in 1964 as a non-profit membership institution, by action of the National Academy of Sciences under the authority of its congressional charter of 1863 establishing it as a private, self-governing corporation to further science and technology and to advise the federal government. The two Academies share those purposes in their fields.

THE NATIONAL RESEARCH COUNCIL was established in 1916 by the National Academy of Sciences to associate the broad community of science and technology with the Academy's purposes of furthering knowledge and of advising the federal government. The Council operates in accordance with general policies determined by the Academy by authority of its Congressional charter of 1863 as a non-profit, self-governing membership corporation. Administered jointly by the National Academy of Sciences, the National Academy of Engineering, and the Institute of Medicine (all three of which operate under the charter of the National Academy of Sciences), the Council is their principal agency for the conduct of their services to the government and the scientific and engineering communities.

THE COMMISSION ON SOCIOTECHNICAL SYSTEMS is one of the major components of the National Research Council and has general responsibility for and cognizance over those program areas concerned with physical, technological, and industrial systems that are or may be deployed in the public or private sector to serve societal needs.

THE NATIONAL MATERIALS ADVISORY BOARD is a unit of the Commission on Sociotechnical Systems of the National Research Council. Organized in 1951 as the Metallurgical Advisory Board, through a series of changes and expansion of scope, it became the Materials Advisory Board and, in January 1969, the National Materials Advisory Board. In consonance with the scope of the two Academies, the general purpose of the Board is the advancement of materials science and engineering, in the national interest. The Board fulfills its purpose by: providing advice and assistance, on request, to government agencies and to private organizations on matters of materials science and technology affecting the national interest; focusing attention on the materials aspects of national problems and opportunities, both technical and nontechnical in nature, and making appropriate recommendations as to the solution of such problems and the exploitation of these opportunities; performing studies and critical analyses on materials problems of a national scope, recommending approaches to the solution of these problems, and providing continuing guidance in the implementation of resulting activities; identifying problems in the interactions of materials disciplines with other technical functions, and defining approaches for the effective utilization of materials technologies; cooperating in the development of advanced educational concepts and approaches in the materials disciplines; communicating and disseminating information on Board activities and related national concerns; promoting cooperation with and among the materials-related professional societies; maintaining an awareness of trends and significant advances in materials technology, in order to call attention to opportunities and possible roadblocks, and their implications for other fields, and recognizing and promoting the development and application of advanced concepts in materials and materials processes.